2013

An experimental study on the deformation behaviour of geosynthetically reinforced ballast

Syed Khaja Karimullah Hussaini
University of Wollongong

Department of Civil, Mining and Environmental Engineering

An Experimental Study on the Deformation Behaviour of Geosynthetically Reinforced Ballast

Syed Khaja Karimullah Hussaini

B.E. (Civil Engineering), M.Tech. (Structural Engineering)

"This thesis is presented as part of the requirements for the award of the Degree of Doctor of Philosophy of the University of Wollongong"

March 2013

CERTIFICATION

I, Syed Khaja Karimullah Hussaini, declare that this thesis, submitted in fulfilment of the requirements for the award of Doctor of Philosophy, in the School of Civil, Mining and Environmental Engineering, Faculty of Engineering, University of Wollongong, is wholly my own work unless otherwise referenced or acknowledged. The document has not been submitted for qualification at any other academic institution.

Syed Khaja Karimullah Hussaini

March, 2013.

LIST OF PUBLICATIONS

The following technical papers are published based on the research carried out as a part of this PhD program;

- Indraratna, B., **Karimullah Hussaini, Sd. K**., and Vinod, J. S. (2012). "On the shear behaviour of ballast-geosynthetic interfaces." *Geotechnical Testing Journal*, ASTM, 35 (2), 305-312 (DOI: 10.1520/GTJ103317).

- Indraratna, B., **Syed Khaja Karimullah Hussaini**., and Vinod, J. S. (2013). "The lateral displacement response of geogrid-reinforced ballast under cyclic loading." *Geotextiles and Geomembranes*, (under review).

- Indraratna, B., **Syed Khaja Karimullah Hussaini**., and Vinod, J. S. (2013). "Application of optical-fiber Bragg grating sensors in monitoring the rail track deformations." *Geotechnique Letters*, (under preparation).

- **Sd K Karimullah Hussaini**, Buddhima Indraratna and J. S. Vinod (2012). "Performance of geosynthetically-reinforced ballast in direct shear conditions." *In G. A. Narsilio, A. Arulrajah & J. Kodikara (Eds.), 11th Australia-New Zealand Conference on Geomechanics: Ground engineering in a Changing World* (pp. 1268-1273). Australia: Engineers Australia.

- **Khaja Karimullah Hussaini SYED**, Buddhima Indraratna and J. S. Vinod (2012). "Some aspects of the shear behaviour of unreinforced and geosynthetic-reinforced rail ballast." *International Conference on Ground Improvement and Ground Control: Transport Infrastructure Development and Natural Hazards Mitigation,* 30 October-2 November, 2012, (pp. 889-894).Wollongong, Australia.

- Indraratna, B., **Syed Khaja Karimullah Hussaini**., and Vinod, J. S. (2013). "The geogrid reinforcement of ballast: Benefits to the rail industry." *World Congress on Railway Research*, Nov 25th-28th, 2013 (abstract submitted).

ABSTRACT

The ballast layer is responsible for distributing the applied wheel load to the subgrade soil and maintaining the track alignment. However, upon repeated load applications, the ballast due to its unbound nature deforms and degrades thereby significantly affecting the performance of the railway track. In this view, it is necessary to stabilise the ballasted rail tracks so that they can carry high-speed trains without creating any major track problem. In recent times, the use of geogrids to stabilise the ballast is on the rise. However, the effectiveness of reinforcement depends on the degree of ballast-geogrid interaction. Therefore, it is necessary to identify a suitable geogrid to stabilise the ballast. Also, it is imperative to investigate in detail the effect of geogrid on the deformation behaviour and degradation characteristics of ballast for typical loading and boundary conditions specific to railway tracks.

In this research, an experimental investigation using the large-scale direct shear apparatus was carried out to study the ballast-geogrid interface behavior and establish the effect of geogrid aperture size on the interface shear strength. A process simulation test (PST) apparatus to simulate the realistic behaviour of ballast was designed in this study. Following the design of apparatus, the influence of geogrid on the permanent deformation and degradation of ballast was assessed by conducting the model track tests. In addition, the study investigated the possible use of optical fiber Bragg grating (FBG) sensors in monitoring the railroad ballast deformations.

The large-scale direct shear tests reveal that the normalized geogrid aperture size (A/D_{50}) has a profound influence on the shear strength of the ballast-geogrid interfaces. In this respect, the ratio A/D_{50} based on the variation of interface shear strength is categorized into three key zones: (a) Feeble Interlock Zone, with $A/D_{50} <$ 0.95 (b) Optimum Interlock Zone, with 0.95 $< A/D_{50} <$1.20 and (c) Diminishing Interlock Zone, with 1.20 $< A/D_{50} <$ 2.50. The best geogrid aperture size to optimize the interface shear strength is determined to be $1.20D_{50}$. The minimum and maximum aperture sizes desired to attain the beneficial effects via geogrids are established as $0.95D_{50}$ and $2.50D_{50}$, respectively.

While the ballast due to its discrete nature is known to undergo non-uniform lateral spreading, the existing state-of-the-art for laboratory testing does not permit such non-uniform lateral spread. Therefore, to realistically simulate the ballast behaviour under cyclic loading, the process simulation test (PST) apparatus available at the University of Wollongong was modified. The modification involved the replacement of the central portion of the side wall of the existing prismoidal chamber with a setup of five independent movable plates assembled along the depth. The free lateral movement of each individual plate under the applied loading is representative of the non-uniform lateral spreading of ballast under track operating conditions.

The model track tests reveal that the geogrid effectively arrests the lateral strains in ballast, thus reducing the extent of ballast settlement and minimizing the particle breakage. However, the effect of geogrid decreases with vertical distance from its placement position. Two new parameters, namely, the lateral spread reduction index (LSRI) and geogrid influence zone (GIZ) are proposed in the current study to assess

the performance of geogrid-reinforced ballast. The GIZ is found to vary from 160 mm ($4.60D_{50}$) to 225 mm ($6.45D_{50}$) based on the geogrid placement position. The study reveals that the LSRI has a profound influence on the settlement and breakage of ballast with both ballast settlement and particle breakage exhibiting a significant reduction with the increase in average LSRI. The ideal geogrid placement location is determined to be a function of A/D_{50} ratio. The study further highlights the ability of FBG sensors to capture the deformations in ballast thereby encouraging their use in the monitoring of track stability under operating conditions.

The current study offers comprehensive understanding of the behavior of ballast-geogrid interfaces and their subsequent effect on the ballast behaviour with potential applications to rail track design. Moreover, it also benefits the rail industry in the form of reduced maintenance costs through enhanced track longevity.

ACKNOWLEDGEMENTS

I am indebted to my research supervisors Prof. Buddhima Indraratna and Dr. Jayan S Vinod for their support and encouragement during the PhD program. Their valuable suggestions and critical comments throughout the research program, including the preparation of this thesis, are gratefully acknowledged.

Thanks are also due to Dr. Cholachat Rujikiatkamjorn and Dr. Sanjay Nimbalkar for their help and comments during the course of research. I would also like to thank Dr. Sujit Kumar Dash for his support and encouragement during his short stay at University of Wollongong.

The financial support from the Cooperative Research Centre for Rail Innovation (established and supported under the Australian Government's Cooperative Research Centres program) in carrying out this research is gratefully acknowledged.

The assistance of Mr. Alan Grant, Mr. Ian Bridge, Mr. Cameron Neilson, Mr. Ritchie McLean, Mr. Frank Crabtree, and Mr. Bob Rowlan, Senior Technical Officers at the Centre of Geomechanics and Railway Engineering, University of Wollongong in the laboratory tests is highly appreciated.

I would like to thank the University of Wollongong for providing me with the necessary facilities for carrying out this research.

Finally, I have to thank my Parents, Brother, Sister, and friends for their support and encouragement.

This Thesis is dedicated with love and respect to my Parents

TABLE OF CONTENTS

LIST OF FIGURES

LIST OF TABLES

LIST OF NOTATIONS

A	geogrid aperture size
B	width of sleeper
BBI	ballast breakage index
C_u	coefficient of uniformity
C_c	coefficient of curvature
$CSDZ$	compressive stable degradation zone
$DUDZ$	dilatant unstable degradation zone
DIZ	diminishing interlock zone
D_{max}	maximum particle size
D_{50}	average particle size
f	frequency of loading
F_2	a factor depending on the sleeper type and track maintenance
FBG	fiber Bragg grating
FIZ	feeble interlock zone
GIZ	geogrid influence zone
H_s	horizontal force required to initiate lateral displacement of the track
J_{sec}	secant tensile stiffness
L	effective length of sleeper supporting the applied load
$LSRI$	lateral spread reduction index
m, n	empirical constants
N	number of load cycles
n_e	the effective refractive index of the fiber core
OIZ	optimum interlock zone

ODZ	optimum degradation zone
P_a	average contact pressure
P_d	the equivalent vertical dynamic wheel load
P_s	the static wheel load
q	deviatoric stress
q_r	maximum rail seat load
S	the standard deviation of the mean accounting for track conditions
T_{ult}	ultimate tensile strength
T	the chosen upper confidence limits
z	distance above the subballast
α	interface efficiency factor
β'	a multiplication factor accounting for the differences in the dynamic performance of unloaded vehicles
δ	apparent friction angle of ballast-geosynthetic interfaces
$\delta_{unreinf}$	lateral displacement of unreinforced ballast
δ_{reinf}	lateral displacement of geogrid-reinforced ballast
σ_v	vertical stress
σ_n	normal stress
σ_c	uniaxial compressive stress
τ	shear stress
φ	friction angle of ballast
ϕ_d	the dynamic factor
ε_1	track vertical strain
ε_2	track longitudinal strain

ε_3	track lateral strain
ε_v	vertical strain
ε_h	horizontal strain
η'	parameter that accounts for the vehicle speed
λ_B	Bragg wavelength of the FBG
Λ	grating period

1 INTRODUCTION

1.1 BACKGROUND

Railways are one of the major modes of transportation around the world. For instance, Australia has a total rail network of about 43000 km of narrow, broad and standard gauge ballasted rail track, and railways are a major contributor to the Australian economy. It is responsible for transporting freight and bulk commodities between major cities, ports and numerous mineral and agricultural industries, apart from carrying passengers in busy urban networks. However, in the recent times, the road transport has become more competitive due to the improvements in road infrastructure and decreasing road transportation costs. To survive the competition and to attract more commuters, railways are forced to introduce many new and faster trains. The introduction of new and faster trains imposes additional cyclic loads on the track thereby leading to track deterioration.

The loss of track alignment, track profile and cross level due to the effect of vibrations imposed on the track elements by complex dynamic loads can lead to various track problems including the derailment. The cost of a single, uneventful derailment is in the order of several million dollars, but when the derailment is a major one involving hazardous goods in an urban area, the consequences can cost several hundreds of millions of dollars and at times, involve human loss (Raymond et al. 1983). It is well recognised that the engineering behaviour of ballast is an important parameter governing the stability and performance of a given railway track structure (Trevizo 1991; Selig and Waters 1994).

In an effort to avoid any rail accident, the rail authorities are compelled to carry out frequent maintenance operations. Worldwide, a major proportion of railway maintenance funds are spent on the geotechnical related problems of substructure layers, including the ballast layer (e.g. Indraratna et al. 2002; Ionescu et al. 1998a). For instance, the track maintenance costs across Australia are substantial and are estimated to be around 15 million dollars per annum in the state of NSW for ballast related maintenance alone. Similarly, the railway authorities in the United States of America spend tens of millions of dollars annually for ballast and related maintenance costs (Chrismer 1985). The Canadian railroads, has reported expenditure of about one billion dollars per year, with 40% of their total track replacement and upkeep costs being on the procurement, distribution, and rehabilitation of ballast (Raymond et al. 1983). Economic studies by Wheat and Smith (2008) into British rail infrastructure showed that more than a third of the total maintenance expenditure for all railway networks that operate on ballasted track goes into substructure. Moreover, the maintenance costs increase dramatically for the tracks subjected to increased train speeds. For instance, the Shinkansen line in Japan required maintenance and tamping operation two to three times per year, and ballast pulverization was observed after only five years of operation. The TGV-Sud-Est line (Paris-Lyon) required tamping and lifting operations once in every three years, after about 40-50 Million Gross Tonnes (MGT) of railway traffic (Eisenmann et al. 1994). These frequent maintenance operations not only require huge funds but also disrupt the rail traffic causing traffic delays. In this view, a thorough understanding of the behaviour of ballast when subjected to high-speed trains and its possible stabilisation

via geogrid reinforcement is imperative if the number of maintenance operations and the track maintenance costs are to be reduced.

1.2 STATEMENT OF PROBLEM

In the recent years, owing to the increased number of rail commuters, railways face the challenge of increasing the competitiveness and attractiveness of rail transport in terms of speed (reduced travel time), increased tonnages, higher frequency of trains, availability and reliability with promising passenger comfort and safety. This in turn necessitates better quality of track that depends upon the better functioning of ballast, a key component of the conventional track structure. Ballast is defined as the selected crushed granular material placed as the top layer of the substructure in which the sleepers are embedded to support the rails. Freshly placed ballast is a narrow-graded material (i.e. contains a limited range of particle sizes), consisting of a large amount of open pore space and a permeable structure. Its importance has grown with increasing axle loads and train speeds.

The inherent effect of traffic loads is the deviation of track geometry (profile, alignment and cross level) from required conditions as a result of deformations that occur in the substructure layers. When the subgrade is stable and proper sub-ballast exists, the track deformations occur mainly in the ballast (Selig 1998). The dynamic effect of traffic causes, apart from deformation of substructure layers, breakdown of the individual ballast particles within the structural ballast section.

Many studies have been carried out in the past to understand the engineering behaviour of railway ballast by both laboratory testing (Schultze and Coesfeld 1961;

Raymond et al. 1975, 1976; Birman. 1975; Selig and Alva-Hurtado 1981; Norman and Selig 1983; Shenton 1985; Jeffs and Marich 1987; Indraratna et al. 1997, 1998, 2001, 2007; Indraratna and Ionescu 1999; Ionescu et al. 1996, 1998b; Indraratna et al. 2010a) and field trials (Dalton 1973; Trevizo 1991; Eisenmann et al. 1994; Selig and Waters 1994; Indraratna et al. 2010b). To stabilize the tracks encountering weak foundation soils and ballast vulnerable to breakage under high-speed loadings, the tracks are reinforced with geosynthetics. Some of the functions of geosynthetics include separating the ballast layer from the subgrade to prevent ballast penetration, reinforcing the ballast layer to reduce ballast settlement and attrition, filtration to prevent subgrade pumping and drainage to prevent excessive wetting of the subgrade. These techniques can reduce the depth of the required granular layer and also reduce the frequency of the required maintenance. For example, Walls and Galbreath (1987) reported that the periods between maintenance operations could be increased by as much as 12 times by the application of geogrid reinforcement to the ballast. However, introduction of geosynthetic layer in ballast may lead to changes in the overall behavior of track in comparison with the conventional tracks, thus elucidating the need to study about the geosynthetic-ballast interface for the better understanding of reinforced tracks.

1.3 RESEARCH OBJECTIVES

The major aim of this research is to evaluate the effect of geogrid reinforcement on the behavior of ballasted rail tracks and to optimise the geogrid type to enhance the track performance. The specific objectives of this study are to:

a) Assess the role of geogrid aperture size (A) on the shear behavior of ballast-geosynthetic interfaces and to identify the optimum geogrid aperture size to maximise the interface shear strength;

b) Design and commission a modified process simulation test (PST) apparatus which enables the accurate simulation of rail track behavior by allowing the free lateral spreading of ballast along its depth;

c) Undertake a series of experiments using the modified PST apparatus to investigate the deformation and degradation behaviour of both unreinforced and geogrid-reinforced ballast using the under high-frequency cyclic loading;

d) Determine the lateral strain profiles along the ballast depth in case of unreinforced and geogrid-reinforced ballast under high-frequency cyclic loading;

e) Determine the distance to which the beneficial effects of geogrid exist in terms of inhibiting the lateral spread of ballast (i.e. geogrid influence zone) and,

f) Establish the role of geogrid aperture size (A) and the geogrid placement position on the ability of reinforcement to reduce the lateral deformations of ballast and hence reduce the track settlement and particle breakage.

1.4 SCOPE OF RESEARCH

The main focus of this project is to thoroughly evaluate the shear behaviour of geogrid-reinforced ballast, and to optimise the type of geogrid and its placement position within the track to improve the track performance. The findings from this study will lead to an efficient track design in order to minimize the deformation and rate of degradation (hence, track settlements), and consequently reduce the track maintenance costs.

1.5 THESIS STRUCTURE

This thesis comprises of eight chapters including the introduction. The organization of the subsequent chapters is outlined below.

A review of the literature is presented in Chapter 2 that begins with a brief background to the structure of railway tracks, followed by a discussion on the loads encountered in a typical track and the behavior of the ballast under those loads. The ballast selection criteria are concisely discussed followed by a critical review of the engineering behavior of ballast. The effect of confining pressure, applied deviatoric stress and other important parameters on the deformation and degradation characteristics of ballast is examined in detail. The influence of increasing train speed on the ballast performance is presented. Emphasis is also laid on the problems associated with the functioning of conventional ballasted tracks and the need for stabilizing ballast. The literature relevant to the geogrid-reinforced ballast is also discussed.

Chapter 3 describes the materials used for this study and their physical characteristics. The description of large-scale direct shear apparatus used in the current study to quantify the geotechnical properties related to the behavior of ballast-geosynthetic interfaces is presented.

Chapter 4 describes the test results pertaining to ballast-geosynthetic interface behavior from the large-scale direct shear tests. The effect of geogrid aperture size (A) on the interface shear strength is highlighted and the probable modes of ballast-geosynthetic interface failure are described.

Chapter 5 explains the layout of the existing large-scale process simulation test (PST) apparatus and highlights the need to modify the equipment to enable a better simulation of the in-field track conditions. This is followed by a description of the modified process simulation test (MPST) apparatus designed and built in order to enable a better simulation of the in-field loading conditions before describing the calibration of instrumentation and various devices used during the experimental work.

Presented in Chapter 6 are the laboratory experimental results from the large-scale model track tests. The permanent deformation and degradation behavior of unreinforced and reinforced ballast is compared and the effect of geogrid type and position on the settlement and breakage characteristics of ballast is highlighted. The geogrid influence zone (GIZ) is determined and the role of geogrid aperture size (A) on the deformation (both vertical and lateral) and degradation of ballast is established.

Chapter 7 describes the application of optical-fiber Bragg grating (FBG) sensors in the rail industry to capture the lateral deformations in ballast. The chapter discusses the lateral strain profiles under the rail for both unreinforced and geogrid-reinforced ballast.

Chapter 8 includes the conclusions of the present study and recommendations for further research. The Chapter concludes with the proposed modifications to existing standards and new design guidelines based on the findings of this study.

In addition, the Appendices that contain some data and a list of references are included at the end of the thesis.

2 LITERATURE REVIEW

2.1 INTRODUCTION

The conventional rail ballasted track is the most common and preferred railroad structure due to its relatively low cost of construction and the ease of maintenance (Chrismer 1985; Jeffs and Marich 1987; Esveld 2001). The ballasted railway track is a layered discrete system that consists of a flat framework made up of rails and sleepers supported on ballast, subballast and subgrade (Figure 2.1).

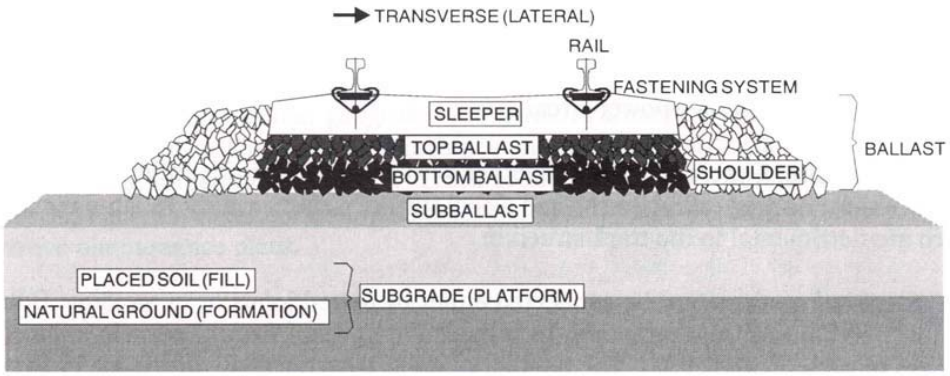

Figure 2.1 Typical ballasted railway track cross section (after Selig and Waters 1994)

2.2 COMPONENTS OF RAIL TRACK

A typical railway track consists of the superstructure and the substructure. The superstructure consists of the rails, the fastening system and the sleepers whereas the components below the sleeper are termed as the substructure. The substructure consists of the ballast, the subballast and the subgrade (Figure 2.2).

Rails are the longitudinal steel members which are placed at a specific distance apart from each other to give tracks of various gauges. The main function of the rails is to

direct the rolling stock and transfer the concentrated wheel loads to the sleepers and subsequently to the substructure. Therefore, rails must have sufficient stiffness to distribute the wheel loads over sleepers and limit deflection between the supports.

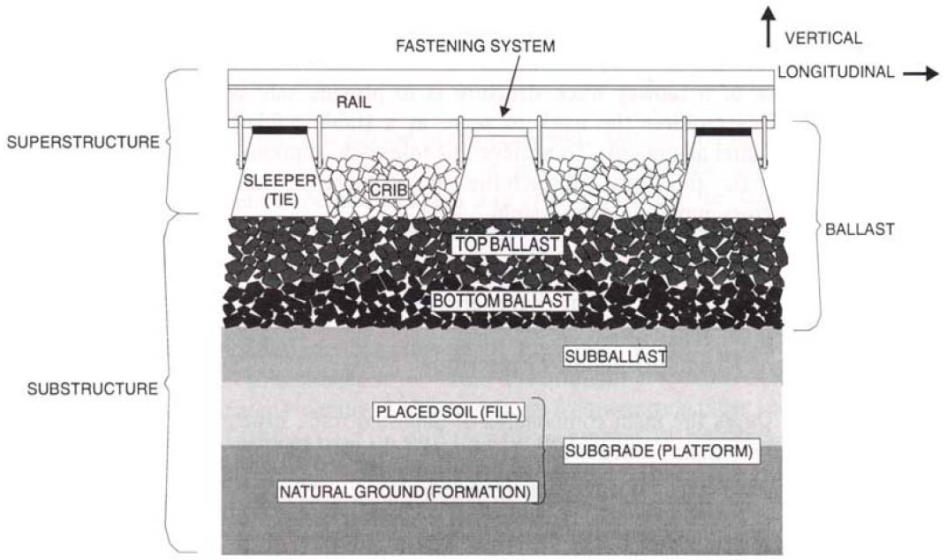

Figure 2.2 Side-layout of a typical ballasted railway track (after Selig and Waters, 1994)

The fastening system retains the rails against the sleepers and resists vertical, lateral, longitudinal, and overturning movements of the rails, thus providing effective bond between the rail and the sleepers. The main function of sleepers is to distribute the wheel loads transferred by the rails and fastening system to the underlying supporting ballast. Sleepers are usually spaced at about 600 mm apart. Ballast, the granular material upon which the rail and the sleeper assembly is laid, is the foundation of the rail track. It performs an important function of transferring the train load to the subballast and maintaining the track alignment. The ballast consists of the crib ballast, the load bearing ballast and the shoulder ballast. Subballast is the

intermediate layer provided in between the ballast and the subgrade. It dissipates the stresses to an acceptable level and prevents the flow of subgrade soil into the ballast. The subgrade is the foundation soil upon which the rail track is laid and hence the load carrying ability of the track is affected by the subgrade soil. The functions and properties of ballast, subballast and the subgrade are described briefly in the subsequent sections.

2.2.1 Ballast

Ballast is the crushed granular material upon which the rail-sleeper assembly is laid. Ballast usually comprises of igneous or metamorphic rocks comprising of medium to coarse gravel-sized aggregates (10-63 mm), with a small percentage of cobble-sized particles. The optimum thickness of ballast is usually 250-350 mm measured from the lower side of the sleeper (Esveld 2001). The ideal material for ballast should be angular, crushed hard rock, uniformly graded, free from dirt and dust, and not prone to cementing action (Selig and Waters 1994).

2.2.1.1 *Functions of ballast*

Ballast, being the principal component of the rail track is responsible for the perfect execution of the following functions to ensure the passenger comfort and safety of the rail tracks. The most important functions are to retain track position, reduce the sleeper bearing pressure for the underlying materials, store fouling materials, provide drainage for water falling onto the track, rearrange during maintenance to restore track geometry as well as to provide damping to the dynamic excitations originated due to the passage of train loads (Robnett et al. 1975; Selig and Waters 1994).

Therefore, ballast is required to be hard, durable, and angular, free from dust and dirt, and have relatively large voids. However, the progressive breakdown of ballast materials, caused by traffic load and maintenance tamping, and the intrusion of external materials, such as wagon spillage and infiltration of underlying materials into the ballast often results in major track deterioration.

2.2.1.2 *Characteristics of railway ballast*

In order to perform the above described functions, the ballast is supposed to be a free-draining granular media used as a load bearing material in railway tracks. The thickness of the ballast bed should be such that the subgrade is loaded as uniformly as possible. Good-quality railway ballast should have angular particles, high specific gravity, high shear strength, high toughness and hardness, high resistance to weathering, rough surface and minimum hairline cracks (Chrismer 1985; Jeffs and Marich 1987; Indraratna et al. 1998, 2000, 2003b; Esveld 2001). However, the sources of such high-quality ballast are limited, and under dynamic loading conditions most ballast properties change progressively because of particle breakage, deformation and fouling. Ballast fouling decreases permeability, and therefore causes hydraulic erosion, reduction in stability due to particle lubrication, subgrade attrition, and ballast deterioration due to the delay in dissipation of excess pore water pressures.

The characteristics required for ballast to perform its intended functions are clearly contradictory in some aspects, and thus a particular type of ballast cannot accomplish all of them completely (Profillidis 1995). It could thus be argued that for high load-bearing characteristics and maximum track stability the ballast needs to be angular,

well graded and compact, which in turn reduces the drainage of the track. Therefore a balance needs to be achieved between bearing capacity and drainage.

2.2.2 Subballast

Subballast generally comprises of broadly graded sand-gravel mixture and is placed between the ballast and the subgrade layers (Selig and Waters 1994). In most countries, the subballast layer is usually about 150 mm thick (Selig and Waters 1994; Profillidis 1995). However, a subballast thickness of greater depths of up to 300 mm is also sometimes provided in the case of weak subgrade soils (Raymond 1978). Alternatively, a structural fill can be placed above the soft subgrade before placing the subballast. In case of higher axle loads, if a greater thickness of granular bed is needed, it is more common and economical to fix the ballast depth and increase the thickness of subballast as required (Shahu et al. 1999). According to Selig and Waters (1994), the main functions of subballast are to:

- ✓ Minimise the subgrade stresses by providing additional load distribution;
- ✓ Provide a load bearing foundation beneath the ballast bed;
- ✓ Prevent the ballast particles from penetrating the subgrade soils;
- ✓ Increase the track resiliency;
- ✓ Provide drainage to the water from the ballast and transfer it away from the subgrade thereby preventing the formation of soil slurry.

Ideal subballast should have a permeability significantly smaller than the ballast layer but sufficient enough to prevent water clogging and poor drainage in the subgrade.

2.2.3 Subgrade

The subgrade comprises of a naturally deposited soil and provides a stable foundation to the rail track. The subgrade characteristics significantly affect the performance of the rail track (Brough et al. 2006). For instance, the subgrade with low bearing capacity or poor drainage may require speed and load restrictions (Zicha 1989). On the other hand, a stiffer subgrade generally enhances the track stability and reduces the ballast settlement (Raymond 1978; Selig and Waters 1994). A sensitivity analysis using different track degradation models conducted by Sadeghi and Askarinejad (2007) revealed that the allowable annual tonnage for a track with a good quality subgrade soil is four times more than that of one with a poor quality subgrade.

2.3 FORCES IMPOSED ON BALLAST LAYER

The knowledge of the various forces acting on the ballast layer is essential to understand its behaviour when subjected to train passage. The wheel load distribution pattern in a typical rail track is shown in Figure 2.3 (Selig and Waters 1994). Although it may not be possible to exactly predict the loading levels on the ballast because of the various factors that affect it such as train speed, axle load and environmental/track conditions, yet the loading level can be estimated reasonably well (Profillidis 1995).

The forces imposed on a rail track could be classified as mechanical forces (both static and dynamic) and the thermal forces. Esveld (2001) has classified the types of forces and their sources as: (a) quasi-static loads induced by the weight of the vehicle, reaction forces in curves and the loads generated due to wind (b) dynamic

loads which are mainly due to speed of trains, track irregularities such as differential settlement in ballast bed, corrugations, discontinuities in welded joints together with vehicle defects such as wheel flats, and (c) thermal loads that are significant in continuously welded rails due to the presence of temperature gradients.

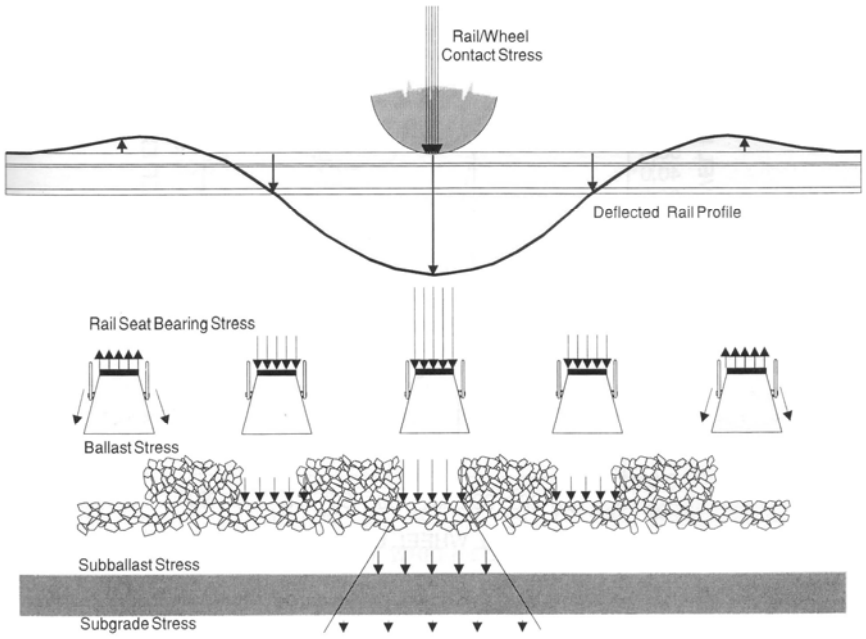

Figure 2.3 Typical wheel load distribution in track (Selig and Waters 1994)

2.3.1 Vertical forces

The pressure level at the sleeper-ballast interface depends on both ballast bed conditions and track characteristics such as stiffness of the rail-sleeper fastening system, the type of sleeper and the distance between them (Shenton 1974; Raymond and Bathurst 1994; Frohling 1998; Esveld 2001). In addition this pressure varies along the sleeper length, with the contact pressure being maximum at the rail seat and smaller towards middle and end of the sleepers (Clarke 1957; Neil 1976; Kerr 1976).

For the purposes of design, the sleeper-ballast contact pressure is generally assumed to be uniform and is given by Equation 2.1 (Jeffs and Tew 1991);

$$P_a = F_2 \times (\frac{q_r}{BL}) \quad 2.1$$

Where P_a = average contact pressure

q_r = maximum rail seat load

B = width of sleeper

L = effective length of sleeper supporting the load q_r

F_2 = a factor depending on the sleeper type and track maintenance.

Alternatively, Atalar et al. (2001) estimated the maximum sleeper-ballast contact stress for a train speed of 385 km/h to be about 479 kPa. Esveld (2001) stated that the maximum permissible sleeper-ballast contact stress can be taken in the vicinity of 500 kPa.

2.3.2 Lateral forces

Selig and Waters (1984) indicated that there are two principal sources of lateral loads: (a) lateral wheel force, and (b) buckling reaction force. Under track operation conditions, the lateral wheel forces are initiated by the lateral force component of friction between the wheel and the rail, plus the lateral force applied by the wheel flange on the rail. On the other hand, buckling forces are developed due to the high compressive stresses caused by high rail temperatures. Although the lateral forces are

critical in terms of both the train safety and the passenger comfort, they are less dependent on train speeds (Birmann 1966; ORE 1970; Eisenmenn 1970).

2.3.3 Longitudinal forces

Longitudinal forces in a typical rail track occur as a result of (a) temperature effects (b) accelerating and breaking of locomotive cars (c) shrinkage stresses caused by welding of rails in the track, and (d) track creep.

2.3.4 Dynamic analysis

It is well known that the dynamic forces in a rail track could increase the applied wheel load by up to a factor of three depending on the defect type of the rail-track system (e.g. Broadley et al. 1981; Frederick and Round 1985; and Harrison et al. 1986). In this view, the design of railway track should be based on the actual stresses in the various components of the track determined from the equivalent dynamic vertical and lateral forces imposed by the moving train. The dynamic factor (ϕ_d) originally proposed by Eisenmann (1972) and subsequently modified by Broadley et al. (1981) and Orange (1988) is currently used by most Australian railway authorities (Equation 2.2);

$$\emptyset_d = 1 + \beta' t \eta' s \qquad 2.2$$

Where, β' is a multiplication factor (accounts for the differences in the dynamic performance of unloaded vehicles), t is the chosen upper confidence limits, η' is a

parameter that accounts for the vehicle speed and S is the standard deviation of the mean (accounts for track conditions).

The equivalent vertical dynamic wheel load (P_d) to be used in the design can then be estimated by Equation (2.3) (Jeffs and Tew 1991);

$$P_d = \emptyset_d P_s \qquad 2.3$$

Where, P_s is the static wheel load and ϕ_d is the dynamic factor.

2.3.4.1 *Lateral resistance*

The lateral resisting forces required to ensure the stability of a loaded track could be determined by the following relationship developed by the SNCF (1950);

$$H_s \ > 10 + \frac{P_d}{3} \qquad 2.4$$

Where, H_s is the horizontal force (kN) required to initiate lateral displacement of the track and P_d is the equivalent vertical dynamic wheel load.

2.4 BEHAVIOUR OF RAIL BALLAST UNDER VARIOUS LOADING CONDITIONS

2.4.1 One-dimensional consolidation behaviour of rail ballast

Ionescu (2004) has carried out one-dimensional compression tests to study the time-dependent deformation characteristics of railway ballast prior to failure. It is reported

that the settlement of ballast under one-dimensional compression occurs in three distinctly different stages. Initially, rapid settlement takes place as particles compact upon loading, thereby increasing the inter-particle contact area. With further loading, primary breakage of highly angular particles takes place as their corners fracture due to increased stress concentration, indicating a gradual compression with time. The final phase is related to secondary breakage of less coarse particles at increased load amplitude or number of cycles, whereby additional but small settlements continue to occur at a diminishing rate (Figure 2.4).

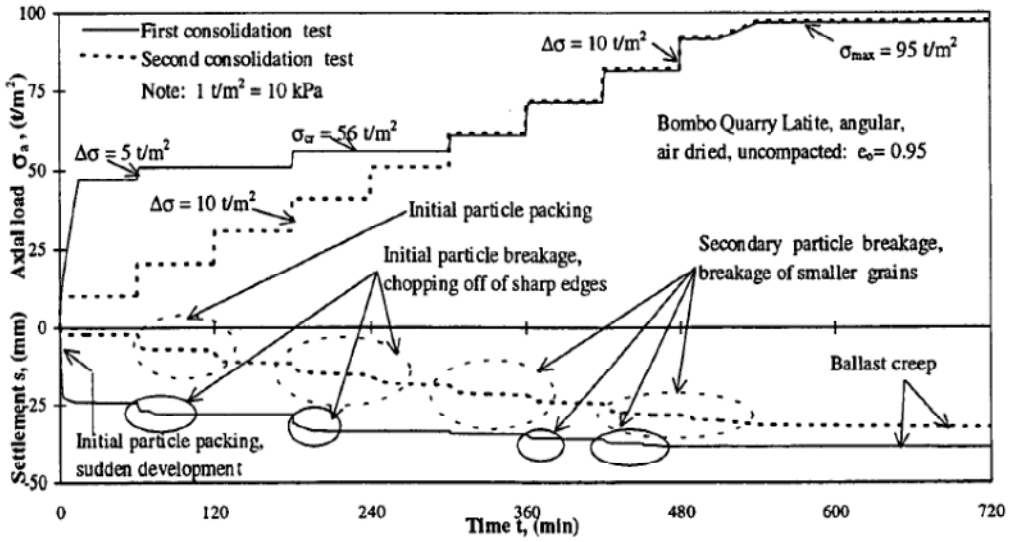

Figure 2.4 Settlement of ballast under one-dimensional compression (Ionescu 2004)

2.4.2 Triaxial shear behavior of railway ballast

2.4.2.1 *Cyclic densification*

Rail tracks undergo millions of loading cycles of varying magnitudes and frequencies during their service life. Under repeated loads, the process of cyclic densification of ballast and associated track deformations are of paramount importance for optimum design, safety and operational efficiency of tracks. In the recent past, several

researchers have studied the deformation and degradation behaviour of ballast under static and cyclic loading conditions (Shenton 1975; Raymond and Williams 1978; Alva-Hurtado and Selig 1981; Selig and Alva-Hurtado 1982; Jeffs and Marich 1987; Indraratna et al. 1998; Indraratna et al. 2005; Indraratna and Salim 2005; Lackenby et al. 2007; Salim and Indraratna 2004; Anderson and Fair 2008; Indraratna et al. 2010a). Jeffs and Marich (1987) conducted a series of cyclic load tests on ballast and indicated an initial rapid increase in settlement, followed by a stabilized zone showing a linear increase in settlement with load cycles. Ionescu et al. (1998) observed highly non-linear deformation of ballast under cyclic loading. They also reported a rapid initial settlement during the first 20,000 load cycles, followed by a gradual compression stage up to about 100,000 cycles, after which the settlement increased at a marginal rate with the increasing load cycles. Under low amplitude cyclic loading, ballast shows a strong tendency towards densification causing a significant increase in strength and stiffness (Suiker et al. 2005; Indraratna and Salim 2005).

2.4.2.2 *Particle breakage*

Crushing of particles in a granular medium has been investigated experimentally by various researchers, and various breakage indices have been proposed based on the changes in the particle size distribution (e.g. Lee and Farhoomand 1967; Marsal 1973; Hardin 1985; Indraratna et al. 2005). The importance of incorporating grain crushing to the plastic behaviour became evident after Bolton (1986) modeled the dilation behaviour of sand under shearing. The breakage of sand particles in triaxial tests was also examined by Nakata et al. (1999). McDowell et al. (1996) developed a conceptual compression model for fractal crushing of a granular medium. They

indicated that the fracture intensity decreases with the reduction in grain size, that results in an increase in particle contact area leading to a more uniform internal stress distribution. McDowell et al. (1996) also concluded that the probability of particle breakage in aggregate increases with an increase in applied stress, increase in particle size, and a decrease in the average coordination number (average number of contacts per particle).

With regards to rail ballast, several researchers have studied the breakage of ballast under static and cyclic loading conditions (Indraratna et al. 1998; Salim and Indraratna 2004; Indraratna and Salim 2005; Indraratna et al. 2005; Lackenby et al. 2007; Indraratna et al. 2010a). Identifying the influence of particle breakage on the deformation behavior of ballast, Indraratna et al. (2005) have proposed a ballast breakage index (BBI) to quantify the particle degradation. The extent of particle breakage is a function of the applied deviatoric stress, confining pressure, loading conditions (i.e. static or cyclic loading) and the loading frequency. For instance, under static loading conditions the particle degradation increases with the increase in confining pressure (Indraratna and Salim 2005). On the other hand, under cyclic loading conditions the particle degradation decreases for an initial increase in confining pressure from about 30 to 60 kPa and increases again with the increase in confining pressure (Indraratna et al. 2005; Lackenby et al. 2007). Similarly, the extent of particle breakage increases with the increase in applied deviatoric stress and the loading frequency (Lackenby et al. 2007; Indraratna et al. 2010a).

2.5 FACTORS INFLUENCING THE PERMANENT DEFORMATION AND DEGRADATION OF BALLAST

There are several factors that influence the deformation and degradation behaviour of railroad ballast. The effect of some of the important parameters like the confining pressure, deviatoric stress, the number of load cycles (*N*), load history, particle size distribution, degree of compaction, loading frequency (*f*), and the parent rock strength are presented in the subsequent sections.

2.5.1 Effect of confining pressure

The effect of confining pressure on the deformation and degradation behaviour of railway ballast has been studied by several researchers (e.g. Barksdale 1972; Knutson 1976; Indraratna et al. 2005; Lackenby 2006; Lackenby et al. 2007). Barksdale (1972) reported a decrease in the permanent deformation with the increase in confining pressure for a given value of the applied deviatoric stress. Similarly, Knutson (1976) has identified the confining pressure to be an important parameter influencing the behaviour of a given granular material.

Indraratna et al. (2005) and Lackenby et al. (2007) have studied the effect of confining pressure on the degradation and deformation response of ballast subjected to cyclic loading. They reported that the axial strains decreased significantly with the increasing confining pressure. They further pointed out that the ballast specimens exhibited dilation at small confining pressure (σ_3 < 30 kPa), but became progressively more compressive as the confining pressure increased from 30 to 240 kPa. It was reported that the ballast breakage index (BBI) of unreinforced ballast initially decreases with the increase in confining pressure, remains almost constant

for a certain range of confining pressure and then increases after a threshold confining pressure. Based on the variation of BBI with the applied confining pressure, the ballast degradation behavior has been categorized into three distinct zones, namely the dilatant unstable degradation zone (DUDZ), the optimum degradation zone (ODZ), and the compressive stable degradation zone (CSDZ) (Figure 2.5). These zones are defined by the level of σ_3 acting on the specimen (i.e. DUDZ, σ_3 < 30 kPa; ODZ, 30 kPa< σ_3 <75 kPa; CSDZ, σ_3 > 75 kPa); however, $q_{max,cyc}$ also plays an important role in characterising the zones.

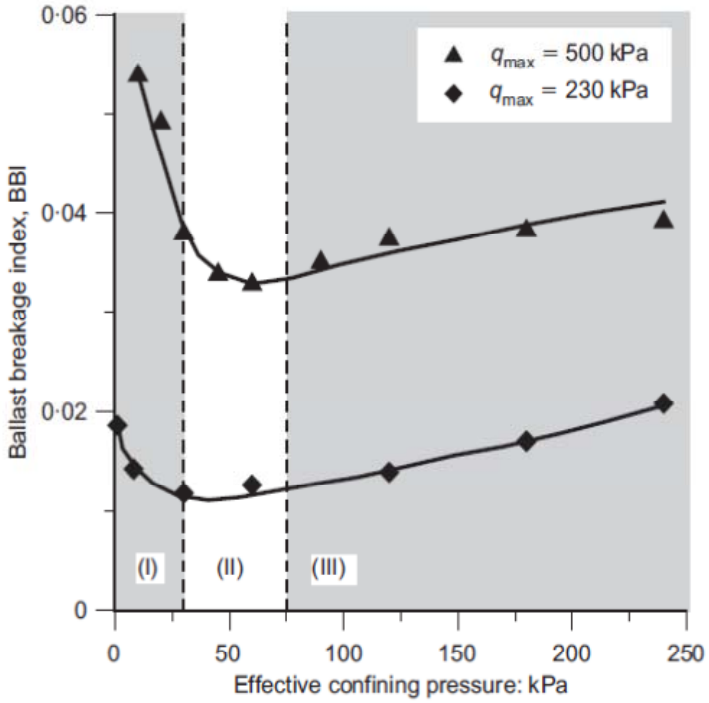

Figure 2.5 Effect of confining pressure on the BBI (Indraratna et al. 2005)

2.5.1.1 *Dilatant unstable degradation zone (DUDZ)*

Indraratna et al. (2005) reported that for σ_3 < 30 kPa, the ballast specimens under cyclic loading experience significant axial and expansive radial strains, resulting in

an overall volumetric increase or dilation. In this zone of high dilation, degradation is attributed mainly to the shearing and attrition of angular projections due to excessive axial and radial (expansive) strains. Because of the small confining pressure applied, specimens in the DUDZ have poorly established contacts and relatively small particle-to-particle contact areas.

2.5.1.2 *Optimum degradation zone (ODZ)*

As the confining pressure is increased, an optimum particle configuration (packing arrangement) is attained, significantly reducing the overall dilation. This behaviour is illustrated in Figure 2.5 for σ_3 in the range 30-75 kPa. The particles in this zone are held together with sufficient lateral confinement to provide an optimum internal contact stress distribution and increased inter-particle contact areas. Consequently, the risk of breakage associated with stress concentrations is reduced, and the coordination number (number of contact points between particles) may increase slightly for each particle compared with the situation in the DUDZ, because the overall volumetric behaviour becomes slightly compressive. Compared with the DUDZ, there is also a significantly reduced axial strain rate due to increased apparent stiffness. With reduced settlement and degradation, rail tracks would benefit from slightly increased lateral confining pressure.

2.5.1.3 *Compressive stable degradation zone (CSDZ)*

As σ_3 is further increased (> 75 kPa), the coordination number is expected to stay approximately constant, and increased breakage in this zone is attributed mainly to increasing stress levels at the particle contacts, and the restriction of internal particle

sliding and rolling. In this zone, the radial strains are much smaller than in the DUDZ. Breakage gradually continues to increase in intensity as the volumetric compression increases at a decreased rate with the confining pressure.

2.5.2 Effect of deviatoric stress, q

The amplitude of loading is an important parameter that significantly affects the deformation and degradation aspects of ballast. Several researchers have reported that the magnitude of permanent deformations increase with the increase in the applied deviatoric stress (e.g. Morgan 1966; Olowokere 1975; Knutson 1976). Stewart (1982) carried out a set of cyclic triaxial tests wherein the loading amplitude was changed at every 1000 load cycles. Based on the results from series of such tests carried out at three different confining pressures it has been concluded that with the increase in deviator stress the extent of plastic deformation at first cycle increased significantly for any given confining pressure. Another prominent conclusion from the study was that when the magnitude of loading was increased beyond any past maximum value, the plastic deformations increased rapidly. Similarly negligible plastic deformations were reported to occur with the load cycles when the magnitude of loading was less than any past maximum value. Shenton (1985) also reported that the permanent strain after the first load application was always larger if the applied stress was higher. These observations correlate well with the field observations by Feng (1984), Bathurst and Raymond (1994) and Sato (1995) that an increase in the axle loads resulted in higher maintenance costs.

The effect of deviatoric stress (q) on the deformation and degradation behavior of ballast was recently studied by Lackenby et al. (2007). They have concluded that the

deformation and degradation of ballast increased significantly with the increase in the applied deviatoric stress for a given confining stress (Figure 2.6 and Figure 2.7).

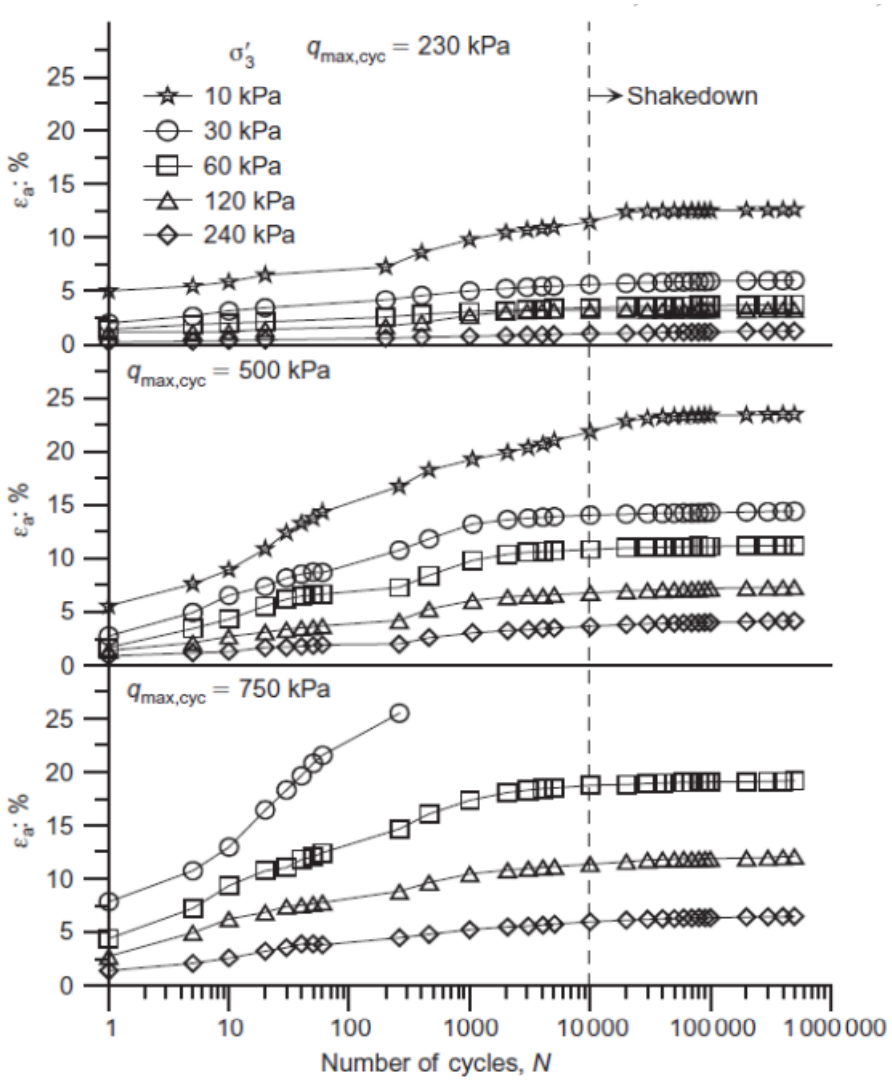

Figure 2.6 Effect of maximum cyclic deviatoric stress on the axial strain of ballast (Lackenby et al. 2007)

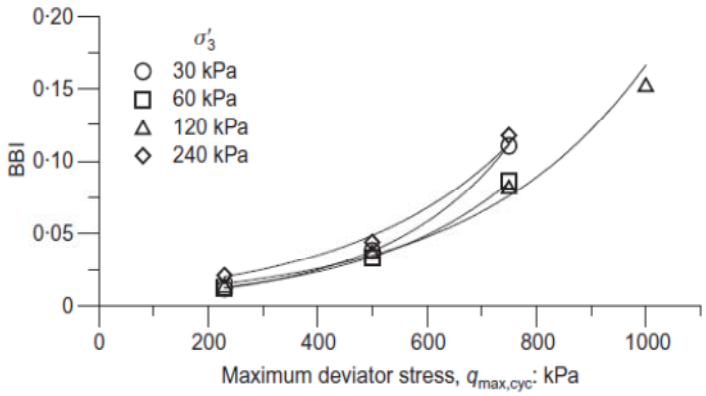

Figure 2.7 Effect of maximum cyclic deviatoric stress on the BBI (Lackenby et al. 2007)

2.5.3 Effect of load history

Several researchers have studied the effect of load history on the behaviour of soil (Drucker et al. 1957; Brown and Hyde 1975; Knutson 1976; Alva-Hurtado 1980; Diyaljee 1987). For instance, Brown and Hyde (1975) and Knutson (1976) reported that the total permanent deformation was less when the specimen was subjected to gradually increasing stress levels than when the highest stress level was first applied. Similarly, Diyaljee (1987) reported that the extent of plastic deformations decreases significantly if the maximum deviatoric stress in the previous stress history is more than 50% of the current applied deviatoric stress.

2.5.4 Effect of number of load cycles (*N*)

According to Collins and Boulbibane (2000) and Werkmeister (2003), a material can respond in four different ways when subjected to repeated loading. The response could be (i) purely elastic, (ii) elastic shakedown, (iii) plastic shakedown and (iv) the incremental collapse or ratchetting. For instance, when the magnitude of the cyclic loading is sufficiently small, the material does not exhibit any permanent strains

(stage 1 in Figure 2.8), and the material response is purely elastic. In stage 2, although the applied load level is appropriate to induce some permanent strains, yet the material behaves completely elastic after a finite number of cycles i.e. leading to zero permanent strain. At this point, the material is said to have reached "elastic shakedown" and the resilient strain becomes constant resulting in constant resilient modulus. At loads higher than these critical loads which cause elastic shakedown, the material behaviour will be either "cyclic plasticity" where a closed cycle of permanent strain is formed (stage 3 in Figure 2.8), or "incremental collapse or ratchetting" wherein permanent strain increases indefinitely (stage 4 in Figure 2.8) with each successive loading until the material fails.

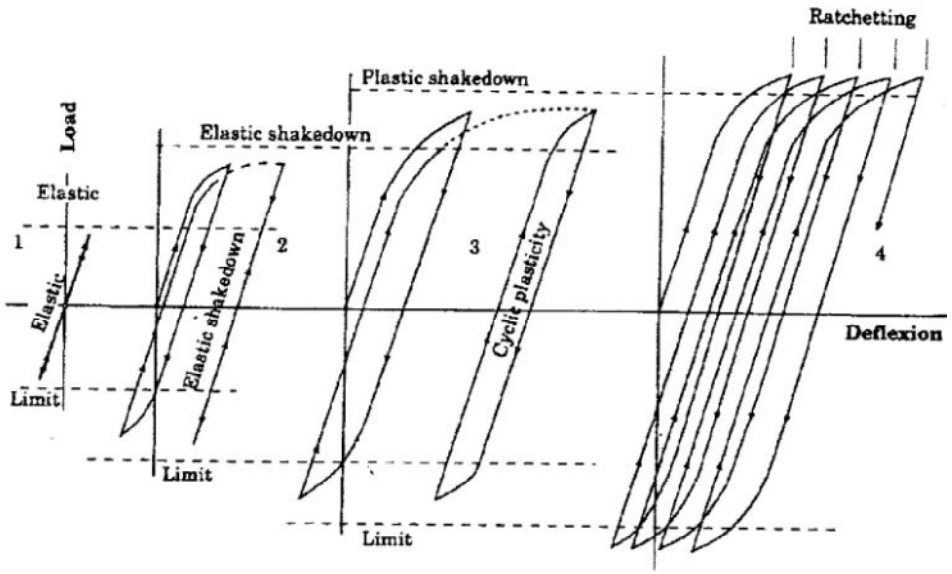

Figure 2.8 Four types of response of elastic/plastic structures to repeated loading cycles (Collins and Boulbibane 2000)

Several researchers have commented that the permanent settlement of ballast increases logarithmically with the number of load cycles, *N* (Barksdale 1972; Shenton 1974, 1985; Olowokere 1975; Raymond and Williams 1978; Lentz and

Baladi 1981; Brown and Selig 1991). Profillidis (1995) concluded that the first cycle causes maximum amount of plastic strain and the rate of plastic strains then decreases with each subsequent cycle until a stable condition is reached. Lackenby et al. (2007) have reported that the ballast reaches a shakedown after 10000 load cycles. Brown (1974), Uzan (1999) and Indraratna et al. (2010a) have commented that the ballast reaches a stable state within the first 10000 load cycles. Moreover, the final permanent strain is a function of the plastic strain at the first cycle (Alva-Hurtado and Selig 1981; Stewart 1986).

Jeffs and Marich (1987) based on a series of cyclic tests concluded that ballast exhibited a rapid increase in settlement in the initial phases, followed by a stabilized zone with further load applications (Figure 2.9). However, in the stabilized (post-compaction) zone the settlements in ballast tend to increase suddenly, which they described as re-compaction of ballast. Jeffs and Marich attributed this to the failure of particle contact points within the ballast bed causing a sudden increase in settlement rate. The effect of re-compaction was noticed for about 100,000 load cycles after which the rate of settlement became almost constant.

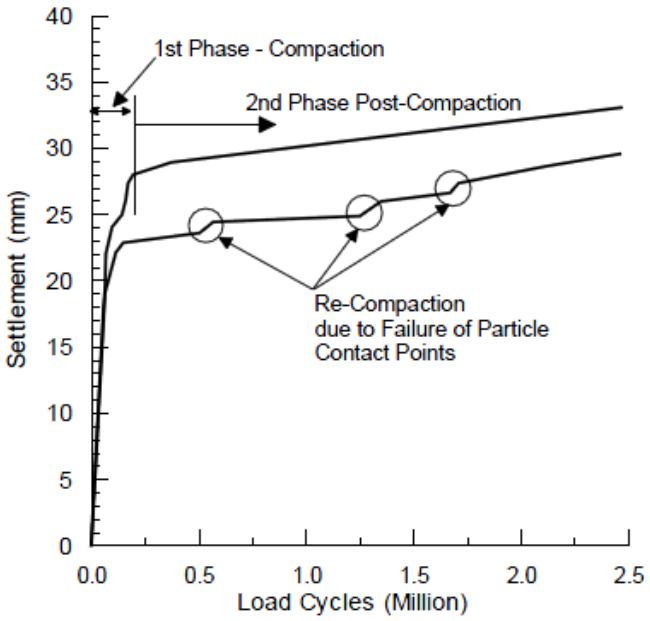

Figure 2.9 Settlement of ballast during cyclic loading (data from Jeffs and Marich 1987)

2.5.5 Effect of particle size distribution

The grain size distribution of ballast significantly controls the ballast performance, which is expected to provide sufficient shear strength and the porosity to allow free drainage. The permanent strains in ballast reduce significantly if a change in particle gradation can lead to increased density of ballast (Dunlap 1966). Raymond and Diyaljee (1979) reported that larger size ballast with a uniform grading caused higher plastic strains than the small sized particles. Thom and Brown (1988) studied the effect of particle size distribution on the behaviour of crushed limestone and concluded that uniformly graded aggregates were a bit stiffer than the well graded aggregate. Similarly, the particle size distribution also affects the resilient behaviour of the granular material. Knutson and Thomson (1977) have reported that well-graded ballast exhibits a higher resilient modulus. Janardhanam and Desai (1983) and Sweere (1990) also reported that the ballast gradation affects the permanent

deformations, volumetric strains and the resilient modulus significantly. Janardhanam and Desai (1983) have commented that the resilient modulus increases linearly with the increase in particle size, particularly at low confining pressures (i.e. < 20 psi).

Indraratna et al. (2004) have carried out the large-scale cyclic triaxial tests to study the influence of grain size distribution on the deformation and degradation behaviour of ballast. An effective confining pressure of 45 kPa was used in their laboratory tests. In order to simulate the train axle loads at a relatively high speed, cyclic loading with a maximum 300 kPa deviator stress was applied at a frequency of 20 Hz. They have concluded that the ballast breakage decreases with the increase in the value of C_u, with the exception of the gap-graded ballast (Figure 2.10). The gap-graded ballast excluded particle sizes that were found to be highly vulnerable to break. Therefore, the gap-graded specimen shows a smaller amount of breakage and higher wet attrition value than the uniform and very uniform gradations. They have further commented that even a modest change in *Cu* significantly affects the deformation and breakage behaviour of ballast. The relationship between the coefficient of uniformity (*Cu*) and particle breakage is shown in Figure 2.10. Indraratna et al. (2004) recommended that a ballast gradation with a uniformity coefficient exceeding 2.2, but not more than 2.6, is most appropriate.

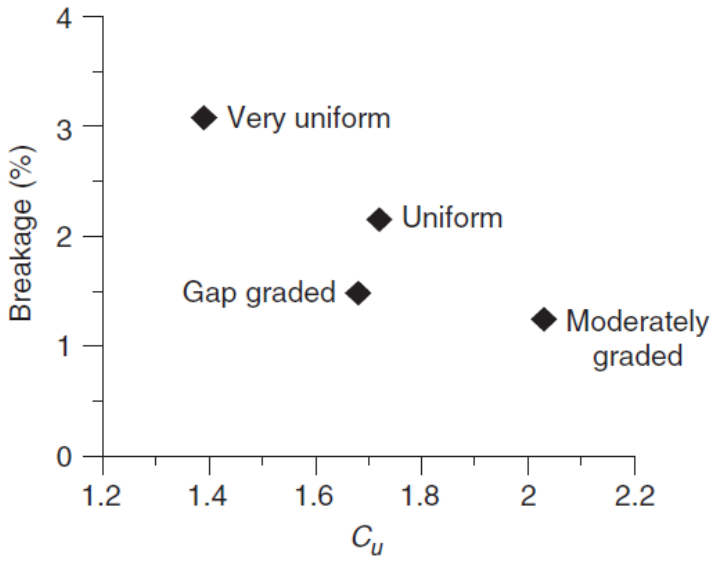

Figure 2.10 variation of BBI with the uniformity coefficient of ballast (Indraratna et al. 2004)

2.5.6 Effect of degree of compaction

The effect of degree of compaction on the deformation under cyclic loading has been widely studied (Barksdale 1972; Allen 1973; Knutson 1976; Selig and Waters 1994; Ionescu 2004). Barksdale (1972) reported that the material was compacted at 95% instead of 100% of maximum compaction density; an average of 185% increase in axial strain was witnessed. Knutson (1976) concluded that the degree of compaction is the most important factor that influences the permanent deformation behaviour of ballast.

2.5.7 Effect of loading frequency, *f*

Timmerman and Wu (1969) carried out cyclic tests on coarse-grained soil at loading frequencies ranging from 2.5 to 25 Hz and concluded that the frequency within this range affected the rate of strain but not the final strain. The effect of loading

frequency, f on the behavior of rail ballast was first studied by Shenton (1975). Based on the test results, Shenton concluded that the frequency of loading does not affect the behavior of ballast (Figure 2.11). However, it was pointed out that in a typical railway track greater dynamic stresses may be induced in ballast when subjected to high-speed trains. Luo et al. (1996) reported that in the high-speed regions, increase in train speed led to increased track settlement and degradation. Kempfert and Hu (1999) carried out in-situ measurements of dynamic forces in track induced by varying train speeds of up to 400 km/h and highlighted that the dynamic stress increased significantly as the train speed increases from 150 to 300 km/h. However, the dynamic stress remains constant for train speeds greater than 300 km/h (Figure 2.12).

The effect of loading frequency on the breakage of railway ballast is recently studied by Indraratna et al. (2010a). They have reported that as the loading frequency increases from 10 to 20 Hz the particle degradation, evaluated in terms of ballast breakage index (BBI), increases significantly. Similarly, the BBI increases significantly as the frequency increases from 30 to 40 Hz. However, there exists an optimum frequency of 20 to 30 Hz at which the ballast densifies without any significant change in the BBI (Figure 2.13). They concluded that a higher confining pressure is needed to reduce the ballast settlement and minimise the particle breakage under high-frequency loading.

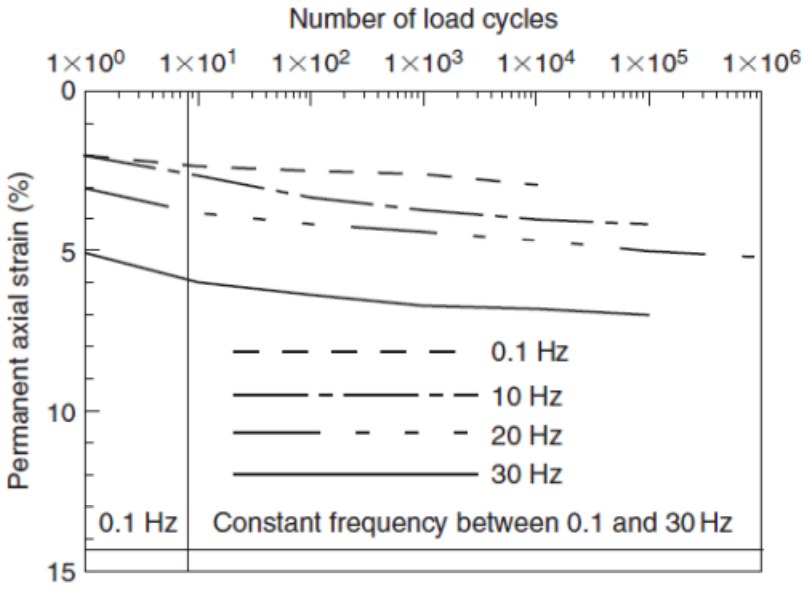

Figure 2.11 Effect of loading frequency on ballast strains (data from Shenton 1975)

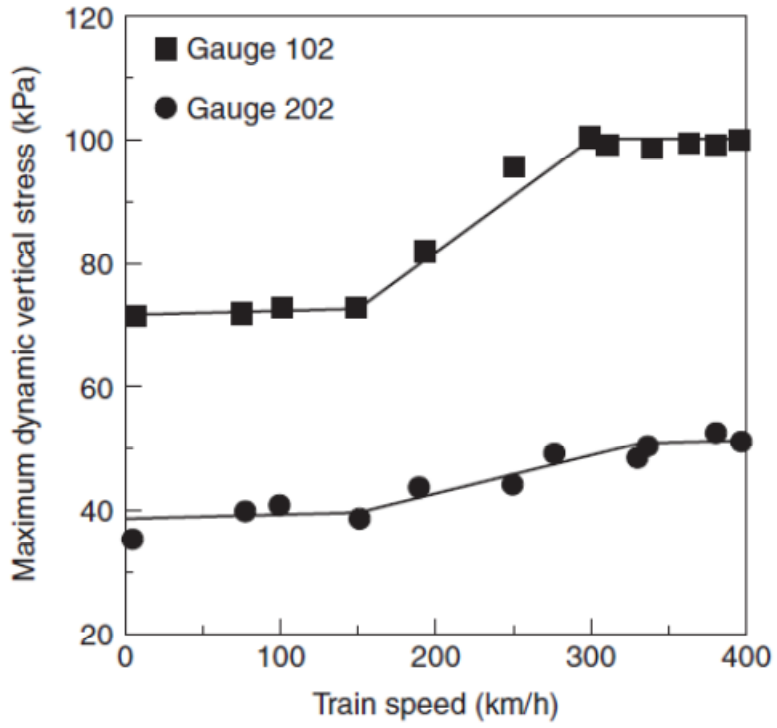

Figure 2.12 Effect of train speed on the maximum dynamic vertical stress (Kempfert and Hu 1999)

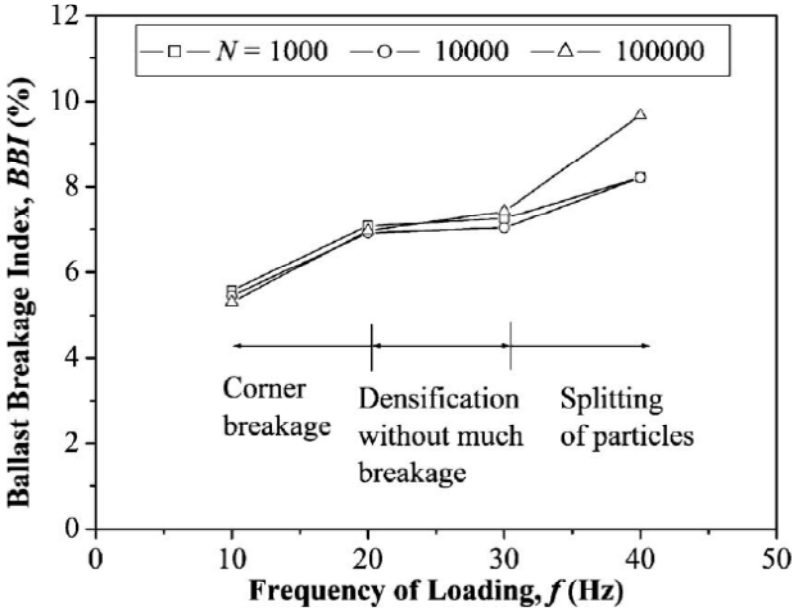

Figure 2.13 Effect of loading frequency on the BBI (Indraratna et al. 2010a)

2.5.8 Effect of parent rock strength

Indraratna and Salim (2005) and Salim (2004) identified the parent rock strength to be an important parameter that influences the deformation and degradation of ballast. This is because the aggregate tensile strength that often governs the particle breakage is a function of the parent rock strength. For example, Jeffs (1989) based on the cyclic tests on three different rock types, reported the vertical settlements to be the highest in case of granite, followed by basalt and quartz.

2.6 PROBLEMS ASSOCIATED WITH BALLASTED RAIL TRACKS

The performance of a railway track is highly affected by the complex interaction of its components in response to train loading. Hay (1982) reported that majority of track failure and maintenance costs are related to the track substructure comprising of ballast, subballast and subgrade layers. Alias (1984) also stated that the track

performance mainly depends on the effective functioning of the ballast layer and the corresponding track deformation and degradation characteristics.

The large vertical train loads combined with relatively small horizontal confining stress leads to lateral flow of ballast under the cyclic loading conditions (Baessler and Rucker 2003). This lateral flow of particles can reduce the horizontal residual stresses that confine the ballast, hence reducing the stability of the track (Selig and Waters 1994). The lateral flow of ballast also leads to attrition, corner breakage and the splitting of particles (Figure 2.14) that contributes towards the vertical deformation of ballast. Moreover, the settlement and breakage of ballast is non-uniform along the track length due to the differences in subgrade characteristics, thus leading to the differential settlement of rails that significantly affects the track safety (Figure 2.15). The other prominent problem in a typical track is due to the fines generated as a result of attrition and particle degradation that migrate downwards and fill the voids between other particles. These fines decrease the void volume, retain moisture and serve to further abrasion (Chrismer 1985). This subsequently reduces the ability of ballast to drain the water due to a decrease in permeability (Figure 2.16). In addition, excessive lateral spreading of ballast owing to the insufficient track confining pressure can also lead to the buckling of rails (Figure 2.17 and Figure 2.18).

The recent study conducted by Dash and Shivadas (2012) also highlighted the lateral flow of ballast as one of the serious track problems. Figure 2.19 shows a rail crossing along with its enlarged view highlighting the track segment that has undergone significant distortion as a consequence of lateral flow of ballast (Dash and Shivadas

2012). The above mentioned track problems increase significantly with the increase in train speed, as higher vibrations contribute to increased track settlement due to higher ballast degradation and the lateral flow of ballast.

Figure 2.14 Particle breakage due to excessive loading of ballast (Indraratna et al. 2011)

Figure 2.15 Track deteriorations and the differential settlement of rails (Suiker 2002)

Figure 2.16 Ponding water in the load bearing ballast at Chester Hill, on the Sydney's Metropolitan line, Australia (Indraratna et al. 2011)

Figure 2.17 Buckling of track due to insufficient lateral confinement (Indraratna et al. 2011)

Figure 2.18 Buckling of track due to insufficient lateral confinement (Indraratna et al. 2011)

Figure 2.19 Track distortion of the crossing at Agthori in Northeast Frontier Railway, India (Dash and Shivadas 2012)

2.6.1 Practical implications

The practical implications of the aforementioned track problems are to either impose speed restrictions on the affected track segments or to repair the concerned portions by replacing the ballast. However, when the rail authorities worldwide are compelled

to introduce high-speed trains to attract the commuters, the imposition of speed restrictions does not seem to be an acceptable solution. Moreover, repairing the tracks that involves ballast replacement and correcting the track alignment is a costly exercise that consumes millions of dollars every year worldwide. For instance, the annual maintenance costs in the state of NSW, Australia are estimated to be around 15 million dollars. In this view, it is necessary to stabilise the ballasted rail tracks so that they can carry high-speed trains without creating any major track problem.

2.7 STABILISATION OF BALLASTED RAIL TRACKS

2.7.1 Use of geosynthetics in railway engineering

The recent studies on ballast have found that the increase in confining pressure could lead to significant improvement in the track performance, in terms of deformation and degradation response, thereby enhancing the overall track stability (Indraratna et al. 2005; Lackenby et al. 2007). Of the several measures used to increase the confining pressure, reinforcing the ballast with geosynthetics is considered to be more suitable and economically viable (Indraratna et al. 2009). Therefore, the use of geosynthetics as reinforcement in rail tracks has been on the rise (Figure 2.20 and Figure 2.21). In a typical rail track, the geosynthetics are usually placed at the subballast-ballast interface. Once placed in the track, the beneficial effects of reinforcement stem from the ballast-geosynthetic interaction that arrests the particle movement thus stabilizing the ballast. The following section describes the various geosynthetics and their usage in the rail industry.

2.7.1.1 *Geosynthetics*

Geosynthetics is the collective term applied to thin, flexible, sheets of polymeric material used to enhance the engineering performance of soils. The purpose of geosynthetics within railway construction, similar to other geotechnical engineering projects, can be subdivided into six categories;

(i) separation
(ii) reinforcement
(iii) filtration
(iv) drainage
(v) moisture barrier/waterproofing and
(vi) protection.

Geosynthetics include the following various products according to their applications and functionality;

2.7.1.1.1 *Geogrid*

Geogrids are polymers formed into a very open, grid-like configuration, i.e., they have large apertures between the adjacent sets of longitudinal and transverse ribs. They function almost exclusively as reinforcement material owing to their apertures that allow the soil to strike-through from one side of the geogrid to the other.

Based on the orientation of the ribs (and the shape of apertures) geogrids are classified into the following categories;

a) Uniaxial geogrids
b) Biaxial geogrids and
c) TriAx geogrids

Biaxial geogrids have rectangular/square shaped apertures while the TriAx has triangular apertures. The key feature of all geogrids is that the openings between the adjacent sets of longitudinal and transverse ribs, called “apertures,” are large enough to allow for soil strike-through from one side of the geogrid to the other.

2.7.1.1.2 *Geotextile*

Geotextile is a permeable planar material made from synthetic fibers/yarns. It can either be of woven or non-woven type. The woven geotextiles are generally used as a filter layer. On the other hand, non-woven geotextile prevents the ballast from fouling due to subgrade fines at the same time providing drainage of water from the ballast. They generally provide the protection to geomembrane against puncture from subgrade aggregates.

2.7.1.1.3 *Geomembrane*

Geomembranes are relatively impermeable sheets of plastic, used as an impermeable layer to check the liquid movement in different civil engineering structures such as landfills, canal lining, pond lining, cut-off trenches etc.

2.7.1.1.4 *Geonet (Drainage Net)*

Geonets are high density polyethylene products consisting of a regular dense network, whose constituents' elements are linked by knots of extrusions and whose openings are much larger than the constituent.

2.7.1.1.5 *Geocells*

Geocells are a three dimensional reinforcement having expandable panels made up of polypropylene arranged systematically to form closed cells. They are often used to help improve the performance of standard construction materials and erosion-control treatments. Since recently, geocells have also been used to stabilize ballast and subballast.

2.7.1.1.6 *Geocomposite*

Geocomposite is a composite material made from different geosynthetics products to serve their functions simultaneously. Usually when used in railroad ballast geocomposite comprises of a layer of geotextile bonded to the geogrid.

The use of geosynthetics in rail track performs various functions like separation and reinforcement. The use of geotextile/geomembrane prevents the upward flow of soil into the ballast, thus reducing the fouling of ballast. On the other hand, the use of geogrid in the track acts as a reinforcement thus increasing the shear strength of ballast. A geocomposite acts as both separation layer as well as reinforcement. Figure 2.20 shows the layer of geocomposite being placed at the subballast-ballast interface in a rail track in Bulli, New South Wales, Australia. Figure 2.21 illustrates the process of track construction with ballast being laid on the layer of geocomposite.

Figure 2.20 Use of geocomposite at the subballast-ballast interface in rail track (after Indraratna et al. 2011)

Figure 2.21 Photo showing the track construction process with ballast being laid on the layer of geocomposite (after Indraratna et al. 2011)

2.8 THE SHEAR BEHAVIOUR OF GEOSYNTHETIC-REINFORCED BALLAST

2.8.1 The interface shear behaviour of geosynthetic-reinforced soils

It is well known that the shear behavior of geosynthetic-reinforced soil depends largely on the soil-geosynthetic interface shear behavior. Moreover, the interface between dissimilar materials acts as a medium through which stresses are transferred from one body to another; thus, relative motions, stress concentrations, and drastic changes in displacement gradients are common features at these interfaces (Desai et al. 1984). Therefore, a thorough understanding of the soil-geosynthetic interface is needed to predict the behavior of geosynthetic-reinforced soils. In the recent past, several researchers have studied the shear behaviour of soil-soil and soil-structure interfaces (Cancelli et al. 1992; Cazzuffi et al. 1993; Bakeer et al. 1998; Abu-Farsakh and Coronel. 2006; Tang et al. 2008; Liu et al. 2009). Although there is vast literature available on the shear behaviour of soil/sand-geosynthetic interfaces, there is no published literature on the shear behaviour of ballast-geosynthetic interfaces. The shear behaviour of soil/sand-geosynthetic interfaces is described in the subsequent paragraphs.

The interface tests are usually performed to determine the internal friction angle of soil and to evaluate the apparent friction angle of the soil-structure interface. The shear behaviour of soil-geosynthetic interfaces depends largely on the soil density and the geosynthetic type. For instance, in case of dense soils the shear strength increases with the shear displacement until it attains a peak value after which it exhibits strain softening. On the other hand, the shear strength of loose soil-

geosynthetic interface increases gradually until it attains a peak value that remains almost constant thereafter. The volumetric behaviour of dense soil-geosynthetic interfaces shows an initial compression of the specimen followed by dilation. On the other hand, the volumetric behaviour of loose soil-geosynthetic interfaces exhibit compression with shearing. However, for both dense and loose soils, with the increasing σ_n the shear strength increases at a decreasing rate and the volumetric behaviour exhibits a decrease in ε_v.

Bakeer et al. (1998) conducted pull-out and direct shear tests on geogrid-reinforced lightweight aggregate. They have concluded that the apparent friction angle of the aggregate-geogrid interface reduced to 48° in comparison to the internal friction angle of 52° of the aggregate. Tang et al. (2008) conducted a series of direct shear and pull-out tests to study the shear behaviour of aggregate-geogrid-soil interfaces. They reported that a good correlation existed between combined geogrid tensile strength at 2% strain, junction strength and interface shear strength. They concluded that the geogrid aperture size does not follow any trend with the interface shear strength. However, based on the results from pull-out tests, they concluded that a strong correlation exists between the aperture size and the interaction coefficient. These observations indicate that the geogrid aperture size plays an important role in its interaction with the aggregate.

Liu et al. (2009) conducted direct shear tests on soil-geosynthetic interfaces for various soils and different types of geosynthetics. They concluded that the shear strength of soil-geogrid interfaces could vary from about 90 to 105% of the shear

strength of unreinforced soil. On the other hand, the shear strength of soil-geotextile interfaces varies from about 70 to 80% in comparison to that of unreinforced soil.

Abdi and Arjomand (2011) have studied the behaviour of sand-geogrid interfaces in direct shear and pullout conditions. They concluded that both the sand-geogrid interface shear strength and the pullout resistance increased with the increase in applied normal stress (Figure 2.22). However, unlike direct shear, the pullout resistance of sand-geogrid samples is gradually mobilized with increase in pullout displacements.

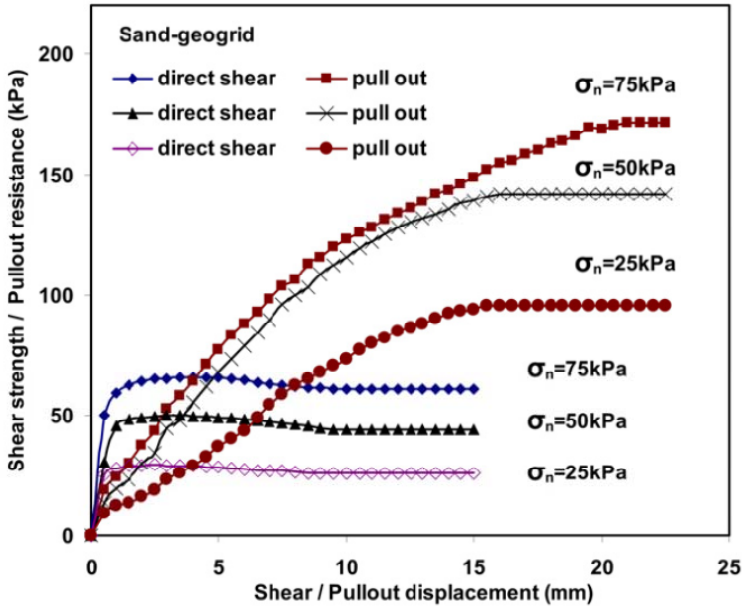

Figure 2.22 Variations of shear strength/pullout resistance versus shear/pullout displacement for sand-geogrid samples (Abdi and Arjomand 2011)

2.8.2 The deformation and degradation response of geosynthetic-reinforced ballast

In the recent past, several studies have described the cyclic behaviour of geosynthetic-reinforced ballast using the large-scale testing facilities (Bathurst and Raymond 1987; Raymond and Bathurst 1987; Raymond and Bathurst 1990; Nancey et al. 2002; Shin et al. 2002; Raymond 1999; Raymond and Ismail 2003; Indraratna et al. 2006; Brown et al. 2007; Fernandes et al. 2008). Bathurst and Raymond (1987) have carried out the large-scale testing of geogrid-reinforced ballast and concluded that the geogrid reduces the rate of settlement of ballast. They further commented that the effect of reinforcement in reducing the permanent deformations of ballast is more pronounced in case of tracks laid on soils with low California bearing ratio (CBR) values. Raymond and Bathurst (1987) commented that inclusion of a biaxial geogrid within the ballast layer lead to a decrease in permanent vertical deformations of up to 50% after 100,000 load cycles. Moreover, the number of load cycles required to cause a permanent vertical deformation of 50 mm increased by a factor of 10 when a geogrid was used.

Amsler (1986) reported a case study in Geneva describing the performance of unreinforced and geosynthetic-reinforced track. In 1982, the left track (Figure 2.23a) was completely rebuilt using a traditional design cross-section (without any geosynthetics). In 1983, the right track (Figure 2.23b) was reconstructed following a new design cross-section incorporating non-woven geotextiles at the subbase/subgrade interface. Both tracks were monitored continuously by a track-quality measuring wagon before and after rehabilitation. The cross slope difference per millimetre between two rails of a track (warp) as a function of travelled distance

was used for assessing the stability and riding comfort. It is evident from pre- and post-renewal monitored data (Figure 2.23) that installation of geotextiles reduces the extent of track deformation.

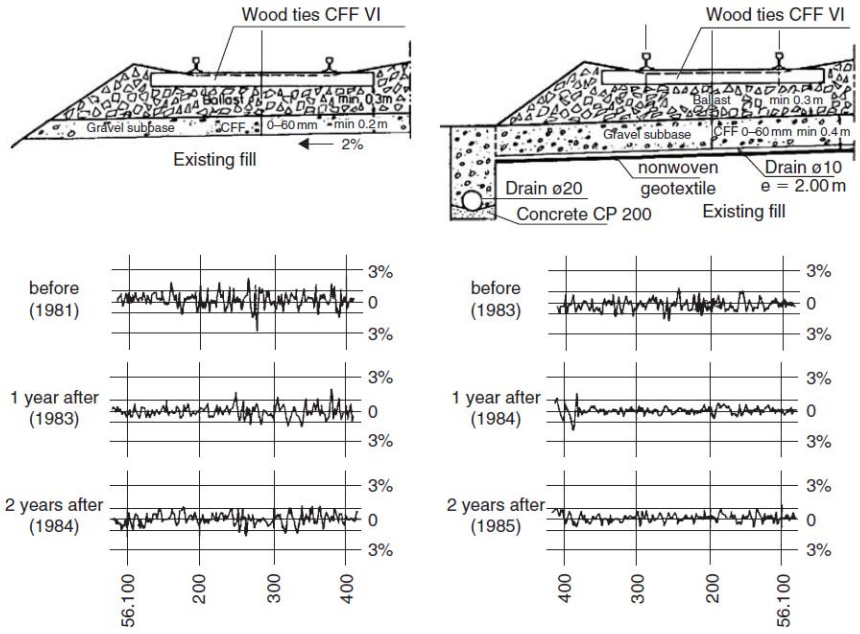

Figure 2.23 Effects of geosynthetics in track, (a) left track without geosynthetics, (b) right track with geosynthetics (after Amsler 1986)

Amsler (1986) further concluded that the use of geotextiles not only significantly improved the track quality but also helped maintaining the track alignment for a relatively long period. However, track rehabilitation without geosynthetics improved the performance for a relatively shorter period of time and deteriorated almost to the pre-renewal level within about 1-2 years (Amsler 1986).

Walls and Galbreath (1987) reported that the inclusion of geogrid improved the performance of a portion of rail track posing serious problems in terms of excessive track settlement due to the subgrade failure. The specific portion of track was laid on

soft subgrade and posed serious problems demanding maintenance operations in about every two to three weeks. Moreover, a speed restriction of about 8 km/h was imposed on the affected portion of track. They reported that the geogrid-reinforcement solved the track problems and removed the need for frequent maintenance operations. In addition, the geogrid reinforcement of track helped increase the speed restriction to be raised to 56 km/h. Similarly, Matharu (1994) has reported reductions in settlement when a geogrid was used in ballasted rail track (Figure 2.24).

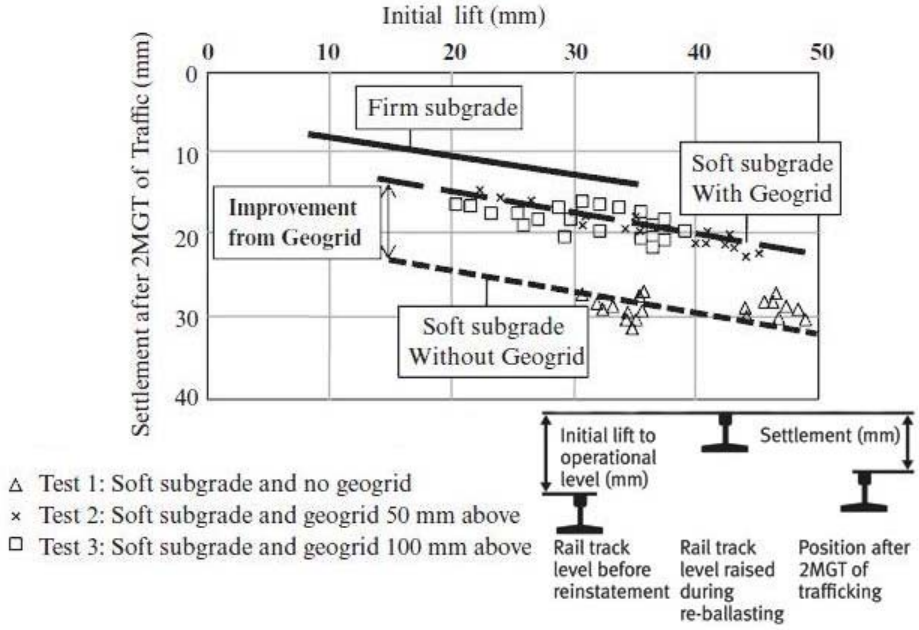

Figure 2.24 Settlement of unreinforced and geogrid-reinforced rail track section (Matharu 1994)

Shin et al. (2002) examined the settlement behavior of railroad ballast under cyclic loading reinforced with different geosynthetic types. They reported that the most beneficial effect of reinforcement in reducing settlement is derived when one layer of

geotextile and one layer of geogrid are placed at the interface of the subgrade soil and subbase course. The field study carried by Ashpiz et al. (2002) also confirmed the effectiveness of geosynthetics in augmenting the track performance. Raymond et al. (2003) have studied the effect of geogrid reinforcement on the behaviour of unbound granular media. They have carried out the model studies at a scale of 1:10, the results of which confirmed that the geogrid reinforcement reduces the settlement of ballast. The optimum position for placing the geogrid reinforcement in the ballast was reported to be 125 mm below the sleeper soffit.

Sharpe et al. (2006) described a full-scale field test undertaken at Coppull Moor on the West Coast Main Line, UK. The track under consideration was constructed over a fairly soft subgrade and had a long history of problems requiring frequent maintenance. In an attempt to ameliorate the track condition, a biaxial geogrid was incorporated within the ballast section during one of the regular track maintenance operations. Regular monitoring of the track was undertaken both prior to and following the geogrid inclusion. The results revealed that the rate of track settlement reduced considerably from 1.40 mm/year to 0.4 mm/year upon the geogrid installation. The reduction in the rate of surface deformation due to the geogrid reinforcement lengthened the time periods between successive ballast cleaning operations.

Indraratna et al. (2006) have investigated the deformation and degradation behavior of recycled and fresh ballast reinforced with geosynthetics using a large-scale prismoidal triaxial chamber. The effectiveness of various geosynthetics in stabilizing fresh and recycled ballast was investigated through laboratory model test results.

Three types of geosynthetics were used including woven geotextiles, geogrids and geocomposites. They have reported that the inclusion of geocomposite in both fresh and recycled ballast improves its resistance to settlement, and that the recycled ballast reinforced with geosynthetics performs as good as the fresh ballast without geosynthetics (Figure 2.25 and Figure 2.26). Indraratna et al. (2006) have further commented that the inclusion of either geotextile or geogrid in recycled ballast improves the settlement behaviour moderately, but not to the same extent as that of the geocomposite. Similarly, the inclusion of geosynthetics in both fresh and recycled ballast reduces the extent of particle degradation as well (Figure 2.27 and Figure 2.28). Fernandes et al. (2008) also reported a reduction in breakage of ballast due to reinforcement. It may be mentioned here that Indraratna et al. (2006) and Fernandes et al. (2008) are the only published literature that highlighted the role of geosynthetics on the particle degradation. The reduction in settlement and breakage of recycled ballast due to reinforcement was reported to be 40-48% respectively.

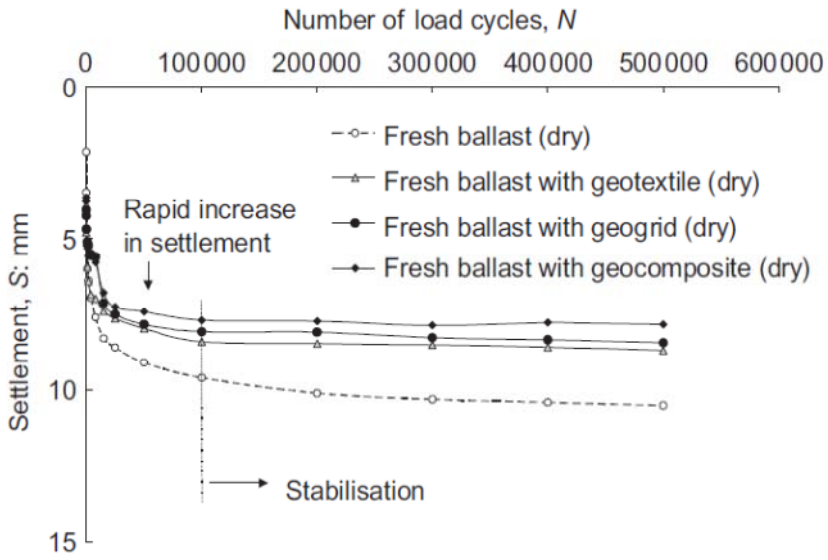

Figure 2.25 Variation of settlement with number of load cycles for fresh ballast reinforced with geosynthetics (Indraratna al. 2006)

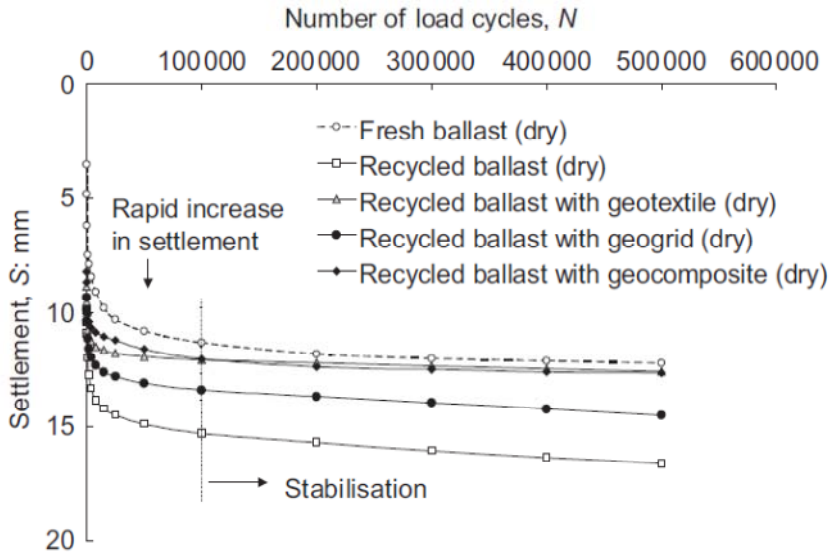

Figure 2.26 Variation of settlement with number of load cycles for recycled ballast reinforced with geosynthetics (Indraratna al. 2006)

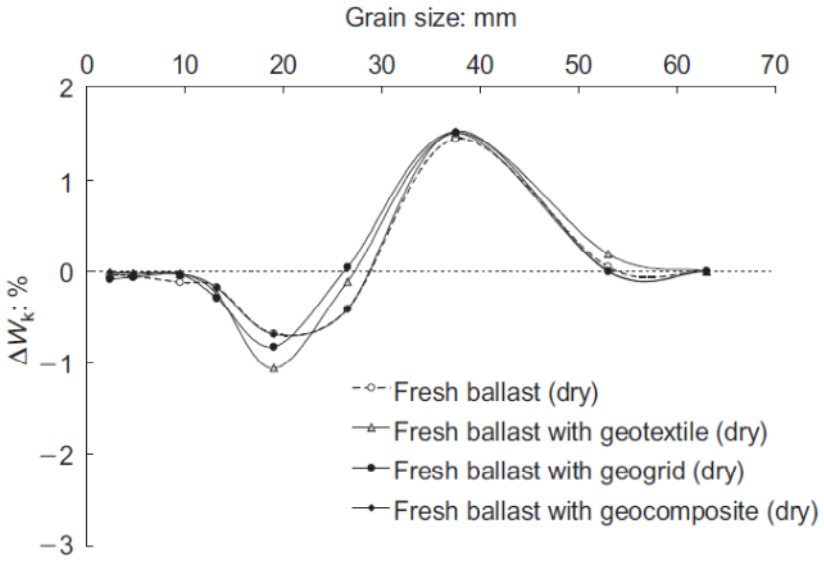

Figure 2.27 Marsal's breakage index for fresh ballast reinforced with geosynthetics (Indraratna al. 2006)

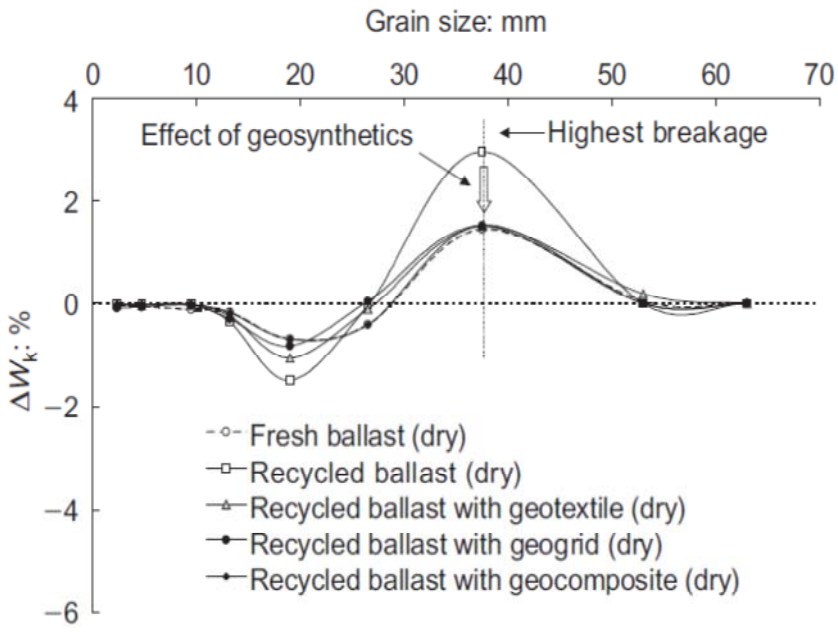

Figure 2.28 Marsal's breakage index for recycled ballast reinforced with geosynthetics (Indraratna al. 2006)

Brown et al. (2007) have studied the effect of different types of geogrid reinforcement on the settlement characteristics of ballast. They have identified geogrid stiffness and geogrid aperture size as the key parameters that influence the settlement behavior of reinforced ballast (Figure 2.29 and Figure 2.30). Recently, Indraratna et al. (2010b) have carried out the field trials to study the effectiveness of reinforcing the track with geosynthetics. The field investigations confirmed that the geosynthetic reinforcement of rail track reduces the vertical settlement and the lateral displacement of fresh and recycled ballast (Figure 2.31 and Figure 2.32). Hornicek et al. (2010) have commented that the geogrid inserted directly under the ballast bed helped reducing the extent of settlement. They have also reported the performance of a railway track trial section with a geocomposite reinforced ballast bed to be exhibiting smaller imperfections in the rail geometric parameters in comparison to unreinforced conditions.

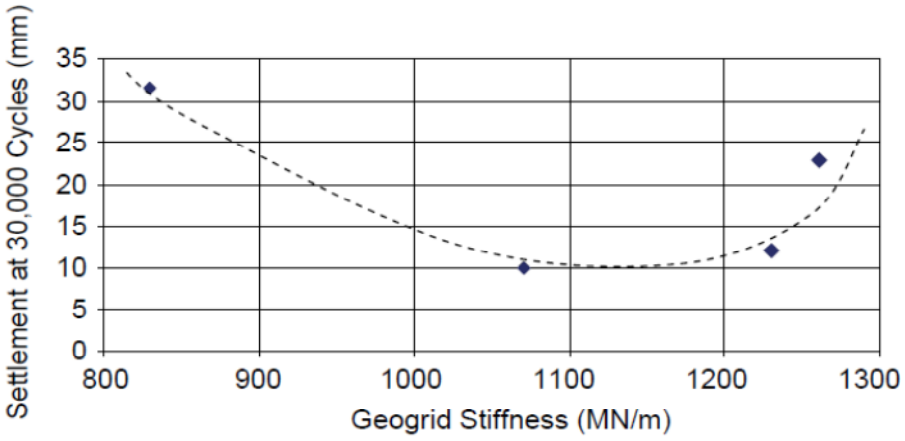

Figure 2.29 Variation of ballast settlement with the geogrid stiffness (Brown et al. 2007)

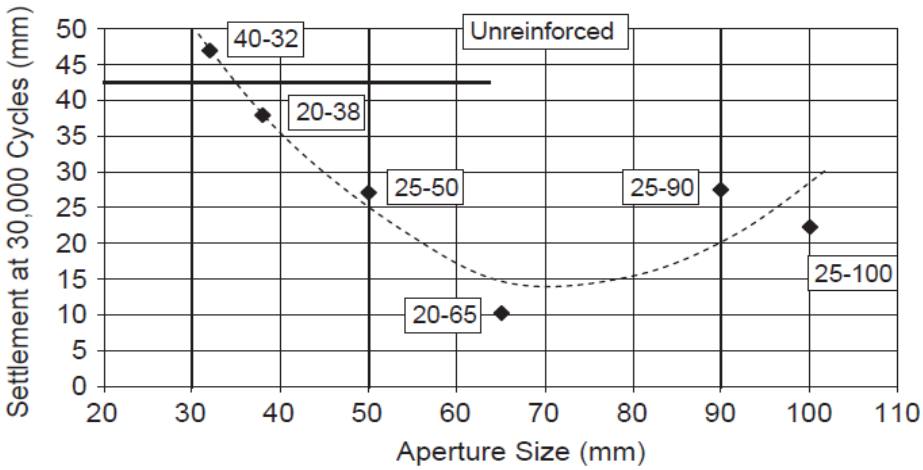

Figure 2.30 Variation of ballast settlement with the geogrid aperture size (Brown et al. 2007)

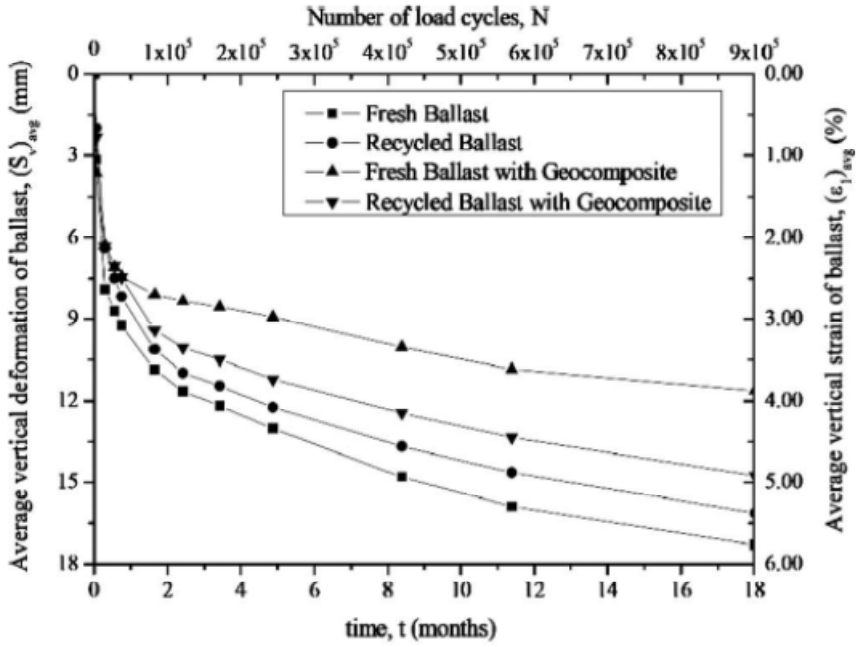

Figure 2.31 Average vertical deformation of unreinforced and geosynthetic reinforced ballast (Indraratna et al. 2010b)

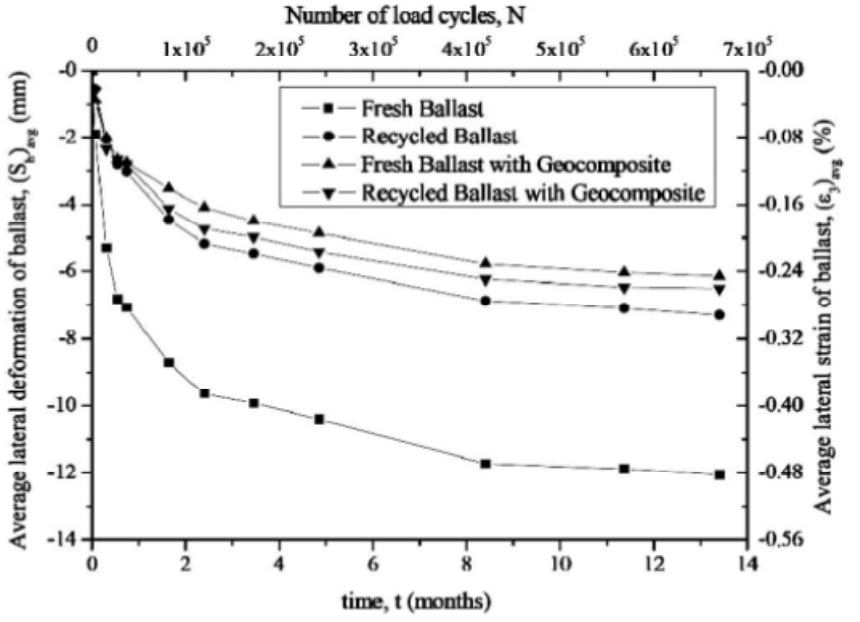

Figure 2.32 Average lateral deformation of unreinforced and geosynthetic reinforced ballast (Indraratna et al. 2010b)

Recently, Kennedy (2011) conducted full-scale tests to assess the influence of different geosynthetic products on the performance of the track. The study found that XiTRACK reinforcement significantly increased track stiffness by about 55-65% thereby reducing the track settlement by around 99%, in comparison to unreinforced track. On the other hand, the geocomposite increased the track stiffness by 9-12% and reduced the track settlement by 25%. However, the geocell reinforcement caused a decrease in the track stiffness by 5-7% and led to an increase in settlement by 37%. The impaired performance in this case was attributed to the difficulty in compacting ballast in the individual cells of geocell.

Geol (2011) has described the case study of a mainline rail track in Nagykanizsa, Hungary, where the decision was made to include a geogrid within the ballast layer during a rehabilitation operation. Prior to replacement of the existing roadbed, the rail line required monthly re-surfacing. Following the inclusion of the geogrid within the track section, a dramatic reduction in the dynamic deflection upon trafficking was observed. The geogrid inclusion has subsequently eliminated the need for frequent maintenance thereby removing the service disruptions. On a similar project constructed near Cologne, Germany, the inclusion of a geogrid within a roadbed constructed over a soft formation allowed the sub-ballast to be reduced from 1050 mm to 700 mm.

2.8.3 Working principle of geogrid-reinforced soils

The benefits of geogrid reinforcement predominantly stem from the interlocking of soil particles in the geogrid apertures that enhances the soil stiffness thereby improving the soil characteristics (Figure 2.33). However, it appears intuitively

obvious that the effect of planar reinforcement like geogrid should reduce with distance away from its placement location. Nevertheless, the current theories ignore the possible reduction in the influence of geogrid and inherently assume the effect of reinforcement to be uniform throughout the sample height (Gray et al. 1984; Athanasopoulos 1994; Ruiken and Ziegler 2010).

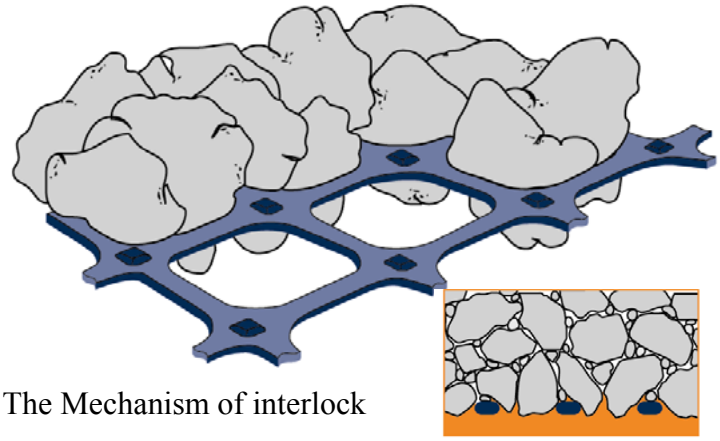

Figure 2.33 The mechanism of particle interlock within the geogrid aperture (Wrigley 1989)

The recent studies by McDowell et al. (2006) have shown the influence of geogrid to exist up to approximately 100 mm on either side of the grid (Figure 2.34). However, this observation is based on the numerical simulations using PFC 3D conducted to study the pull-out behaviour of the geogrid-reinforced ballast. Bauer et al. (2009) carried out numerical simulations on granular soil-geogrid interface and reported that the soil-geogrid interaction occurs up to a distance of about $7D_{50}$. Schuettpelz et al. (2009) reported that the reinforcing effect of geogrid in stiffening the granular road base material extends up to about 30 mm on either side of the geogrid. However, there is no reported literature that explains the variation in the degree of rail ballast-

geogrid interaction with distance away from the grid under high-frequency cyclic loading. Moreover, the influence of the degree of ballast-geogrid interaction on the deformation and degradation characteristics of ballast also remains to be studied.

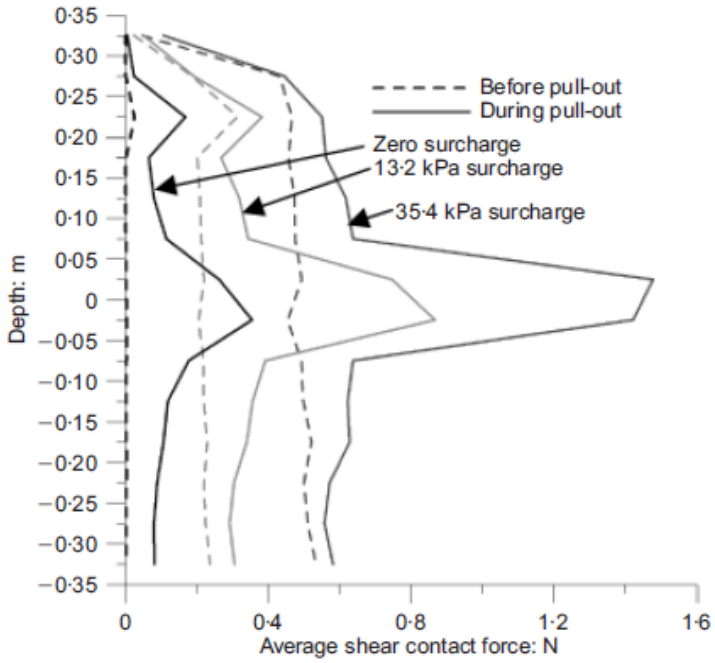

Figure 2.34 Average shear contact force under pullout conditions with distance from the geogrid (Mc Dowell et al. 2006)

2.9 SUMMARY

In this Chapter, the basic components of a rail track including the functions and characteristics of each component were briefly enumerated. Of all the track components, ballast is the principal component and is responsible for retaining track position, and to reduce the sleeper bearing pressure for the underlying materials (e.g. subballast and subgrade soils). The Chapter then described the literature pertaining to the behaviour of ballast under various loading conditions. The effect of various important factors like the confining pressure, deviatoric stress, the number of load

cycles (N), load history, particle size distribution, degree of compaction, loading frequency (f), and the parent rock strength on the deformation and the degradation behaviour of ballast were highlighted.

The Chapter highlighted the various track problems that occur as a consequence of the lateral flow of ballast upon traffic loading. For instance, the way the lateral flow of ballast led to attrition, corner breakage and the splitting of particles that contributed towards the vertical deformation of ballast were described. Furthermore, instances of buckling of rails occurring from excessive lateral spreading of ballast owing to the insufficient track confining pressure were enumerated. The practical implications of track problems on the effective functioning of railways were discussed. The Chapter then emphasized the need for stabilizing ballast if the track problems were to be minimized especially in view of the introduction of newer and faster trains. The various types of geosynthetics and their use in rail industry to stabilize the ballast were described. The shear behaviour of soil-geosynthetic interfaces was presented. In addition, the laboratory experimental studies and the field trials including the case studies that described the role of geosynthetics on the deformation and the degradation behaviour of geogrid-reinforced ballast were presented.

The next chapter discusses the various laboratory experiments carried out in this research to study the engineering behaviour of geogrid-reinforced rail ballast.

3 LABORATORY EXPERIMENTAL INVESTIGATIONS OF THE SHEAR BEHAVIOUR OF BALLAST-GEOSYNTHETIC INTERFACES

3.1 INTRODUCTION

In this Chapter, the laboratory investigation of the response of ballast-geosynthetic interfaces under direct shear conditions is described. In order to study the shear strength characteristics of ballast-geosynthetic interfaces, a series of tests was conducted in the laboratory using the large-scale direct shear apparatus. The details regarding the large-scale testing equipment, test materials, specimen preparation methods, and the experimental procedure followed including the instrumentation used to measure the deformations of ballast are discussed in the subsequent paragraphs.

3.2 SHEAR BEHAVIOR OF BALLAST-GEOSYNTHETIC INTERFACES USING THE LARGE-SCALE DIRECT SHEAR APPARATUS

In recent times, the rail authorities around the world have resorted to the geosynthetic reinforcement of ballast in an effort to improve the track performance and hence reduce the maintenance costs. However, the effectiveness of reinforcement in providing any benefit towards track stabilisation depends on the level of interaction between ballast and geosynthetic. In such a scenario, the ballast-geosynthetic interface shear strength could be treated as a measure of the ability of geosynthetic to inhibit the lateral spread of particles; thus, providing guideline about its suitability as

reinforcing material for stabilising ballast. In view of this, the shear behaviour of ballast-geosynthetic interfaces was investigated using the large-scale direct shear apparatus available at the University of Wollongong (Figure 3.1). Drained shearing tests were conducted on ballast-geosynthetic interfaces at various values of applied normal stresses under constant normal loading conditions. In order to optimise the geogrid type to be used to enhance the performance of a track with given ballast gradation, geogrids with different aperture sizes were used for the testing. This is particularly important owing to the availability of various geosynthetics commercially available in the market and the various particle gradations of ballast adopted by different rail authorities.

3.2.1 Apparatus description

The large-scale direct shear apparatus consists of two 300 x 300 mm square boxes. The upper immovable box is 100 mm deep and the lower moveable box is 90 mm deep. The maximum allowable shear displacement of the lower movable box is 36 mm that corresponds to a horizontal strain of 12%. The vertical/normal load on the sample could be applied by suspending required weights from the weight hanger. The apparatus can be used to study the shear behavior of interfaces under constant normal loading (CNL) conditions with the applied normal stress ranging from zero to about 70 kPa. It can operate at a shearing rate in the range of 2.75-14 mm/min.

Figure 3.1 Photograph of the large-scale direct shear apparatus used in the current study

3.2.2 Characteristics of test materials

3.2.2.1 *Ballast*

Fresh latite basalt from Bombo quarry, situated 100 km South of Sydney NSW, Australia, was used for the current study. The sample consisted of hard, robust, highly angular, quite similar shape of unweathered, dark grey aggregates of basalt (latite). The essential minerals present in latite basalt are plagioclase (feldspar) and augite (pyroxenes) (Indraratna et al. 2011). The durability, shape and strength properties of ballast used in the laboratory study are summarised in Table 3.1.

The ballast was first washed using a high pressure hose to remove any dirt and clay adhering to the particles. The ballast was then sorted into various sizes by passing it

through the sieves of required sizes. Upon drying, the specimens were prepared by thorough mixing of the correct weight of each particle size to match the selected gradation curve shown in Figure 3.2. The amount of mixing was sufficient to make samples with reasonable degree of homogeneity. The ballast samples used for the investigation conformed to the standards specified by Technical Specification TS 3402 of Rail Infrastructure Corporation (RIC), and the particle size distribution (PSD) conformed to AS 2758.7. The maximum particle size (D_{max}) of ballast is 50 mm. This satisfies the general requirement that the ratio of minimum size of the shear box to the maximum size of particle is not less than six, so that the sample size effects become negligible (e.g. Marachi et al. 1972; Indraratna et al. 1993). The grain size characteristics of Latite ballast are tabulated in Table 3.2.

Table 3.1 Characteristics of fresh ballast (Latite basalt) (after Indraratna et al. 1998)

Characteristics test	*Test result*	*Recommendations by Australian Standard*
Durability		
Aggregate crushing value	12%	<25%
Los Angeles Abrasion	15%	<25%
Wet attrition value	8%	<6%
Strength		
Point load index	5.39 MPa	-
Shape		
Flakiness	25%	<30%
Misshapen particles	20%	<30%

Table 3.2 Grain size characteristics of Latite ballast

Material	*Particle shape*	D_{max} *(mm)*	D_{10} *(mm)*	D_{30} *(mm)*	D_{50} *(mm)*	D_{60} *(mm)*	C_u	C_c
Fresh ballast	angular	50	20	29	35	37.5	1.87	1.12

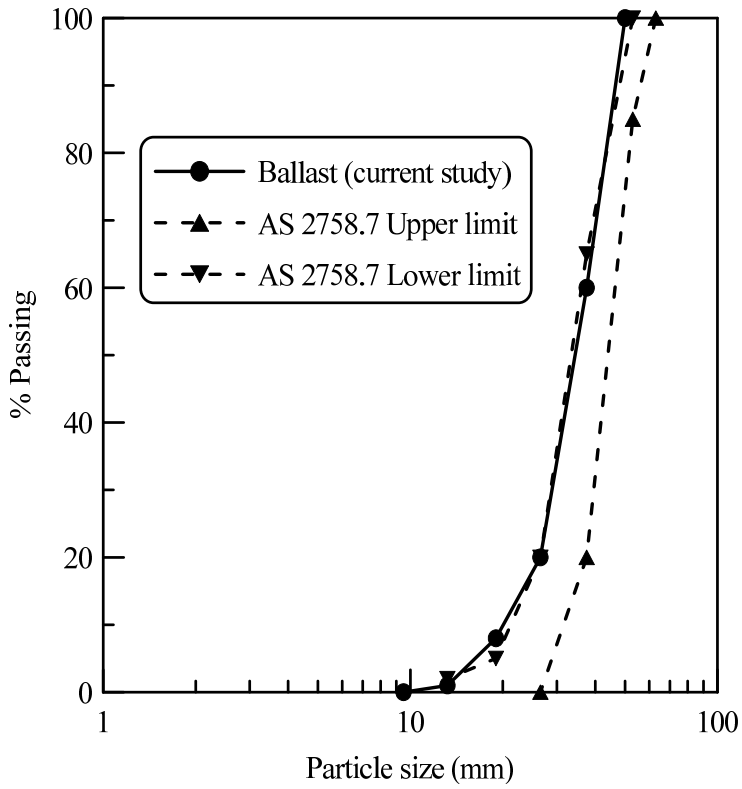

Figure 3.2 Particle size distribution (PSD) of ballast used for the direct shear tests

3.2.2.2 *Geogrids*

In order to establish the effect of geogrid aperture size (A) on the shear strength of ballast-geogrid interfaces, seven geogrids with different aperture sizes (labelled G1 to G7) were used in this current study. The physical characteristics and technical specifications of the geogrids used are listed in Table 3.3 (Photographs shown in Appendix A). The geogrid G2 had triangular apertures with each side measuring 36

mm, while geogrid G7 had large apertures which were obtained by removing one and two ribs in either direction of the geogrid G6. The size of the newly formed aperture for G7 was measured to be approximately 70 × 110 mm. The tensile strength of this geogrid will be reduced to half and one third in either direction due to the removal of ribs (analysis based on the trend reported by Liu et al. 2009). All the geogrids used in the study were of biaxial type except G2. Tests were also conducted for ballast-geotextile (GT) interface to compare its performance with that of various geogrids. The non-woven geotextile used was made up of polypropylene and had a mass per unit area of 140 g/m^2.

Table 3.3 Physical characteristics and technical specifications of the geogrids used for the study

Geosynthetic type	*Aperture shape*	*Aperture size (mm)*		*Rib thickness (mm)*		T_{ult} [a] (kN/m)		J_{sec} [b] *(2% strain) (kN/m)*	
		MD	CMD	MD	CMD	MD	CMD	MD	CMD
G1[*]	Square	38	38	2.2	1.3	30	30	525	525
G2[*]	Triangle	36	36	2.0	2.0	19	19	230	230
G3[*]	Square	65	65	1.7	1.5	30	30	550	600
G4[+]	Rectangle	44	42	1.0	1.0	30	30	500	500
G5[#]	Rectangle	36	24	1.0	1.0	55	30	500	350
G6[*]	Square	33	33	2.2	1.4	40	40	700	700
G7[*]	Rectangle	70	110	2.2	1.4	20	14	350	233

[*] extruded type; [+] welded type; [#] knitted type; MD: Machine direction; CMD: Cross Machine direction; [a] Ultimate tensile strength (manufacturer supplied values); [b] Secant tensile stiffness (manufacturer supplied values).

Table 3.4 The geogrid open area in plan

Geosynthetic type	*G1*	*G2*	*G3*	*G4*	*G5*	*G6*	*G7*
Area (mm^2)	1444	562	4225	1848	864	1089	7700

Figure 3.3 Photograph illustrating the geogrid installed at the interface of upper and lower shear boxes

3.2.3 Preparation of test specimens

The ballast samples prepared following the procedure described in section 3.2.2.1 was placed and compacted in the large-scale direct shear apparatus in three layers of approximately 60 mm height. After the compaction of first 60 mm layer, additional 30 mm ballast was placed to fill the lower box, and the geosynthetic was placed at the interface of the lower and the upper boxes with the machine direction placed parallel to the direction of shearing (Figure 3.3). An additional 40 mm layer of ballast was then placed in the upper box and compacted. This was followed by the

placement and compaction of the third 60 mm layer of ballast. The compaction was carried by using a hand held electric vibrating plate. To minimize the particle breakage during vibration, a 5 mm thick rubber pad was placed underneath the vibrating plate. A predetermined amount of ballast to achieve the desired field density of 1550 kg/m^3 (relative density of 75%) was placed in the given volume of the shear box apparatus in each case and compacted.

Figure 3.4 Photograph showing the prepared ballast specimen, with the required vertical load applied, ready for testing

3.2.4 Test procedure

The tests were conducted at normal pressures of 26.3, 38.5, 52.5 and 61.0 kPa, at a constant shear rate of 2.75 mm/min. A photograph of the prepared ballast specimen

with the required vertical load applied on it that is ready for testing is shown in Figure 3.4. Fresh samples of aggregates and geosynthetics were used for each test. The vertical displacement exhibited by the sample upon shearing is measured during the tests by means of a dial gauge. The horizontal movement of the lower shear box and the corresponding shear force to cause the displacement are also recorded during the test. The direct shear apparatus and the associated measuring devices (e.g. proving ring and the dial gauges) were calibrated prior to each test. The calibration procedure included the testing of a granular material (sand) with a known effective friction angle (37°) and the comparison of the obtained friction angle with the already available value. All the tests were conducted up to a shear displacement of 36 mm that corresponds to a horizontal strain (ε_h) of 12%.

The results from the large-scale direct shear tests are presented and discussed in Chapter 4 of the thesis.

4 EXPERIMENTAL RESULTS FROM LARGE-SCALE DIRECT SHEAR TESTS

4.1 INTRODUCTION

This Chapter presents the results from the large-scale direct shear tests performed following the test procedure described in Section 3.2 of Chapter 3. The focus of discussion is on the shear behaviour of ballast-geosynthetic interfaces (i.e. variation of shear stress with the shear strain and the evolution of vertical strains during the shearing). This Chapter then compares the performance of various ballast-geosynthetic interfaces in relation to the shear behaviour of unreinforced ballast. The effect of applied normal stress (σ_n) on the angle of internal friction of ballast and apparent friction angle of ballast-geosynthetic interfaces is discussed. The influence of geogrid aperture size (A) on the shear strength of ballast-geogrid interface is presented, and the way in which the most suitable geogrid is selected to optimise the performance of given ballast is described.

4.2 SHEAR STRESS-SHEAR STRAIN BEHAVIOUR

4.2.1 Unreinforced ballast

The behaviour of unreinforced ballast upon shearing is presented in terms of the variation of stress ratio (τ/σ_n) and vertical strain (ε_v) with the horizontal strain (ε_h) (Figure 4.1), for various values of applied normal stress (σ_n). It is observed from Figure 4.1 that τ/σ_n increases with ε_h and attains a peak value at 6-7% horizontal strain after which it exhibits slight strain softening. A similar shear behaviour of

granular materials was reported in the past by several researchers (e.g. Bolton 1986; Asadzadeh and Soroush 2009; Yan and Ji 2010). Moreover, it is clear that the value of τ/σ_n decreases with the increase in σ_n. This reduction in τ/σ_n with σ_n is primarily due to the suppression of dilation, which agrees with the findings of the earlier studies (Indraratna et al. 1998; Ni et al. 2000; Cui and O'Sullivan 2006).

The volumetric behaviour shows an initial compression of the specimen until ε_h of about 3% followed by dilation. The volumetric behaviour remains essentially the same with the increase in the applied normal stress barring a decrease in ε_v with increasing σ_n. For example, ballast exhibits a vertical strain of 4.81% at the end of test for an applied normal stress of 26.3 kPa in contrast to 3.15% for σ_n of 61.0 kPa. The replicate test results closely match with that of original results (Figure 4.1).

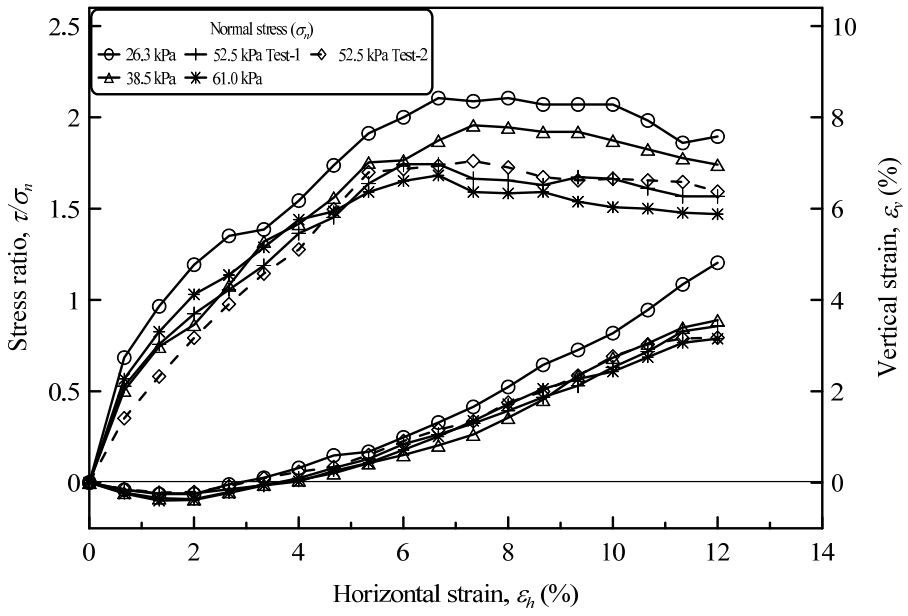

Figure 4.1 Plots of stress ratio (τ/σ_n) and vertical strain (ε_v) versus horizontal strain (ε_h) for unreinforced ballast

4.2.2 Ballast-geosynthetic interfaces

4.2.2.1 *Geogrid G1*

Figure 4.2 shows the interface shear behaviour of ballast reinforced with geogrid G1 in the form of stress ratio (τ/σ_n) and vertical strain (ε_v) versus horizontal strain (ε_h), for various values of the applied normal stress (σ_n). It is evident from Figure 4.2 that similar to the shear behaviour of unreinforced ballast, τ/σ_n increases with ε_h and attains a peak value at 7-8% horizontal strain. The post-peak behaviour shows a slight strain softening. Similar interface behaviour of geosynthetic-reinforced granular material was reported earlier by Liu et al. (2009). The replicate test results closely match with that of original results (Figure 4.2).

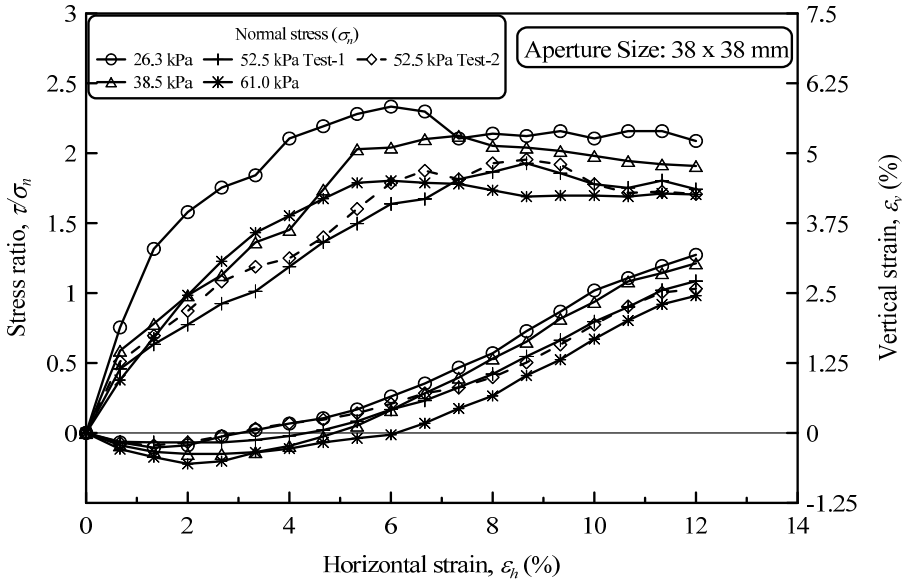

Figure 4.2 Plots of stress ratio (τ/σ_n) and vertical strain (ε_v) versus horizontal strain (ε_h) for reinforced ballast (G1)

Similar to the behaviour of unreinforced ballast, τ/σ_n of reinforced ballast decreases with the increase in σ_n. However, the volumetric behaviour shows a decrease in ε_v due to the reinforcement (Figure 4.2).

4.2.2.2 *Geogrids G2-G7 and Geotextile*

The shear behaviour of different ballast-geosynthetic interfaces (G2 through G7 and GT) is presented in Figure 4.3-Figure 4.9. These plots also depict the effect of the applied normal stress (σ_n) on the interface shear behaviour. It is evident from Figure 4.3 through Figure 4.9 that similar to the shear behaviour of unreinforced ballast and that reinforced with G1, τ/σ_n increases with ε_h and attains a peak value at 6-8% horizontal strain beyond which a slight strain softening occurs.

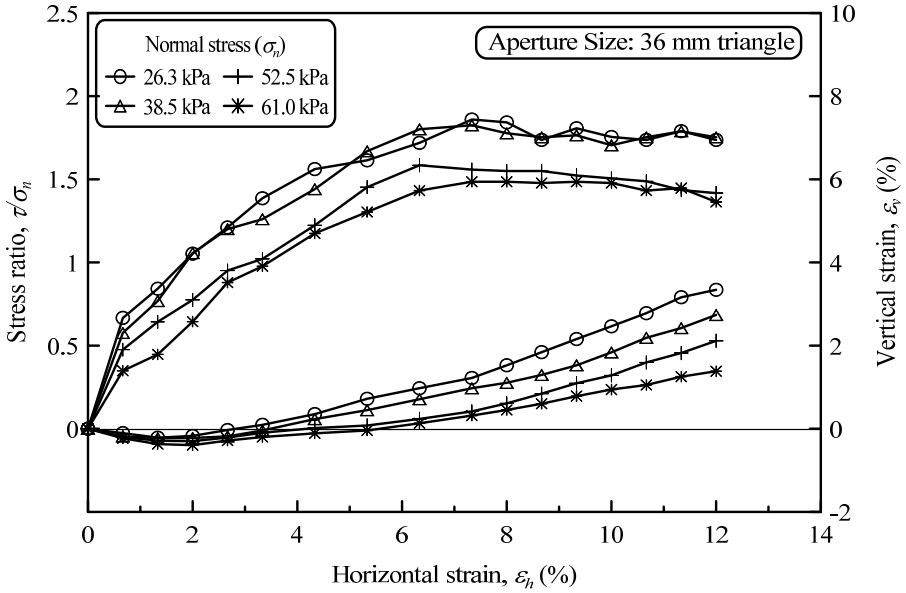

Figure 4.3 Plots of stress ratio (τ/σ_n) and vertical strain (ε_v) versus horizontal strain (ε_h) for reinforced ballast (G2)

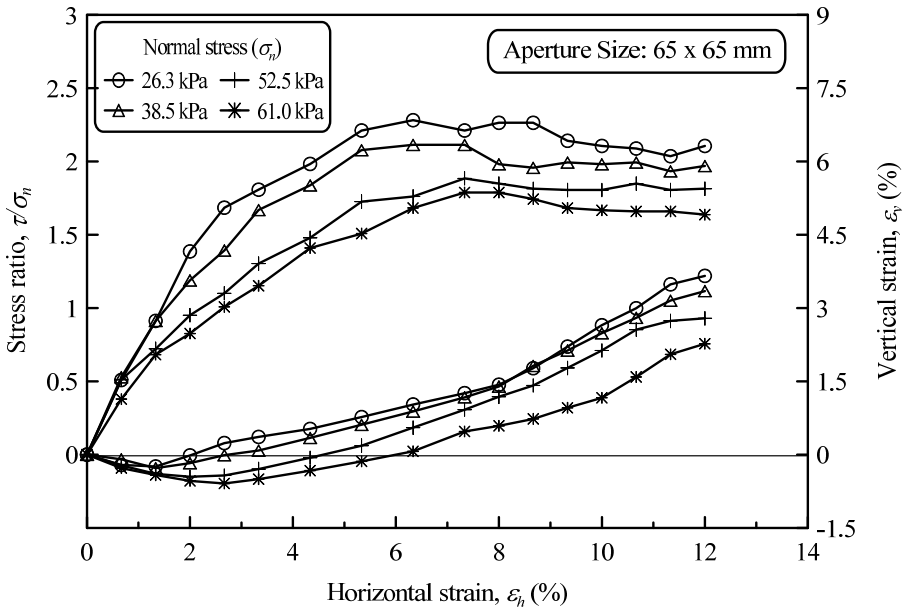

Figure 4.4 Plots of stress ratio (τ/σ_n) and vertical strain (ε_v) versus horizontal strain (ε_h) for reinforced ballast (G3)

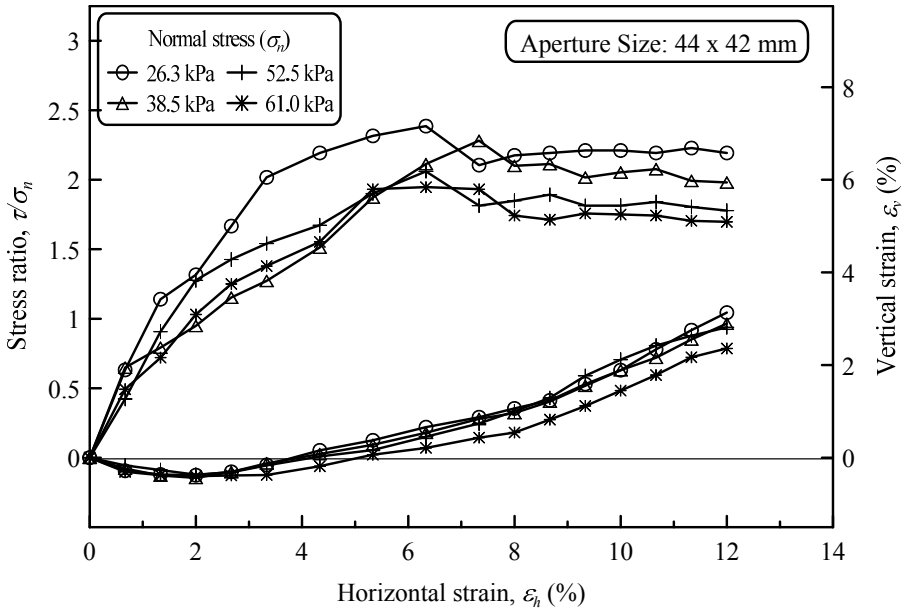

Figure 4.5 Plots of stress ratio (τ/σ_n) and vertical strain (ε_v) versus horizontal strain (ε_h) for reinforced ballast (G4)

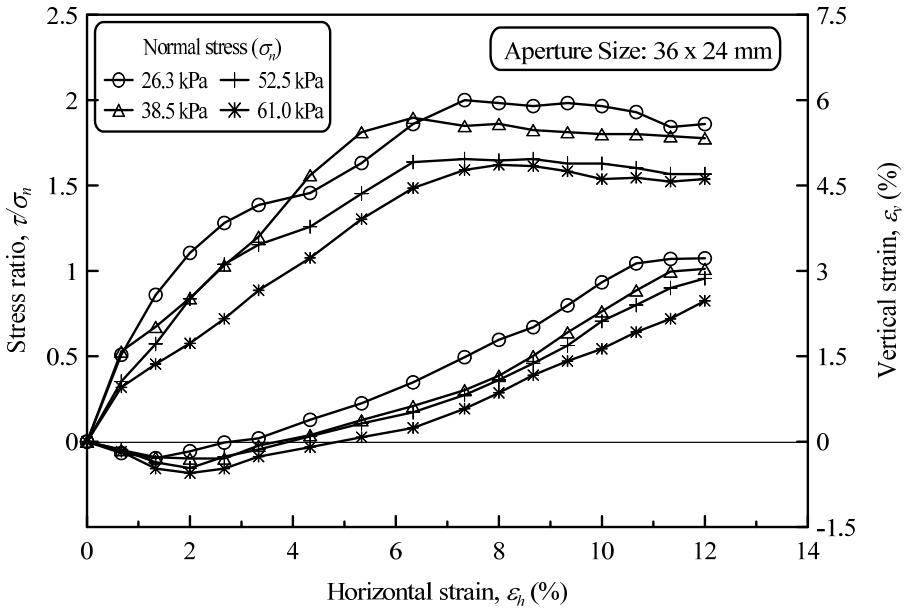

Figure 4.6 Plots of stress ratio (τ/σ_n) and vertical strain (ε_v) versus horizontal strain (ε_h) for reinforced ballast (G5)

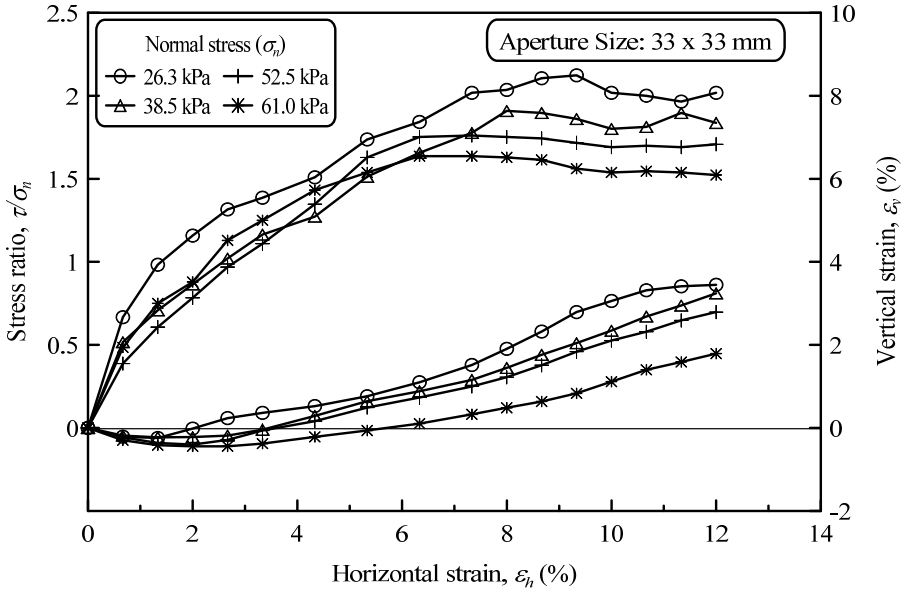

Figure 4.7 Plots of stress ratio (τ/σ_n) and vertical strain (ε_v) versus horizontal strain (ε_h) for reinforced ballast (G6)

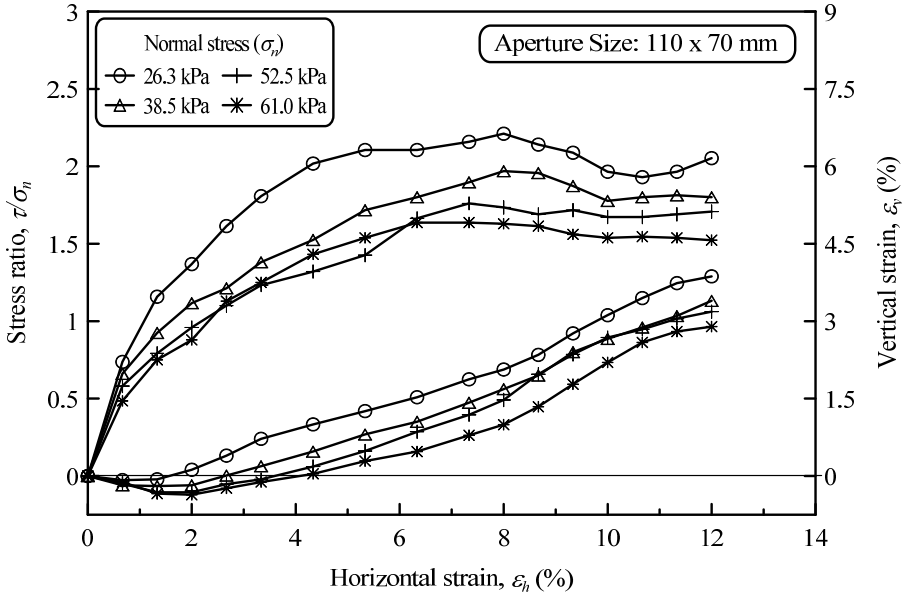

Figure 4.8 Plots of stress ratio (τ/σ_n) and vertical strain (ε_v) versus horizontal strain (ε_h) for reinforced ballast (G7)

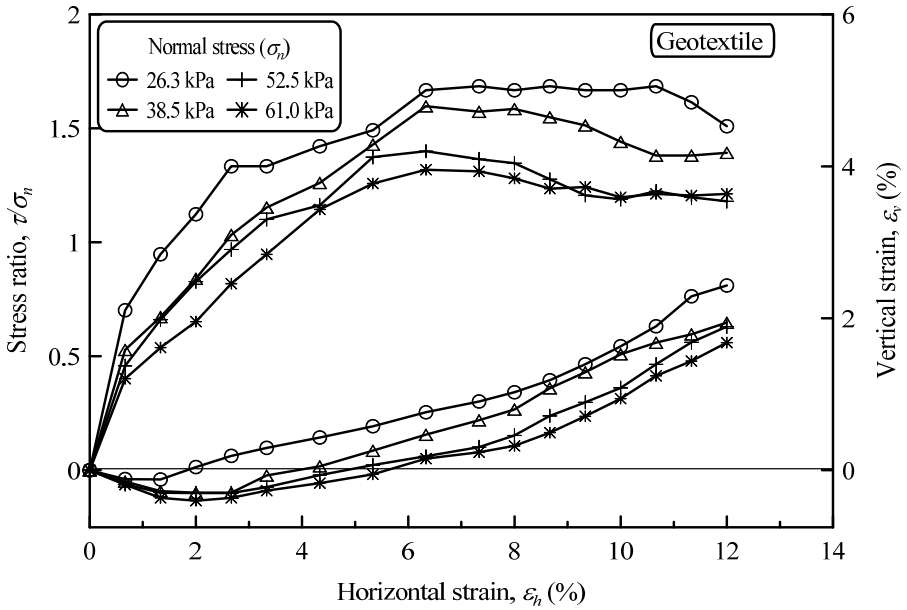

Figure 4.9 Plots of stress ratio (τ/σ_n) and vertical strain (ε_v) versus horizontal strain (ε_h) for reinforced ballast (GT)

4.2.3 Comparison of the shear behaviour of unreinforced and reinforced ballast

4.2.3.1 *Applied normal stress of 26.3 kPa*

Figure 4.10 and Figure 4.11 show the effect of geosynthetic type on the shear behaviour of the ballast-geosynthetic interfaces for an applied normal stress of 26.3 kPa. It is observed from Figure 4.10 that the use of geogrids G1, G3 and G4 increases the value of τ/σ_n in comparison to unreinforced ballast. This can be attributed to the interaction between the ballast and geogrid in the form of particle interlocking. In this case, τ/σ_n increases until 5-7% of the horizontal strain and remains constant thereafter. However, Figure 4.11 indicates that ballast reinforced with G2, G5 and GT exhibit lower values of τ/σ_n compared to unreinforced ballast. This may be attributed to the lack of particle interlocking, as will be described in detail later. It is clear from Figure 4.10 and Figure 4.11 that reinforcement of ballast also reduce the extent of dilation, an observation that agrees with several earlier studies (e.g. Haeri et al. 2000; Liu et al. 2009).

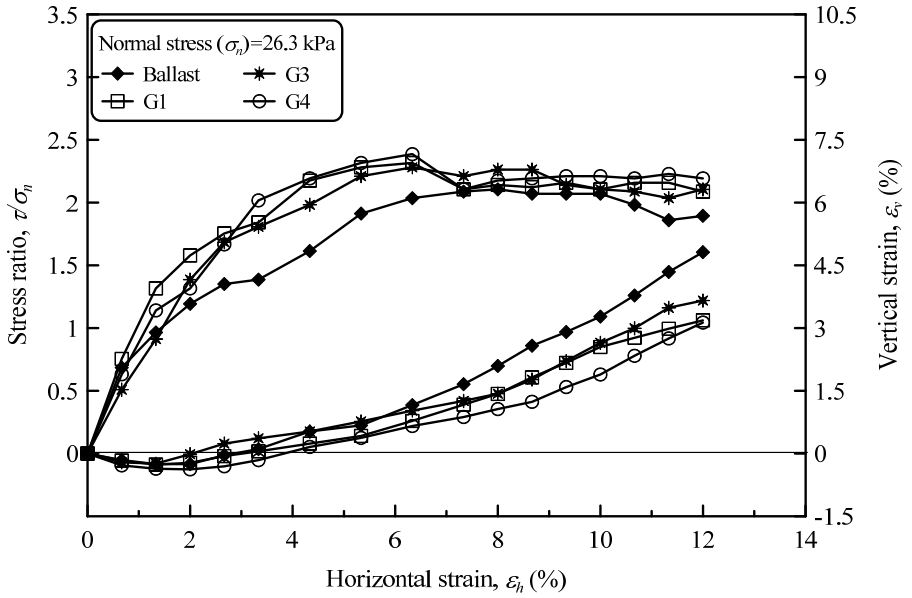

Figure 4.10 Comparison of stress ratio (τ/σ_n) and vertical strain (ε_v) versus horizontal strain (ε_h) for unreinforced and reinforced ballast (σ_n = 26.3 kPa)

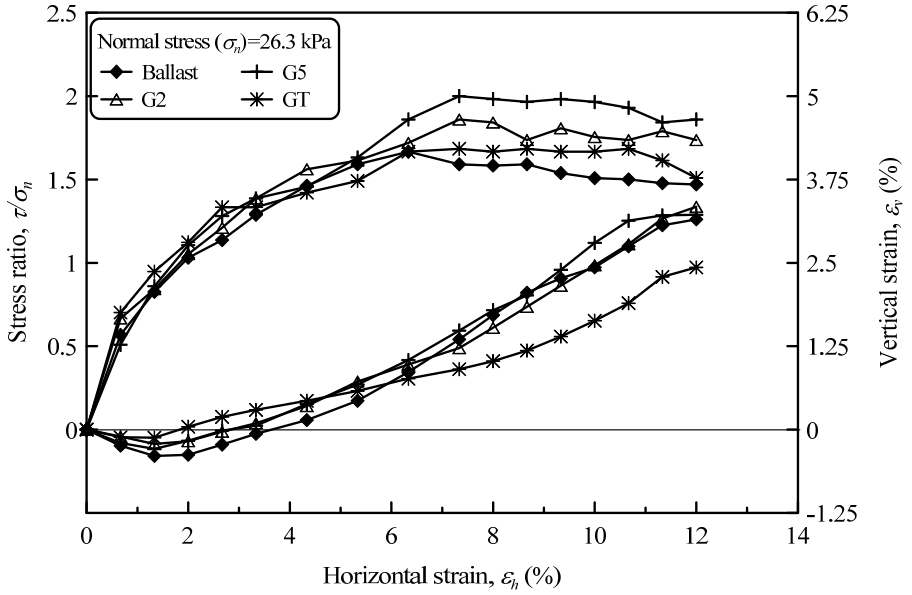

Figure 4.11 Comparison of stress ratio (τ/σ_n) and vertical strain (ε_v) versus horizontal strain (ε_h) for unreinforced and reinforced ballast (σ_n = 26.3 kPa)

4.2.3.2 *Applied normal stress of 38.5, 52.5 and 61.0 kPa*

A comparison of the shear behaviour of ballast-geosynthetic interfaces for applied normal stress of 38.5, 52.5 and 61.0 kPa is presented in Figure 4.12 through Figure 4.16. It is evident that similar to that observed at a normal stress of 26.3 kPa, the use of geogrids G1, G3 and G4 (Figure 4.12, Figure 4.14 and Figure 4.16) increases the value of τ/σ_n ratio while the geogrids G2, G5 and GT (Figure 4.13, Figure 4.15 and Figure 4.17) decrease the value of τ/σ_n in comparison to unreinforced ballast. This highlights that the performance of a particular geogrid in improving the characteristics of ballast remains essentially the same with the change in applied normal stress.

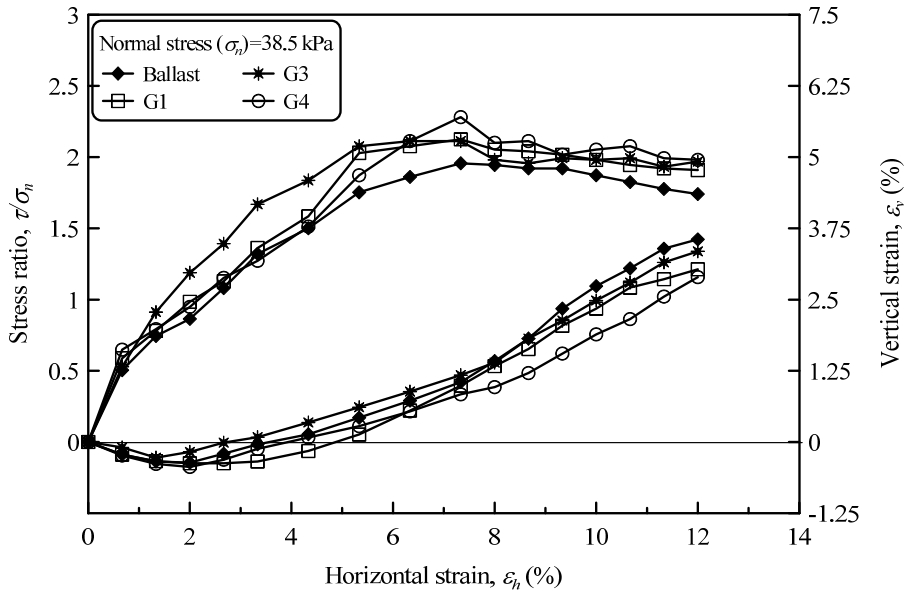

Figure 4.12 Comparison of stress ratio (τ/σ_n) and vertical strain (ε_v) versus horizontal strain (ε_h) for unreinforced and reinforced ballast (σ_n = 38.5 kPa)

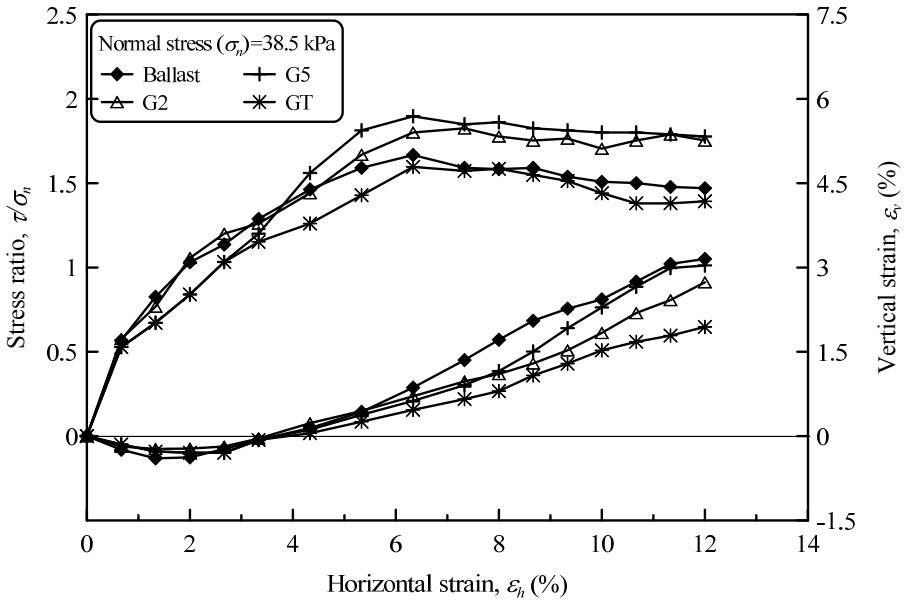

Figure 4.13 Comparison of stress ratio (τ/σ_n) and vertical strain (ε_v) versus horizontal strain (ε_h) for unreinforced and reinforced ballast (σ_n = 38.5 kPa)

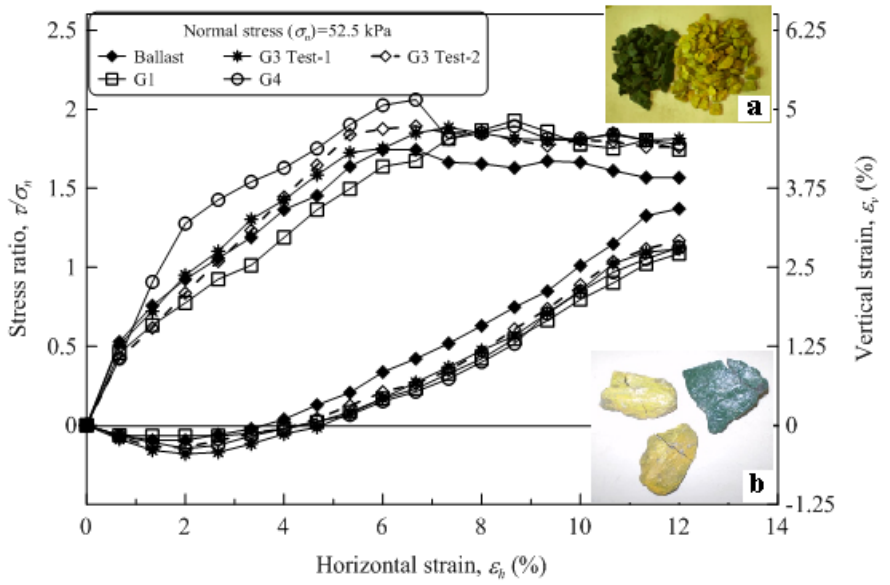

Figure 4.14 Comparison of stress ratio (τ/σ_n) and vertical strain (ε_v) versus horizontal strain (ε_h) for unreinforced and reinforced ballast (σ_n = 52.5 kPa). Inset (a) the colored ballast used at the interface (b) broken particles at the ballast-G4 interface

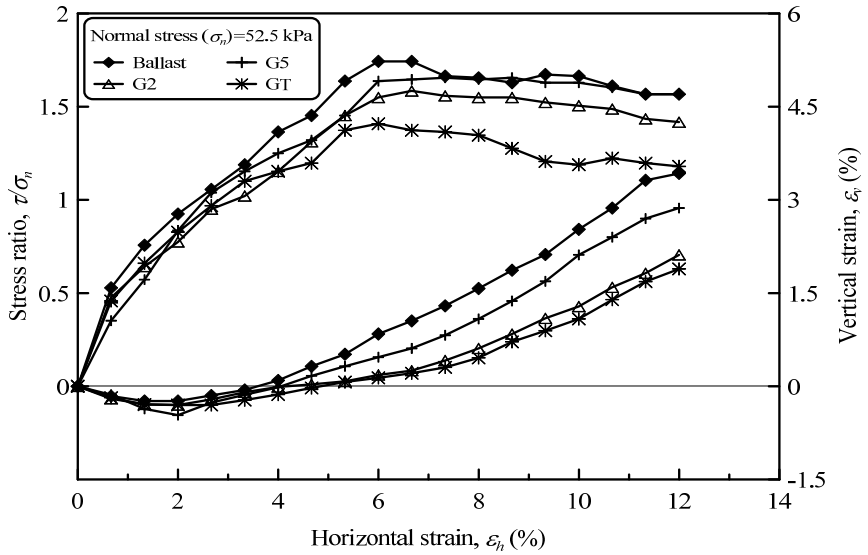

Figure 4.15 Comparison of stress ratio (τ/σ_n) and vertical strain (ε_v) versus horizontal strain (ε_h) for unreinforced and reinforced ballast (σ_n = 52.5 kPa)

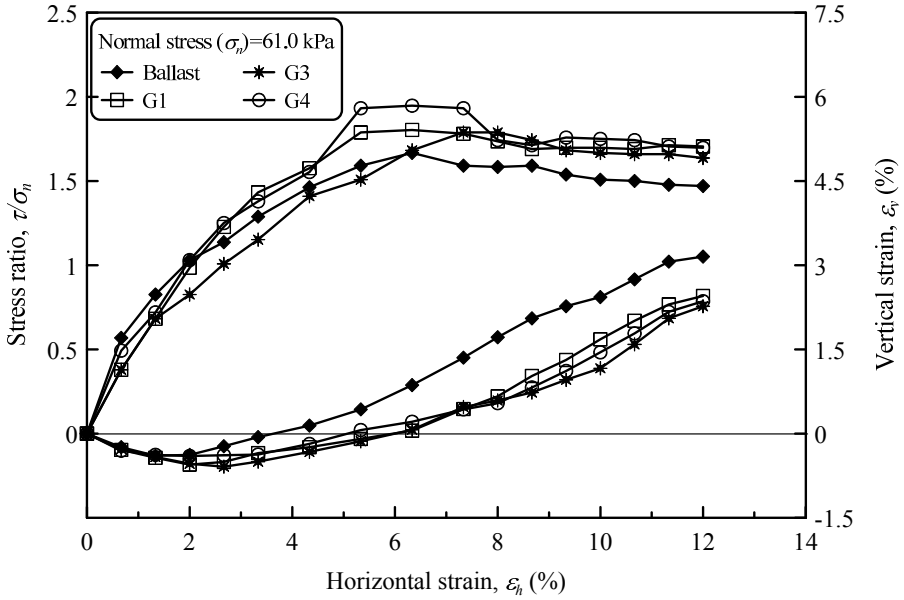

Figure 4.16 Comparison of stress ratio (τ/σ_n) and vertical strain (ε_v) versus horizontal strain (ε_h) for unreinforced and reinforced ballast (σ_n = 61.0 kPa)

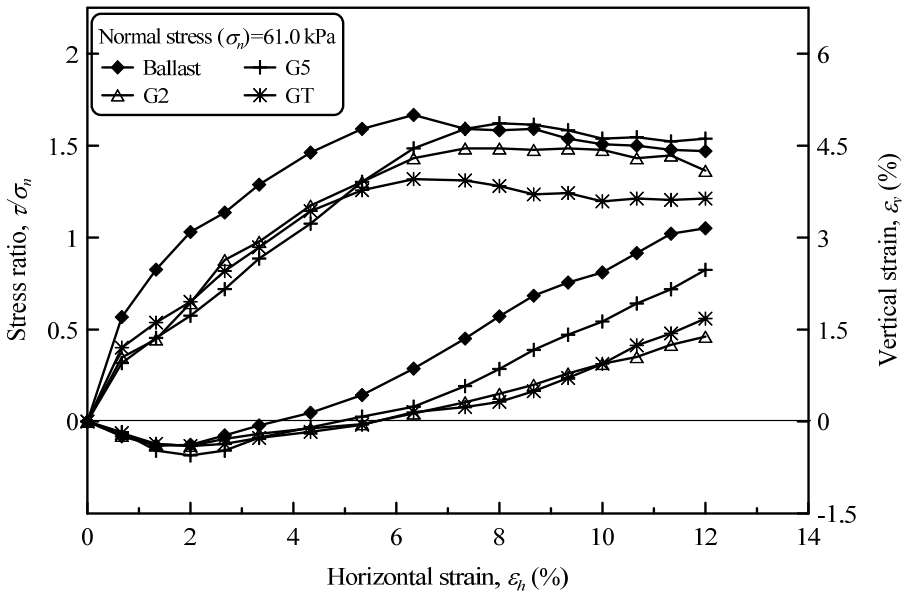

Figure 4.17 Comparison of stress ratio (τ/σ_n) and vertical strain (ε_v) versus horizontal strain (ε_h) for unreinforced and reinforced ballast (σ_n = 61.0 kPa)

4.3 RELATIONSHIP BETWEEN SHEAR STRESS AND NORMAL STRESS

It is well known that the shear behaviour of granular materials follows a non-linear trend at low confining pressures (Marsal. 1967, 1973; Marachi et al. 1972; Charles and Watts. 1980; Indraratna et al. 1998). As expected, a significant non-linearity is observed in the shear behaviour of ballast from the current study. In addition, all the ballast-geosynthetic interfaces also exhibit non-linear shear behaviour with the increase in the applied normal stress (Figure 4.18). The non-linear shear behaviour at low confining pressures can be expressed by the following normalized relationship (Eq. 4.1; Indraratna et al. 1998);

$$\left(\frac{\tau}{\sigma_c}\right) = m\left(\frac{\sigma_n}{\sigma_c}\right)^n \qquad 4.1$$

Where, τ/σ_c is the normalized shear strength, σ_n/σ_c is the normalized normal stress, σ_c is the uniaxial compressive strength of parent rock, and m and n are empirical constants.

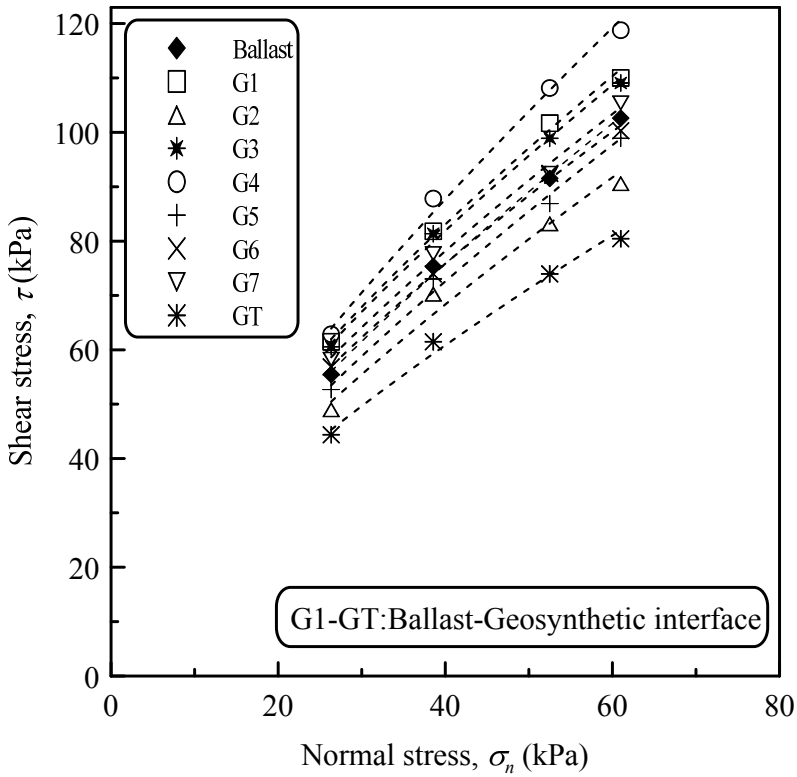

Figure 4.18 Failure envelopes for unreinforced and geosynthetic-reinforced ballast

The uniaxial compressive strength (σ_c) of this tested latite basalt from Bombo quarry is 130 MPa. The data from the current study in a normalized form are re-plotted in log scales (Figure 4.19) to evaluate the degree of non-linearity exhibited by ballast and the ballast-geosynthetic interfaces under direct shear conditions and compare the same with that evaluated from different testing conditions. The values of m and n for

ballast, ballast-geogrid interfaces along with results from Indraratna et al. (1998) are summarized in Table 4.1. These values provide preliminary guidance to the practicing engineers in the design and analyses of geogrid-reinforced railway tracks. Currently, there is no constitutive model available in the literature to predict the shear strength of ballast-geogrid interfaces; hence this empirical model offers practical benefits.

Table 4.1 Values of coefficients *m* and *n* for the normalized failure criterion

Material	*Range of σ_n (kPa)*	*m*	*n*
Ballast*	26.3-61	0.2	0.72
Ballast*-G1	26.3-61	0.18	0.70
Ballast*-G2	26.3-61	0.18	0.72
Ballast*-G3	26.3-61	0.18	0.70
Ballast*-G4	26.3-61	0.31	0.76
Ballast*-G5	26.3-61	0.21	0.73
Ballast*-G6	26.3-61	0.15	0.68
Ballast*-G7	26.3-61	0.16	0.69
Ballast*-GT	26.3-61	0.14	0.71
Ballast+ (Indraratna et al.,1998)	1-240	0.18	0.69
Ballast++ (Indraratna et al.,1998)	1-240	0.14	0.65

*D_{50}=35 mm; + D_{50}=38.9 mm; ++ D_{50}=30.3 mm

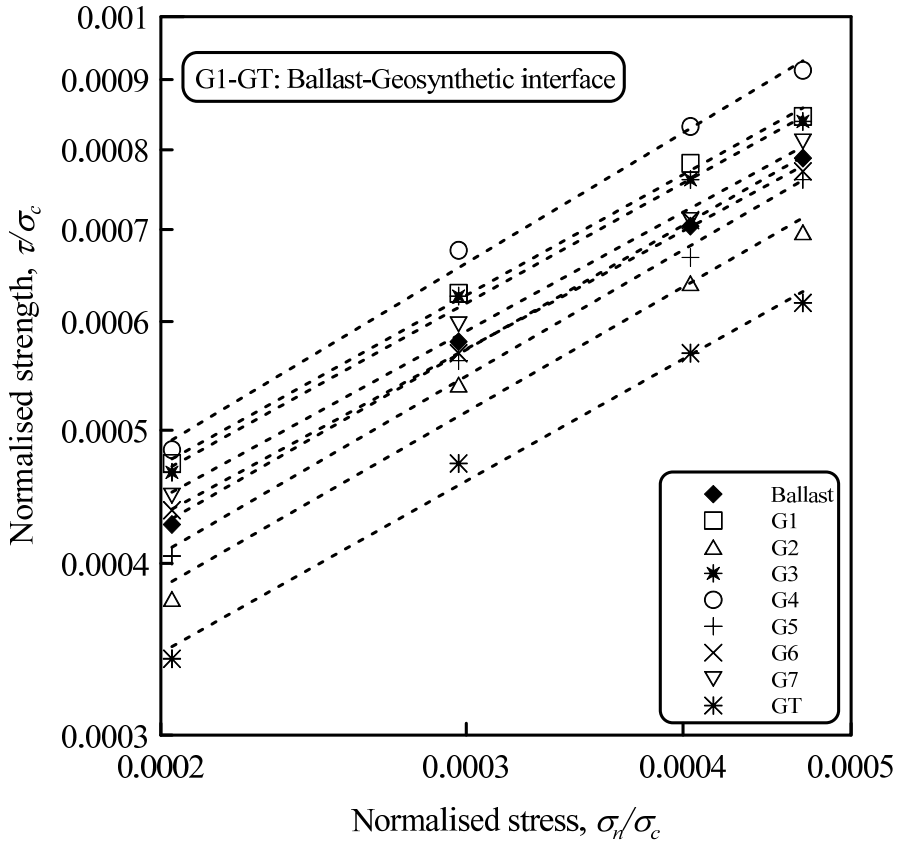

Figure 4.19 Variation of normalized shear strength with normalized normal stress for ballast and ballast-geosynthetic interfaces

The values of *m* and *n* determined here for ballast are close to those obtained from triaxial shear tests presented earlier by Indraratna et al. (1998). The values of *n* lie in the range of 0.68-0.76, which is an indication of significant non-linearity. It is to be mentioned here that the closeness of *m* and *n* values from the current study and that reported by earlier studies (e.g. Indraratna et al. 1998) highlight that ballast exhibits similar degree of non-linearity in both triaxial and the direct shear conditions, especially under low confining pressures. It is further observed from Table 4.1 that the values of *m* and *n* for unreinforced ballast and the ballast-geosynthetic interfaces lie in a narrow band highlighting that both geosynthetic-reinforced and the

unreinforced ballast exhibit a similar degree of non-linearity under direct shear conditions. However, with the increase in confining pressures the value of n is expected to approach unity and subsequently m approaches the tangent of the interface friction angle.

4.4 EFFECT OF NORMAL STRESS ON THE FRICTION ANGLE OF INTERFACES

It is well known that the friction angle (φ) of granular materials decreases with the increase in confining pressure (σ_n) (Leps 1970; Marachi et al. 1972; Charles et al. 1980; Indraratna et al. 1993, 1998). It is seen from Figure 4.20 that the friction angle of ballast (φ) decreases from 64° to 59° when σ_n is increased from about 26 to 61 kPa. A similar conclusion was made by Indraratna et al. (1998) based on the triaxial shear behaviour of ballast. They reported that the friction angle of ballast decreased from about 67° to 46° when the confining pressure increased from 1 to 240 kPa. The friction angle of the ballast-geosynthetic interfaces (δ) also decreased with an increase in σ_n, a trend similar to that of unreinforced ballast.

A comparison of friction angle of ballast determined from direct shear and triaxial tests reveal that direct shear testing gives a relatively higher friction angle (φ) of ballast (by about 2-3^o) determined at any given confining stress (σ_n) (Figure 4.20). This observation is in line with the trends reported earlier by Liu et al. (2005) and Asadzadeh et al. (2009) for sand and rockfill material respectively. This may be attributed to the different boundary conditions, failure planes and stress paths

associated with these two testing conditions. The other prominent reason behind such a difference in the observed friction angle is the associated ballast degradation under triaxial conditions. It may be mentioned here that the friction angle of ballast reduces significantly with the reduction in particle angularity or with the increase in particle breakage (Indraratna et al. 1998); thus, leading to lower friction angle in case of triaxial testing.

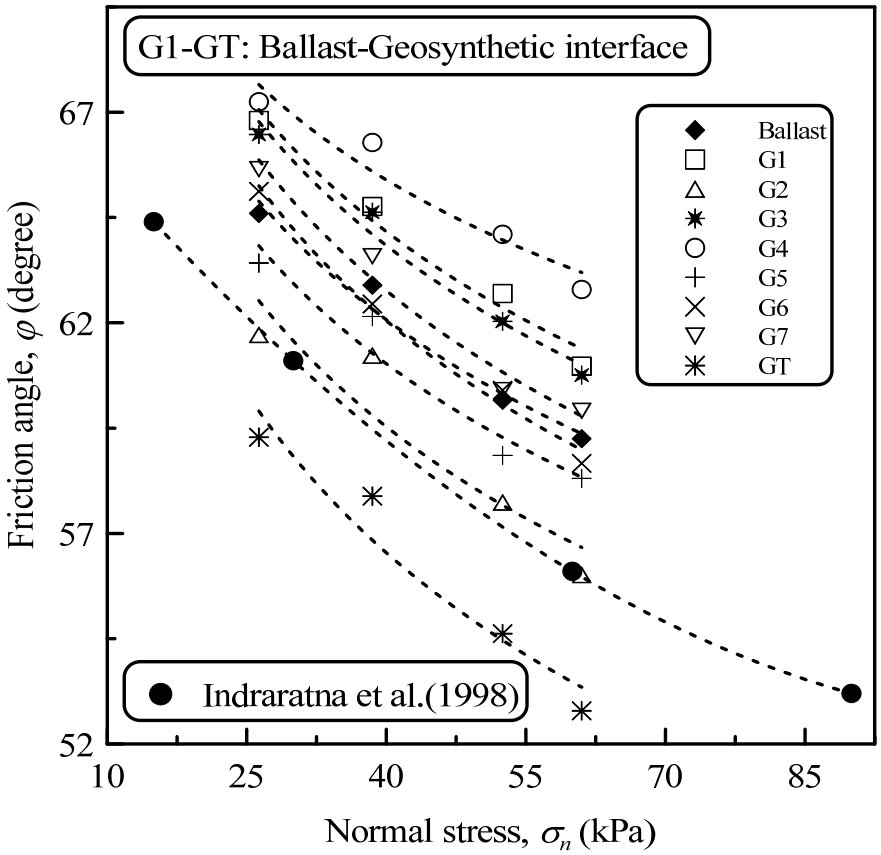

Figure 4.20 Variation of friction angle of ballast and ballast-geosynthetic interfaces with normal stress

4.5 INTERFACE EFFICIENCY FACTOR (α)

The improvement in the behaviour of soil-structure interfaces can be determined in terms of the interface efficiency factor (α), defined as the ratio of the shear strength of the interface to the internal shear strength of the soil (Koerner 1998), hence:

$$\alpha = \frac{\tan \delta}{\tan \varphi} \qquad 4.2$$

Where, δ is the apparent friction angle of the interface and φ is the friction angle of the soil. Note that for granular materials, the role of any cohesion intercept is neglected.

Table 4.2 Efficiency factors for the ballast-geosynthetic interfaces

Geosynthetic type	*Aperture size, A (mm)*	*Interface efficiency factor(α)*
G1	38	1.09
G2	20.8*	0.90
G3	65	1.07
G4	42.5*	1.16
G5	29.4*	0.96
G6	33	0.99
G7	88*	1.03
GT	NA	0.8

* Equivalent aperture size

The efficiency factors (α) for various ballast-geosynthetic interfaces are presented in Table 4.2. The equivalent aperture size has been considered for geogrids with rectangular and triangular apertures in Table 4.2. In the case of a geogrid with rectangular apertures (G4, G5 and G7), the square root of the aperture opening area has been considered as the 'equivalent aperture size', while for the geogrid with triangular apertures the diameter of the largest circle inscribed in the aperture has been adopted in the analysis.

Ballast-geotextile (GT) interface tests were conducted to compare the efficiency factors. Interface efficiency factor (α) for the tested interfaces ranges from 0.8 to 1.16. It is the lowest for ballast-GT interface and becomes highest for the ballast-G4 interface. Efficiency factors for ballast-GT, G2 and G5 interfaces are less than unity, but are greater than unity for ballast-G1, G3, G4 and G7 interfaces. An efficiency factor exceeding unity represents the beneficial effect of geogrids in reinforced soils. The shear strength of the ballast-geogrid interface derives its major share from interlocking that depends on the size of the apertures and the particles. However, the internal shear strength of ballast is primarily a function of inter-particle interaction. The increase in shear strength of the ballast-geogrid interface is mainly due to the interface particles (i.e. particle-aperture interlock) being restricted from sliding or rotate freely compared to the particle-particle interaction. The relatively low shear strength of ballast-GT interface is due to the absence of interlocking, i.e. both particle-particle and particle-aperture interaction.

A sketch of the particle-particle interlock and the interlocking of particles (particle-grid interlock) for both unreinforced and reinforced ballast is illustrated in Figure 4.21. An efficiency factor of less than unity for ballast-G2 and G5 interfaces is attributed to the lack of particle-grid interaction mainly owing to the small aperture sizes of the geogrid. Therefore, the apparent strength is lower than unreinforced ballast, but is higher than that of the ballast-GT interface (e.g. Figure 4.15). A good level of particle-grid interlock plus inter-particle interaction results in values of α greater than unity (Figure 4.10, Figure 4.12, Figure 4.14, Figure 4.16). The theory pertaining to the levels of interlocking is described in the latter sections of the manuscript. Figure 4.14 indicates that the shear strength of reinforced ballast (G1 and G4) increases significantly after some initial horizontal strain (ε_h). This is because some rearrangement of particles is needed for a significant interlocking between particles and grid to take place. The post-peak behaviour of ballast-G4 interface exhibits a sudden decrease in shear strength. This is caused by the breakage of interlocked particles as was clearly evident by broken particles at the interface observed during examination of ballast after the testing. Photograph showing the breakage of colored particles that were laid at the interface is shown in inset of Figure 4.14.

4.6 PROPOSED MODES OF INTERFACE FAILURE

Based on the experimental observations, two possible failure modes at ballast-geogrid interface can be proposed. Failure may take place due to either of the following modes,

(i) Loss of interlock: the mobilization of interface shear strength continues as long as the particle-grid interlock exists. Loss of interlock (slip of interlocked particle) causes free movement of particles leading to the interface failure.

(ii) Breakage of the interlocked particles: the inability of interlocked particles to slide or rotate freely offers the resistance to shearing. However, it causes the interlocked particles to experience high stresses leading to their breakage and subsequent failure of the interface.

The peak shear strength of the ballast-geogrid interface would not be attained if none of the above phenomena occur (i.e. loss of interlock or the breakage of interlocked particles).

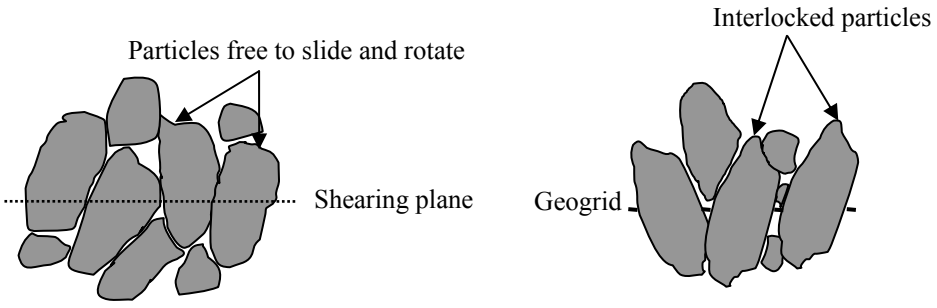

(a) Unreinforced ballast (b) Reinforced ballast

Figure 4.21 Particle-particle interlock and interlocking of particles in (a) unreinforced ballast and (b) geogrid-reinforced ballast

4.7 ROLE OF GEOGRID APERTURE SIZE ON THE INTERFACE SHEAR STRENGTH

To highlight the effect of aperture size (A) on the interface shear strength, the data is plotted in the form of variation of interface efficiency factor (α) with A/D_{50} ratio (Figure 4.22).

It is observed that the value of α is a function of the A/D_{50} ratio, where α increases with A/D_{50} until it attains a maximum value of 1.16 at A/D_{50} of 1.21, and then it decreases towards unity as A/D_{50} approaches 2.5. A similar behaviour was reported by Sarsby (1985) for fine sand-geogrid interfaces. Moreover, it is observed that the value of α is less than unity (i.e. unreinforced ballast) for $A/D_{50} < 0.95$, and is greater than unity for $A/D_{50} > 0.95$. However, α for all the tested ballast-geogrid interfaces exceeds 0.8, the efficiency factor for the ballast-geotextile interface, which can be attributed to the interlocking of particles. The value of $\alpha < 1$ indicates an ineffective interlocking of particles, whereas $\alpha > 1$ indicates acceptable interlocking which contributes towards higher shear strength. In other words, the A/D_{50} value at which $\alpha = 1$ represents the minimum condition required to generate the benefits of geogrid reinforcement.

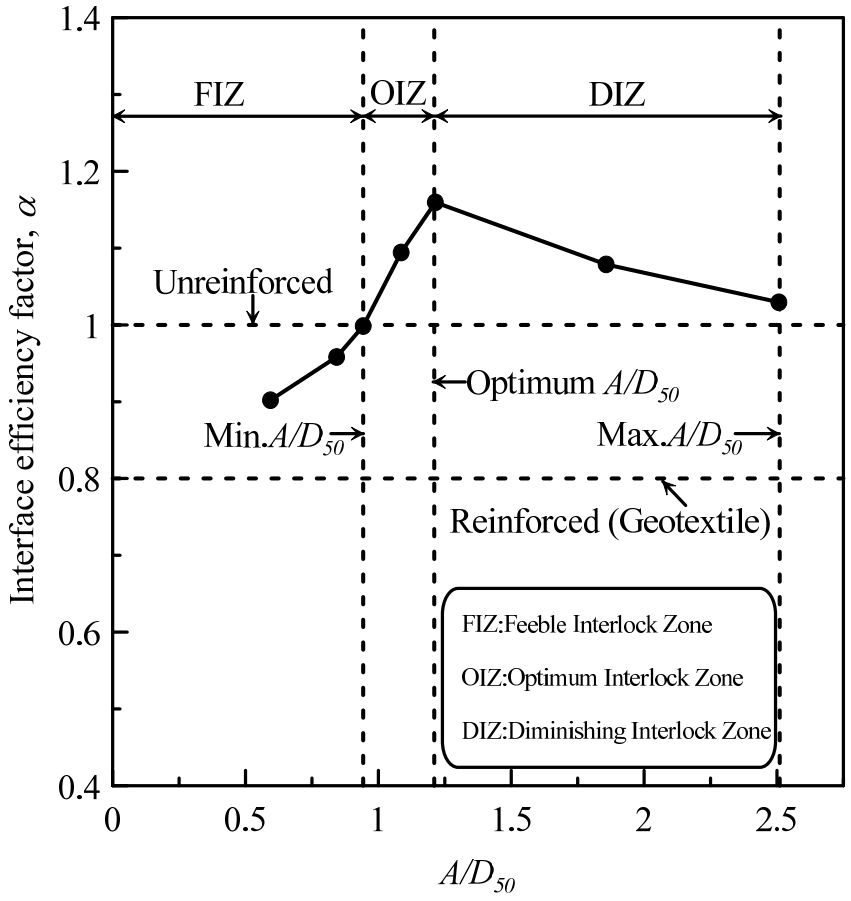

Figure 4.22 Interface efficiency factor (α) versus $A/D_{50,}$ a dimensionless parameter

Based on the variation of α, the ratio A/D_{50} is classified into three primary zones, as defined below.

4.7.1 Feeble interlock zone (FIZ)

For A/D_{50} ratio ranging from 0 to 0.95, relatively smaller particles interlock and hence, the values of α are less than unity. In this zone, the particle-grid interlock is weaker than the inter-particle interaction achieved without geosynthetics. This is because the particle-grid interlock is attributed to smaller particles alone (< 0.95 D_{50}) when compared to the particle-particle interlock with respect to all sizes. In this zone of interlock, an examination of ballast after testing showed insignificant particle

breakage, which suggests that the interface failure stemmed from the loss of particle-grid interlock during shearing.

4.7.2 Optimum interlock zone (OIZ)

For A/D_{50} ratio from 0.95 to 1.20, interlocking of relatively larger particles occurs thereby leading to the values of α exceeding unity. The value of α attains a maximum of 1.16 at an optimum A/D_{50} ratio of about 1.20. An examination after shearing showed there were many broken particles at the interface, suggesting that the failure is caused by the breakage of initially interlocked particles. As also described earlier by Lade et al. (1996), this is probably due to the presence of increased number of natural flaws (e.g. micro-cracks) in the larger particles.

4.7.3 Diminishing interlock zone (DIZ)

For $A/D_{50} > 1.20$, the values of α are greater than unity but the degree of interlocking decreases rapidly leading to a reduction in α with increasing A/D_{50} ratio. It is observed that α decreases to almost unity when A/D_{50} exceeds 2.50, implying that the interface now becomes similar to condition of unreinforced ballast, as the aperture size become exceedingly higher in relation to the particle size. Based on the test results, the maximum realistic ratio A/D_{50} is considered as 2.50, beyond which the geogrid plays an insignificant role. This reduction in α may be further attributed to the number of particles entrapped within a given aperture. Here, the free movement of relatively small particles within the aperture boundary approaches the displacement condition of unreinforced ballast.

From the above defined interlocking zones, it is clear that $\alpha > 1$ for $A/D_{50} > 0.95$, although the effect of geogrid is less significant with the increasing A/D_{50}. This highlights that the effect of larger geogrid aperture size for a given particle gradation is neutral, if not beneficial in terms of the interface shear strength. On the contrary, the effect of smaller geogrid aperture size is detrimental in terms of the interface shear strength (i.e. for $A/D_{50} < 0.95$, $\alpha < 1$). These observations, in practical sense, discourage the use of geogrids with $A/D_{50} < 0.95$ for reinforcing the ballast.

4.8 EFFECT OF APPLIED NORMAL STRESS ON THE INTERFACE EFFICIENCY FACTOR (α)

The effect of applied normal stress (σ_n) on the interface efficiency factor (α) is shown in Table 4.3. It is seen that the efficiency factor for a given ballast-geosynthetic interface is almost constant with the applied normal stress (σ_n), suggesting that the attained interface shear strength or the degree of ballast-geogrid interlock is primarily a function of the ratio A/D_{50} alone. Therefore, it can be said that the degree of interlocking achieved is primarily a function of geometrical dimensions/sizes of materials at the interface, i.e. both geogrid and ballast. This implies that the extent of reduction in dilation due to the increase in normal stress is constant irrespective of whether the ballast is in the unreinforced or reinforced state. In other words, both ballast and ballast-geosynthetic interfaces exhibit similar degree of non-linearity at low normal stresses. This fact is further substantiated by the similar range of n values computed as per the normalized shear stress-normal stress relationship given by Indraratna et al. (1998) for unreinforced and reinforced ballast.

Table 4.3 Efficiency factors for the ballast-geosynthetic interfaces for different values of applied normal stress

Geosynthetic type	*Interface efficiency factor (α)*			
	σ_n= 26.3 kPa	σ_n= 38.5 kPa	σ_n= 52.5 kPa	σ_n= 61.0 kPa
G1	1.10	1.08	1.11	1.07
G2	0.89	0.92	0.90	0.88
G3	1.09	1.08	1.08	1.06
G4	1.14	1.16	1.18	1.15
G5	0.95	0.96	0.95	0.96
G6	1.02	0.98	1.02	1.02
G7	1.04	1.03	1.01	1.03
GT	0.80	0.81	0.80	0.79

4.9 OPTIMIZATION OF APERTURE SIZE IN TERMS OF PARTICLE SIZE DISTRIBUTION

From this current study, the minimum, optimum and maximum aperture sizes of geogrid required to optimize the shear strength are identified as $0.95D_{50}$ (D_{45}), $1.20D_{50}$ (D_{80}) and $2.50D_{50}$ respectively. However, for all practical purposes, the optimum aperture size of geogrid can be treated as $1.15\text{-}1.3D_{50}$. The minimum size of aperture is to ensure that the particles effectively interlock, while the maximum limit on aperture size is required to ensure that there are not too many particles in any one aperture, because their free movement does not offer much resistance to shearing. In this view, the minimum and optimum aperture sizes in terms of PSD are shown in Figure 4.23.

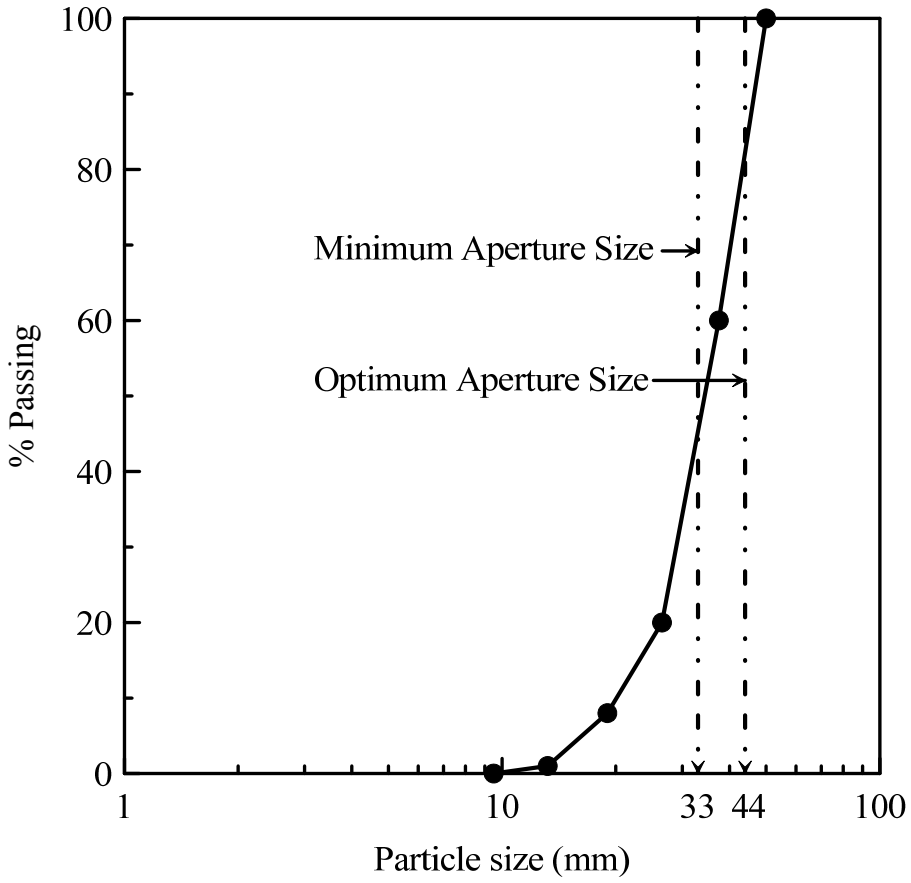

Figure 4.23 Minimum and optimum aperture sizes in terms of PSD

An optimum aperture size of 1.40 D_{50} was reported in the past by Brown et al. (2007). However, this was based on the settlement behaviour from the full-scale model testing of geogrid-reinforced ballast with ballast gradation as per Railtrack (2000) specification. In contrast, the optimum aperture size from the current study is based on the ballast-geogrid interface behaviour in the direct shear mode. The closeness in the optimum aperture value with that reported earlier by Brown et al. (2007) though determined from different testing conditions confirms the accuracy of results from the current study.

4.10 SUMMARY

The chapter presented the results from the large-scale direct shear tests carried out to study the behaviour of ballast-geosynthetic interfaces. The behaviour of various ballast-geosynthetic interfaces was explored and the efficiency factors were determined. The value of α for ballast used in the study was found to vary in the range of 0.8-1.16. This was lowest for the ballast-geotextile interface and highest for the ballast-geogrid (G4) interface. It was observed that the angle of shearing resistance of the ballast (φ) and that of the ballast-geosynthetic interfaces (δ) decreased non-linearly at relatively low confining pressures (σ_n < 100 kPa), where φ decreased from 64° to 59° when σ_n is increased from about 25 to 60 kPa. The non-linear shear behaviour of ballast was expressed by a normalized relationship, and the values of the relevant empirical constants (i.e. *m* and *n*) for various interfaces were determined.

Two possible modes of ballast-geogrid interface failure were proposed in this Chapter. The loss of interlock and the breakage of interlocked particles were identified as the potential modes of ballast-geogrid interface failure. It was observed that the ratio A/D_{50} has a profound influence on α. In this respect, the ratio A/D_{50} based on the variation of α is categorized into three key zones: (i) Feeble Interlock Zone (ii) Optimum Interlock Zone and (iii) Diminishing Interlock Zone. The best geogrid aperture size to optimize the interface shear strength is determined to be $1.20D_{50}$. The minimum and maximum aperture sizes desired to attain the beneficial effects via geogrids are established as $0.95D_{50}$ and $2.50D_{50}$, respectively.

The conclusions from the current study are relevant to the direct shear mode of failure and, hence, may not directly represent the interface behavior under pullout conditions.

5 LABORATORY EXPERIMENTAL INVESTIGATIONS OF THE PERMANENT DEFORMATION AND DEGRADATION ASSESSMENT OF BALLAST

5.1 INTRODUCTION

In this Chapter, the laboratory investigation of the permanent deformation and degradation characteristics of ballast under cyclic loading using state-of-the-art large-scale process simulation test (PST) apparatus is described. In order to study the shear strength characteristics of ballast-geosynthetic interfaces, a series of tests were conducted in the laboratory using the large-scale direct shear apparatus. Following the direct shear tests, in order to investigate the permanent deformation and degradation behaviour of geogrid-reinforced ballast under high-frequency cyclic loading, a small section of track was simulated in the laboratory. Representative field lateral stresses were applied to the ballast specimens and a cyclic vertical load equivalent to a typical trainload was applied to the specimens. The details regarding the large-scale testing equipments, test materials, specimen preparation methods, and the experimental procedures followed including the instrumentation used to measure the deformations of ballast are discussed in the subsequent paragraphs.

5.2 MODEL TRACK TESTS TO STUDY THE BALLAST BEHAVIOUR UNDER CYCLIC LOADING

The behaviour of ballast should ideally be studied through tests conducted on a real track under actual loading conditions. However, these tests are not only costly and

time consuming but also disrupt traffic schedules. Moreover, many variables which affect the proper formulation of definitive ballast relationship are often difficult to control in the field (Jeffs and Marich 1987). Therefore, laboratory experiments simulating field load and boundary conditions are usually carried out on ballast specimens.

In the recent past, several studies have described the cyclic behaviour of ballast using large-scale model testing facilities (Eisenmann et al. 1993; Goebel and Weisemann 1994; Raymond et al. 1994; Guerin et al. 1996; Atalar et al. 2001; Raymond 2002; Hornícek et al. 2010). However, the testing chambers used by them had rigid and immovable (rigid) boundaries and therefore they have restricted the lateral movement of ballast. Consequently, some investigators developed semi-confined devices for ballast modelling (Jeffs and Marich 1987; Norman and Selig 1983). Recently, Indraratna et al. (2000) have designed a process simulation test (PST) apparatus to simulate the lateral movement of ballast under imparted loadings (Figure 5.1). The apparatus can accommodate test specimens of dimensions 600 x 800 x 650 mm. It consists of a prismoidal steel box having about a 1 mm gap between the vertical walls and the base plate, to allow the free movement of the vertical walls when subjected to a horizontal force. A system of linear-bearings mounted on steel rod placed near the corners of each wall allows the lateral displacement of the vertical walls, thereby simulating the lateral spreading of ballast. The vertical walls of this PST apparatus are named based on the orientation of the device within the laboratory, for the ease of reference and monitoring. Accordingly, the walls parallel to the sleeper direction were named North wall and South wall,

respectively, and the walls perpendicular to the sleeper direction are named East wall and West wall, respectively.

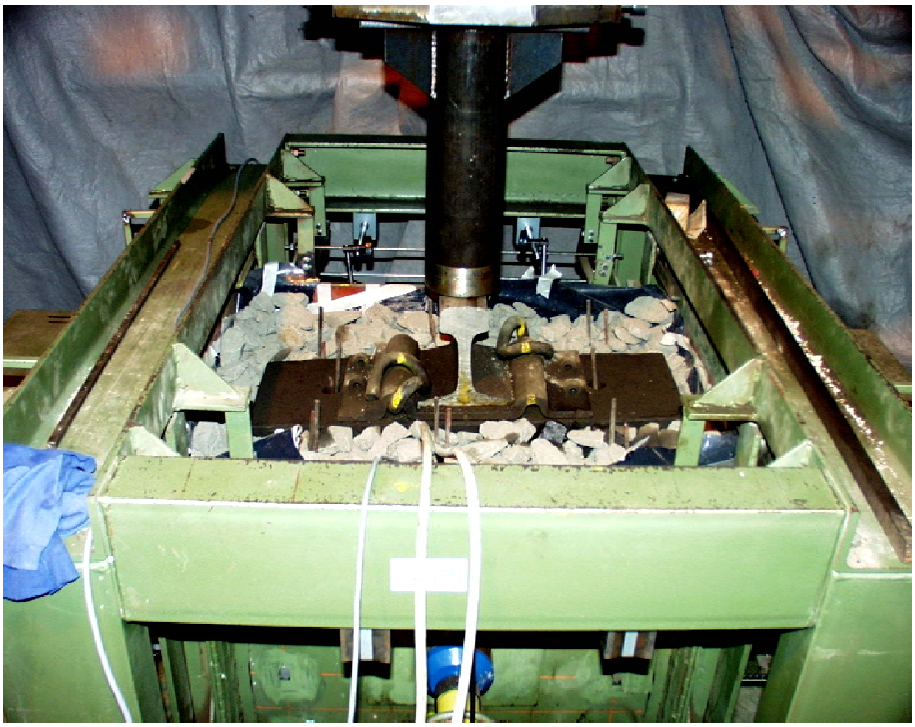

Figure 5.1 A general view of the PST apparatus available at University of Wollongong (adapted from Indraratna et al. 2000)

While this large-scale PST apparatus available at the University of Wollongong (UOW) allowed lateral movement of ballast, it still did not permit a more realistic non-uniform lateral displacement with depth owing to the side plate that could move only as a rigid body in the horizontal direction. This is not a major concern for loading frequencies in the range of 10-15 Hz (train speeds < 100 km/h) where the magnitude of lateral strains is small. However, the lateral strains are not only a function of axle load and the loading frequency, but they also vary with depth. Therefore, the modification of the existing prismoidal triaxial equipment was

necessary to capture a more realistic lateral displacement of ballast with depth under high-frequency loading.

5.3 MODIFIED PROCESS SIMULATION TEST (MPST) APPARATUS

5.3.1 Description

The apparatus proposed herein is a modification of the existing cubical triaxial apparatus designed and built at the University of Wollongong (Indraratna et al., 2000; Figure 5.1). It has plan dimensions of 800 x 600 mm and can accommodate samples measuring 650 mm in height. The modification involved the replacement of the central portion of the side wall of the existing prismoidal chamber (Figure 5.2) with a setup of five independent movable plates each measuring 600 mm in width and 64 mm in height assembled along the depth (Figure 5.3). A small gap of 1 mm is provided between the adjacent plates to ensure free lateral movement of each individual plate under the applied loading. While a greater number of moving plates would mimic the reality even better, it is infeasible to have plates of width less than 60-65 mm owing to the size of actuators needed to apply the confining stress on to these movable plates. Therefore, for a ballast depth of 300-350 mm, a maximum of five movable plates were considered to be sufficient. In a real track, subballast containing smaller particles compacted to a higher density than the overlying ballast does not indicate significant lateral movement. Also, the top 150 mm of the specimen should represent crib ballast that does not carry the load but confines the ties (sleepers). This crib ballast rarely undergoes significant lateral movement. In this context, the movable plates are required only at the central portion of the side wall where the load carrying ballast is subjected to lateral movement.

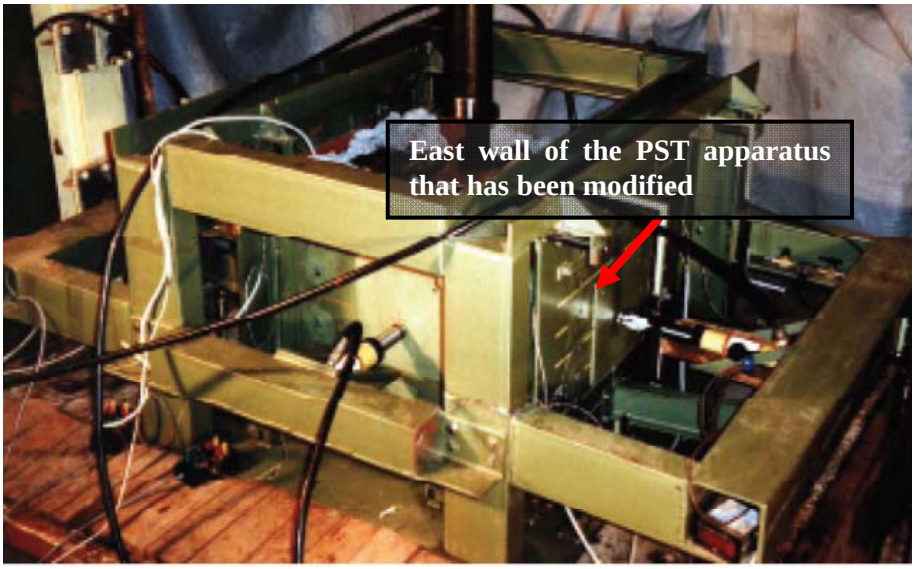

Figure 5.2 Photograph highlighting the east wall of the PST apparatus that has been modified

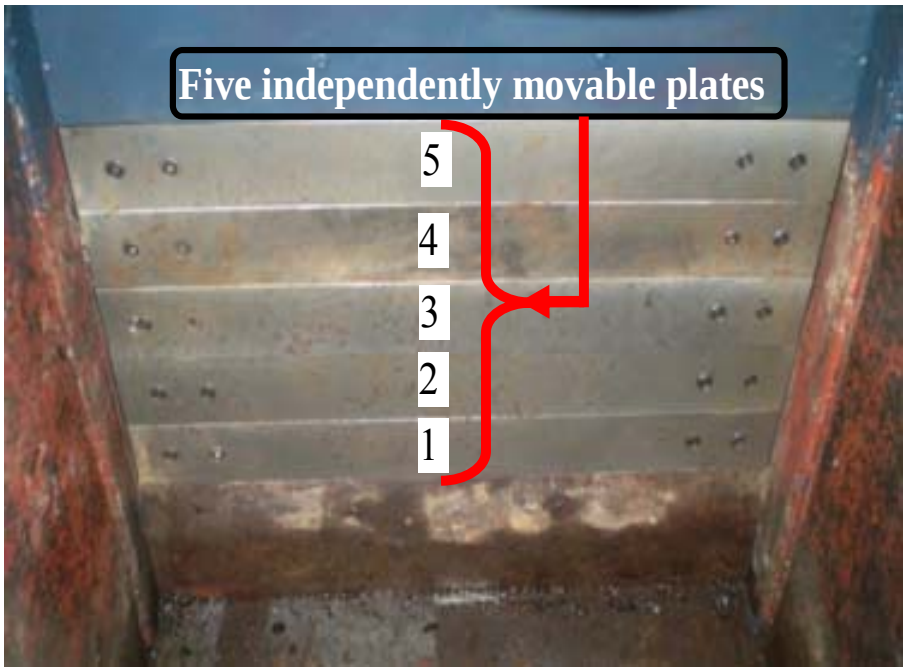

Figure 5.3 Internal view of the five-plate setup of the modified cubical apparatus

The lateral movement of plates is facilitated by means of linear bearings mounted on a steel guide rail. These bearings were placed at the ends of each plate, two on each

plate, hence totally ten. The allowable lateral displacement is 45 mm, representing a maximum lateral strain of 5.63%. A desired confining pressure, to simulate the confining effect of shoulder ballast, can be applied to each of the five movable plates by means of servo-controlled actuators (Figure 5.4).

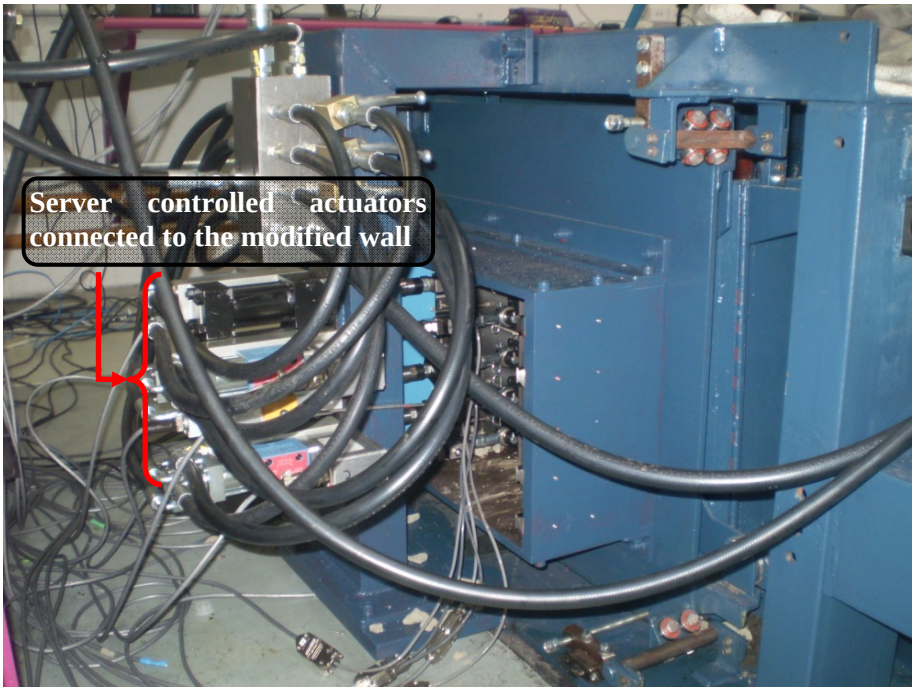

Figure 5.4 Server controlled actuators used to apply the confining pressure on to the five movable plates

The shorter dimension of the MPST apparatus (i.e. 600 mm) represents the centre-to-centre distance between the ties while the longer side (i.e. 800 mm) represents the track width. Figure 5.5 illustrate the contact stress distribution at the ballast-tie interface for broad gauge tracks based on the simplified analysis proposed by Jeffs and Tew (1991) and Atalar et al. (2001), respectively. Figure 5.6 shows the plan view of a typical track highlighting the specific portion that the modified apparatus is

designed to simulate in the laboratory. The simulated portion is representative of the track section stressed due to the applied wheel loading.

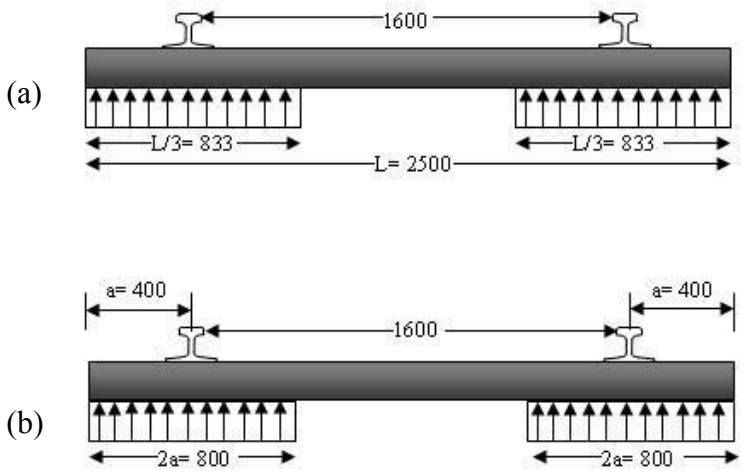

Figure 5.5 (a) Simplified ballast-tie contact pressure distribution (modified after Jeffs and Tew. 1991) (b) Ballast-tie contact pressure distribution as per the Japanese standards (modified after Atalar et al. 2001)

The individual walls of the MPST apparatus could be either released or held fixed to simulate the boundary conditions in accordance with real track conditions. In a typical track under applied loading, the lateral spread of ballast is essentially in the outward direction (parallel to ties) with almost a zero lateral movement at the track centreline. Therefore, exploiting symmetry with respect to sleeper axis (Figure 5.6), only one of the two side walls (i.e. the modified East wall with five movable plates) can be allowed to move laterally while the West wall could be held fixed. Although a moving train can cause a slight forward and backward movement of ballast parallel to rails, the net effect is zero strains in the longitudinal direction. Such plane strain

conditions could be ensured by fixing the North and South boundaries of the apparatus too.

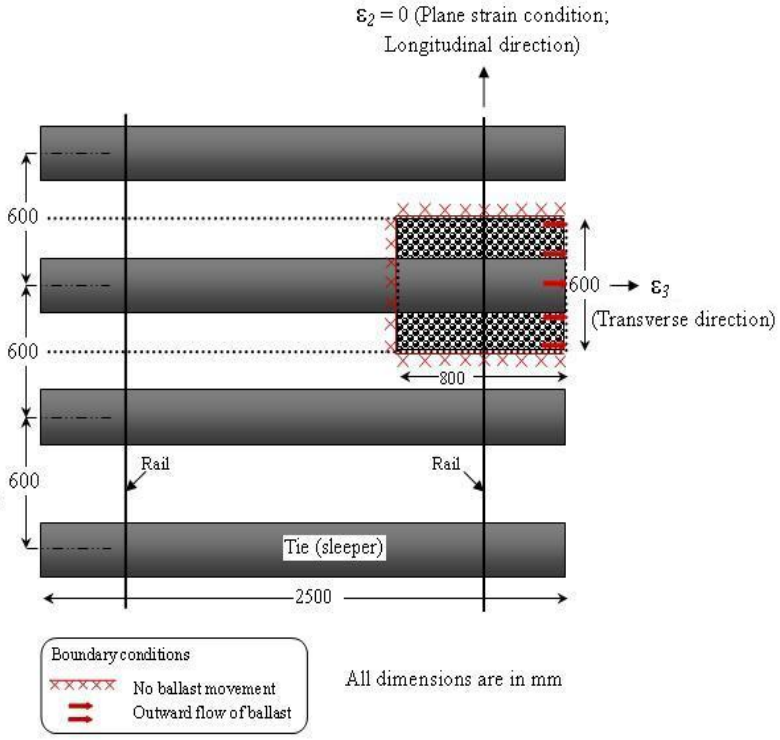

Figure 5.6 Plan view highlighting the section of track simulated in the laboratory by MPST apparatus

5.4 THE DEFORMATION AND DEGRADATION BEHAVIOR OF GEOGRID-REINFORCED BALLAST UNDER CYCLIC LOADING

5.4.1 Laboratory experiments using the MPST apparatus

In the recent past several researchers have studied the shear behaviour of ballast under monotonic and cyclic loading (e.g. Shenton 1975; Raymond 2002; McDowell and Stickley 2006; Brown et al. 2007; Lackenby et al. 2007; Anderson and Fair.

2008; Aursudkij et al. 2009; Indraratna et al. 2009; Hornícek et al. 2010; Tutumluer et al., 2012). Lackenby et al. (2007) have found that an increased ballast confinement is necessary to counteract the increased train axle loads and enhance the track performance. Of the several measures used to increase the confining pressure, reinforcing the ballast with geosynthetics is considered to be more suitable and economically viable (Indraratna et al. 2009). Therefore, the use of geosynthetics as reinforcement in rail tracks has been on the rise. Once placed in the track, the beneficial effects of geogrid reinforcement stem from the ballast-geogrid interaction in the form of interlocking of particles in the geogrid apertures that stabilizes the ballast. While it is known that geogrids stabilize the ballast, the extent by which they arrest the lateral spread of ballast and the lateral strain variation with vertical distance away from the reinforcement placement position is not yet explored. Therefore, experiments were carried out on unreinforced and geogrid-reinforced ballast using the MPST apparatus to investigate the effect of geogrid type and its placement location on the lateral displacement variation along the ballast depth and its subsequent effect on the vertical settlement and particle breakage. All the tests were carried at a cyclic loading frequency of 20 Hz that corresponds to a train speed of 146 km/h, for an axle spacing of 2.02 m. In order to study the influence of reinforcement placement position on the performance of ballast, the geogrid was placed at either (a) the subballast-ballast interface (i.e. z = 0 mm) or (b) 65 mm above the subballast (i.e. z = 65 mm); with z defined as the distance above the subballast. These placement positions of the reinforcement were chosen keeping in view the track maintenance operations that require about 250 mm of ballast free from geogrid(s).

5.4.2 Characteristics of test materials

5.4.2.1 *Ballast*

Fresh Latite ballast from Bombo quarry, situated 100 km South of Sydney NSW, Australia, was used for the studying the behaviour of unreinforced and geogrid-reinforced ballast under cyclic loading. The durability, shape and strength properties of ballast used in the laboratory study are summarised in Table 3.1.

The ballast was first washed using a high pressure hose to remove any dirt and clay adhering to the particles. The ballast was then sorted into various sizes by passing it through the sieves of required sizes. Upon drying, the specimens were prepared by thorough mixing of the correct weight of each particle size to match the selected gradation curve shown in Figure 5.7. The amount of mixing was sufficient to make samples with reasonable degree of homogeneity. The ballast samples used for the investigation conformed to the standards specified by Technical Specification TS 3402 of Rail Infrastructure Corporation (RIC), and the particle size distribution (PSD) conformed to AS 2758.7. The maximum particle size (D_{max}) of ballast is 53 mm, with D_{50} of 35 mm and a coefficient of uniformity, c_u of 1.87.

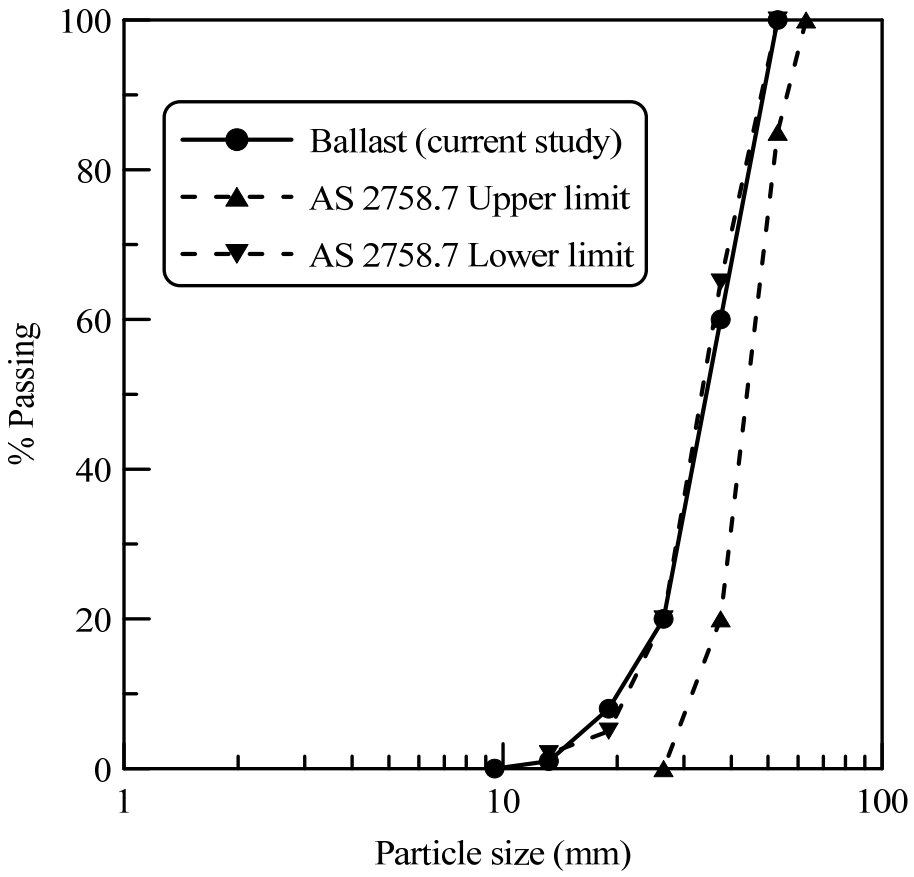

Figure 5.7 Particle size distribution of ballast used to study the cyclic behaviour of geogrid-reinforced ballast

5.4.2.2 *Geogrids*

Four types of geogrids labeled G1 to G4 with different aperture sizes were used as reinforcement in this current study. The physical characteristics and the technical specifications of the geogrids used are summarized in Table 5.1. The specific geogrids used in the study were decided based on the interface efficiency factor (α), defined as the ratio of the ballast-geogrid interface shear strength to the internal shear strength of ballast, obtained from direct shear testing (Indraratna et al. 2012).

Table 5.1 Physical characteristics and technical specifications of the geogrids used in the model track tests

Geogrid type	*Aperture shape*	*Aperture size (mm)*		*Rib thickness (mm)*		T_{ult} [a] (kN/m)		J_{sec} [b] *(2% strain) (kN/m)*	
		MD	CMD	MD	CMD	MD	CMD	MD	CMD
G1	Square	38	38	2.2	1.3	30	30	525	525
G2	Triangle	36	36	2.0	2.0	19	19	230	230
G3	Square	65	65	1.7	1.5	30	30	550	600
G4	Rectangle	44	42	1.0	1.0	30	30	500	500

[a] Ultimate tensile strength (manufacturer supplied values); [b] Secant tensile stiffness (manufacturer supplied values); MD-Machine direction; CMD-Cross machine direction.

5.4.3 Preparation of test specimens

A subballast layer composed of a sand-gravel mixture (150 mm thick) having a particle size distribution as presented in Figure 5.8 was placed at the bottom of the test chamber. The subballast layer was placed in three lifts of 50 mm each and compacted to attain a density of 2100 kg/m^3. A layer of load bearing ballast (325 mm thick) was then placed above the compacted subballast layer. The ballast specimens were prepared by sieving and mixing of aggregates to match the gradation curve shown in Figure 5.7. Pressure plates were also placed in the ballast, as described in the subsequent paragraphs (Figure 5.9). The ballast was compacted in three layers using a vibrating plate to achieve a target field density of 1550 kg/m^3. To minimize particle breakage during vibration, a 5 mm thick rubber pad was placed underneath

the vibrator. An assembly of sleeper (tie) and rail section was placed above the compacted ballast, and the space between the tie and vertical walls was filled with crib ballast up to 150 mm in thickness (Figure 5.10). Settlement plates were installed at the subballast-ballast interface and at the sleeper-ballast interface to record the settlement upon loading. All the test specimens were prepared in a similar manner except that a layer of geogrid was placed at either (a) the subballast-ballast interface or (b) 65 mm above the subballast layer in case of reinforced ballast. Four types of geogrids labeled G1 to G4 with different aperture sizes were used as reinforcement in this current study.

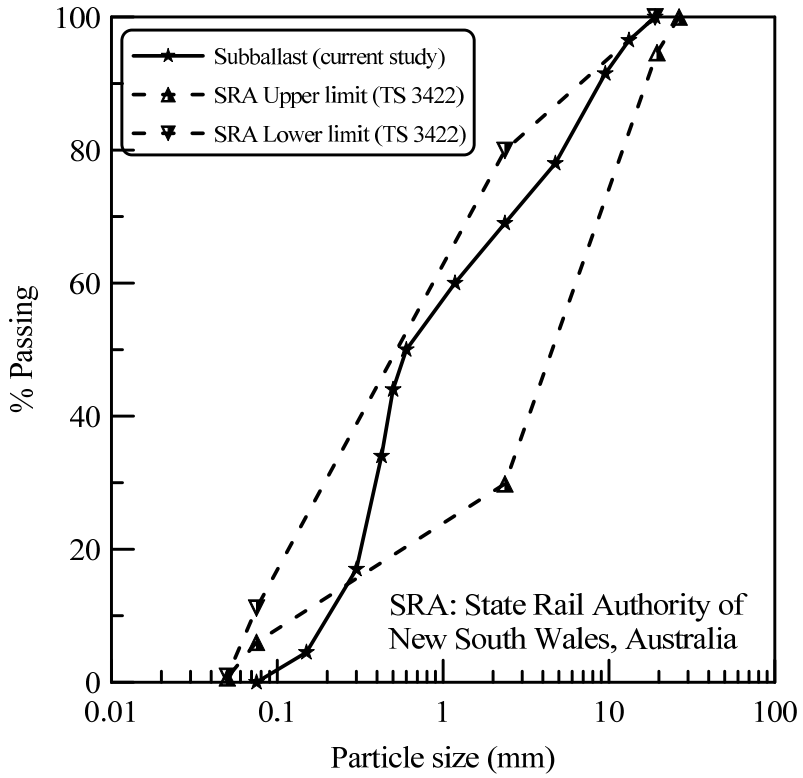

Figure 5.8 Particle size distribution of subballast

Two pressure cells were placed in the test chamber to capture the vertical stress variation along the ballast depth and establish the role of geogrid reinforcement in

reducing the subgrade stresses (i.e. vertical stress at the subballast-ballast interface). One of the pressure cells was aimed at capturing the stress at the subballast-ballast interface. The pressure cell was placed with its top surface slightly (i.e. 5 mm) below the surface of subballast layer, upon which the layer of sand-gravel mixture was laid (Figure 5.9). This was carried out to simulate a uniform subballast-ballast interface throughout the test specimen. This pressure cell would give the extent of vertical stress at the subballast-ballast interface. The second pressure cell was placed at the sleeper-ballast interface. The pressure cells used in the current study had a thickness of 12 mm and a diameter of 230 mm. They were rapid-response hydraulic earth pressure cells with grooved thick active faces based on semiconductor type transducers satisfying the aspect ratio and size of the cell requirements as formulated by previous researchers (e.g. Selig 1980; Weiler and Kulhawy 1982; Dunnicliff 1988; Clayton and Bica 1993).

In addition, optical fiber Bragg grating (FBG) sensors were also installed in the test tank under the rail to explore their possible use in railway applications to measure the lateral movement of ballast parallel to sleeper (tie). Four FBG sensors with a centre to centre spacing of 81 mm were attached to a polymeric sheet which was placed at the desired location to record the lateral strains in ballast at different depths below the sleeper soffit (Figure 5.9). A dynamic 4 channel optical sensing interrogator (Si 425) was employed for the demodulation of FBG sensors. More details on the history and characteristics of FBG sensors, the basic structure and working principle including the wavelengths of sensors used in this study are explained in detail in Chapter 7 of the thesis.

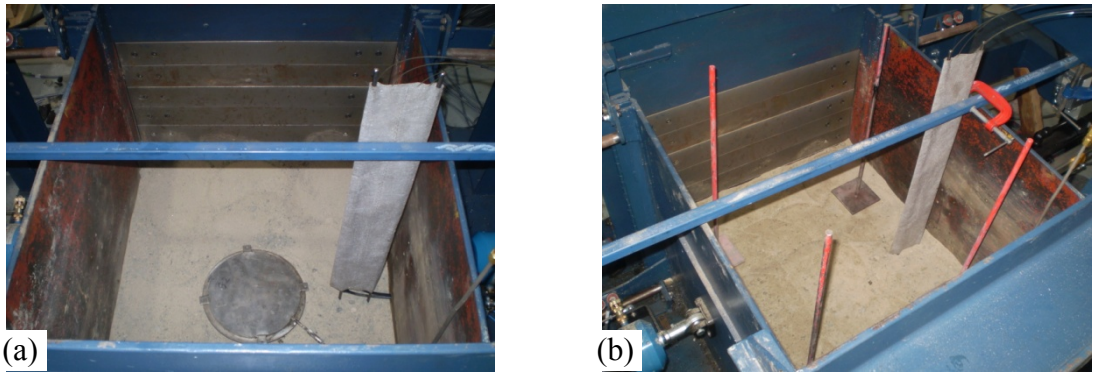

Figure 5.9 (a) Pressure cell placed at the subballast-ballast interface (b) Photograph showing the compacted subballast and the arrangement of settlement plates.

5.4.4 Test procedure

The electronic potentiometers used for recording the lateral movement of the plates were calibrated prior to each test. Three walls of the test tank were fixed and only the modified side wall was allowed to move laterally. The linear bearings were well lubricated to ensure the free movement of plates during the test. The boundary conditions adopted for testing are in accordance with real track conditions, as described earlier. A vertical stress of 460 kPa that corresponds to an axle load of 225 kN moving at a speed of 146 km/h was applied by means of a dynamic actuator (Esveld 2001; Atalar et al. 2001). A lateral pressure of 10 kPa was applied onto the modified side wall. The lateral pressure was applied at the middle of movable plates to eliminate any non-uniform distribution of the confining pressure. Le Pen and Powrie (2011) have shown that for a usual ballast depth of about 300 to 350 mm, the total confining pressure along the depth varies from 9.7 kPa to 10.1 kPa of which the predominant component is from the shoulder ballast, with relatively small contribution from weight of crib ballast, rail and sleeper. In this context, the

application of a uniform lateral pressure of 10 kPa on all the five movable plates is justified. This value of confining pressure also falls within the range of in-situ confining pressure of 10-30 kPa measured earlier by Indraratna et al. (2011). Tests were conducted up to 250000 load cycles. The lateral movement of the individual plates was recorded continuously by the potentiometers connected to a data acquisition system. The tests were halted at selected number of load cycles (i.e. N = 1, 100, 1000, 3000, 5000, 10000, 30000, 50000, 100000 and 200000) to record the readings from the settlement plates.

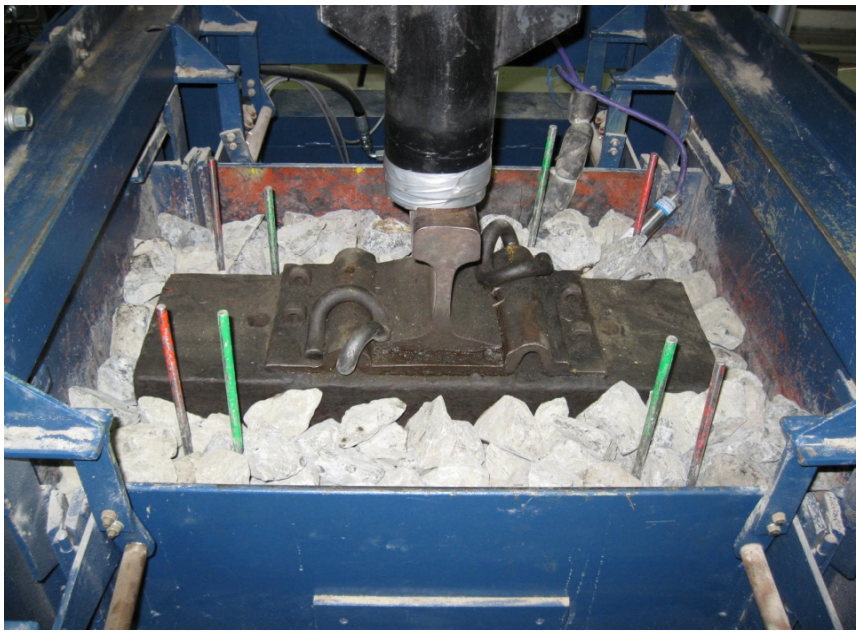

Figure 5.10 Plan view of the prepared ballast specimen ready for testing

5.4.5 Degradation assessment of ballast

5.4.5.1 *Ballast breakage index (BBI)*

The ballast specimen was sieved at the end of test to evaluate the change in gradation and quantify the breakage of particles. The degradation of ballast was quantified in

terms of ballast breakage index (BBI) proposed originally by Indraratna et al. (2005). The evaluation of BBI employs the change in the fraction passing a range of sieve sizes due to the loading (Figure 5.11). By utilizing a linear particle size axis, BBI can be found from Equation 5.1, where the parameters A and B are defined in Figure 5.11. The BBI can theoretically vary from zero to 100%. Higher the value of BBI, the greater is the degree of ballast degradation.

$$BBI = \frac{A}{(A+B)} \tag{5.1}$$

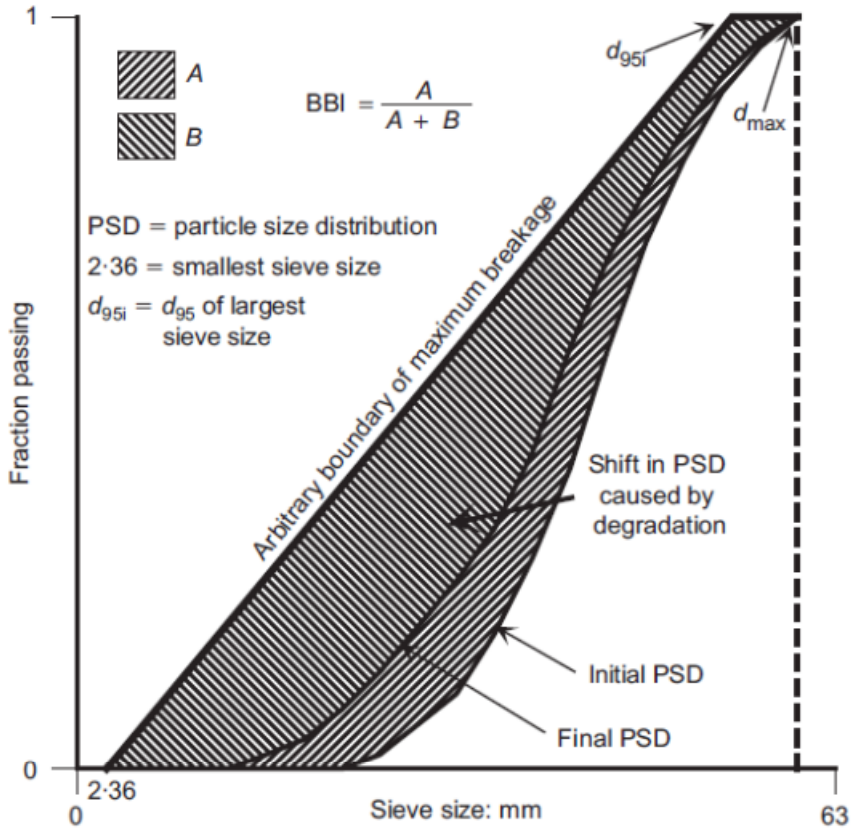

Figure 5.11 Ballast breakage index (after Indraratna et al. 2005)

5.5 SUMMARY

The laboratory experiments conducted to explore the engineering behavior of geogrid-reinforced ballast were described in this Chapter. It also presented the details related to the large-scale process simulation test (PST) apparatus, test materials, specimen preparation methods, and the experimental procedure followed including the instrumentation used to measure the deformations of ballast. The large-scale process simulation test (PST) apparatus available at University of Wollongong was modified to allow the non-uniform lateral spreading of particles along the ballast depth. One of the side walls of PST apparatus was replaced by five independent movable plates to monitor the variation of lateral displacement with depth parallel to the ties (sleepers). Only one side required this modification exploiting symmetry along the longitudinal centreline.

The results from the model track tests conducted using MPST apparatus are presented and discussed in Chapter 6.

6 DEFORMATION AND DEGRADATION BEHAVIOUR OF GEOGRID-REINFORCED BALLAST

6.1 INTRODUCTION

The permanent deformation and degradation behaviour of unreinforced and geogrid-reinforced ballast under cyclic loading has been investigated using a large-scale modified process simulation test (MPST) apparatus (Figure 5.10) simulating a small track section. The stabilisation aspects of ballast using various types of geogrids were also studied in these model tests. To quantify ballast degradation, each specimen was sieved before and after testing. This Chapter describes the deformation and degradation behaviour of unreinforced and geogrid-reinforced ballast under cyclic loading. The influence of geogrid aperture size (A) and the geogrid placement position on the ability of geogrid to arrest the lateral deformations in ballast are presented and discussed through laboratory model test results.

6.2 LATERAL DISPLACEMENTS IN BALLAST BENEATH THE SLEEPER EDGE

Ballast being an unbounded granular medium, spreads laterally when subjected to cyclic loading. The lateral displacement of ballast in the current study is captured by monitoring the movement of the side wall of the MPST apparatus comprising of five independently movable plates.

Figure 6.1 shows the variation of lateral displacements in unreinforced and geogrid-reinforced ballast with the number of load cycles (N) determined from the movement

of the bottom plate (i.e. plate 1). It is observed from Figure 6.1 that the lateral displacements occur mainly during the initial 50000 load cycles after which the displacements remain relatively constant. As expected, Figure 6.1 indicates that the geogrid-reinforced ballast undergoes lesser lateral displacement in comparison to unreinforced ballast. This could be attributed to the ballast-geogrid interaction in the form of interlocking of particles in the geogrid apertures that inhibits the particle movement. The almost constant lateral displacement for $N > 50000$ suggests that the degree of ballast-geogrid interlock remains unaffected upon repeated load applications. In a practical sense, this implies that once the required ballast-geogrid interlock is attained, the geogrid continues to perform its intended purpose of arresting the lateral displacement of ballast even at 250000 load cycles. However, the extent of reduction in lateral displacement varies depending upon the geogrid type and its placement position. The effectiveness of geogrid in stabilising ballast under cyclic loading has a significant bearing on the maintenance of rail tracks. For example, the reduction in the lateral movement of ballast decreases the need for additional layers of crib and shoulder ballast during maintenance.

The variation of lateral displacements in unreinforced and geogrid-reinforced ballast with the number of load cycles (N) obtained from the movement of other movable plates (i.e. plates 2 to 5) is shown in Figure B.1-Figure B.4 of Appendix B.

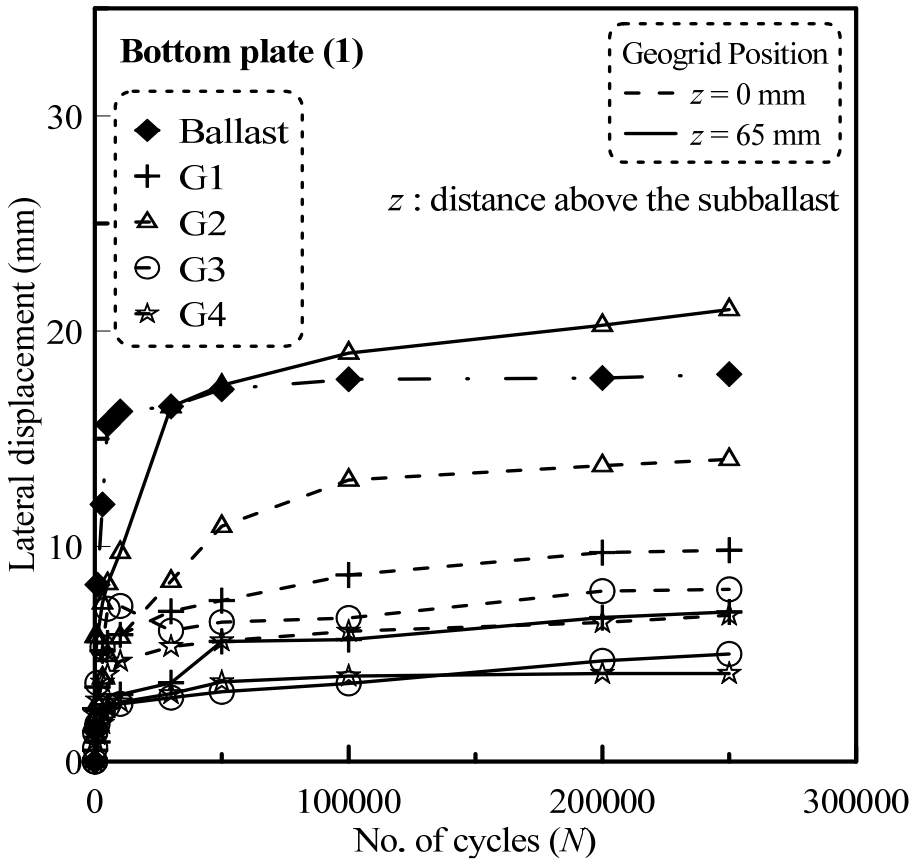

Figure 6.1 Lateral displacement in unreinforced and geogrid-reinforced ballast at the bottom plate (plate 1)

6.2.1 Lateral strain profile along the ballast depth

Figure 6.2 (a) and (b) show the lateral strain profile of unreinforced ballast and that reinforced with various geogrids, for geogrid placed at z = 0 and 65 mm respectively (with z defined as the distance above the subballast). The lateral strains presented here correspond to N = 250000. From Figure 6.2 (a) and (b) it is evident that the lateral strains in geogrid-reinforced ballast are smaller in comparison to unreinforced ballast. This is due to the non-displacement boundary conditions at the ballast-geogrid interface due to the interlocking of particles. For instance, for z = 0 mm, the geogrids G3 and G4 reduces the lateral strains at the subballast-ballast interface by

55% and 60% respectively. Although a planar reinforcement, geogrid also confines the ballast that is away from its placement position. This is attributed to the high angularity of ballast that facilitates transfer of reinforcing benefits away from its placement position albeit less efficiently. As expected, with increasing vertical distance, the lateral strain increases, and subsequently becomes similar to that of unreinforced ballast (Figure 6.2 (a) and (b)).

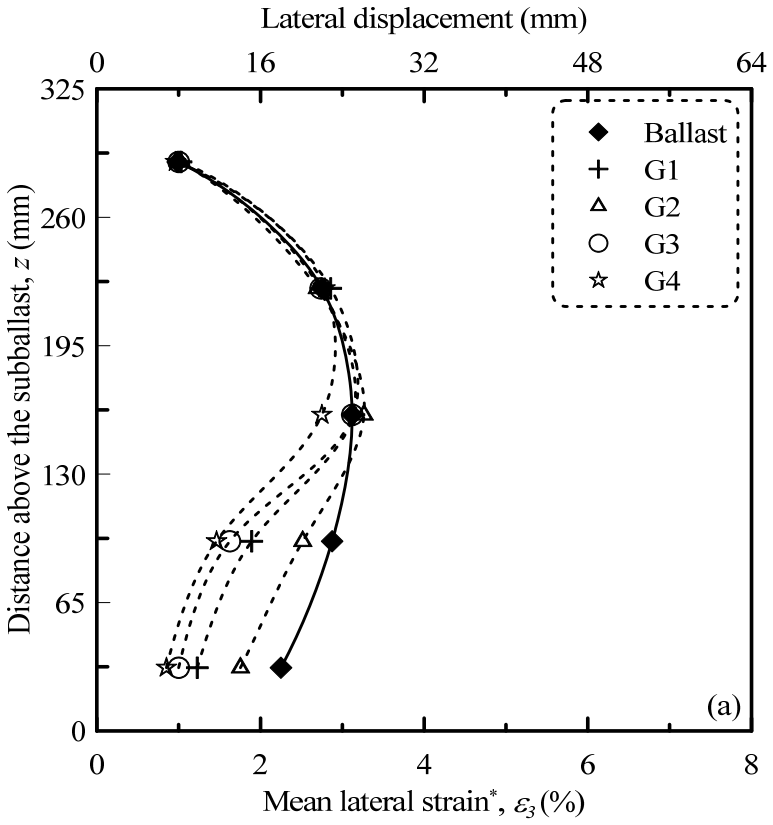

*Mean lateral strain is determined over the original width of specimen of 800 mm

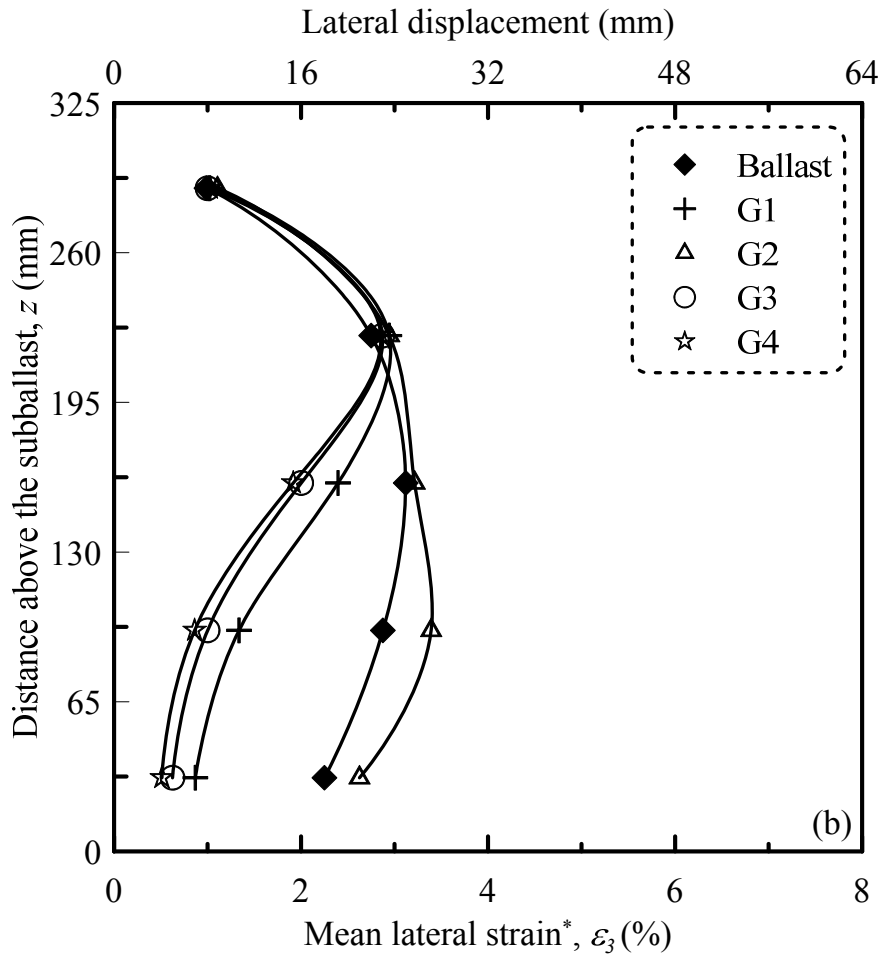

Figure 6.2 Lateral strain profile of unreinforced and geogrid-reinforced ballast beneath the sleeper edge for geogrid placed at (a) z = 0 mm and (b) z = 65 mm

Figure 6.2 (b) indicates that geogrids have a significantly higher effect on restraining the lateral strains in ballast when placed at z = 65 mm. For this placement location, the geogrids G3 (square) and G4 (rectangular) decreases the lateral strains at the subballast-ballast interface by 65% and 70% respectively. However, the ballast reinforced with geogrid G2 (triangular) exhibits higher lateral strains when compared to unreinforced conditions due to ineffective interlocking of particles. It may be mentioned here that for reinforcement placed within the ballast, a ballast-geogrid interlock stronger than the inter-particle interlock in an unreinforced sample is a

prerequisite to arrest the lateral displacement of ballast. This is attained only in the case of geogrids with A/D_{50} (i.e. the ratio geogrid aperture size to the mean particle size of ballast) lying in the optimum interlock zone (OIZ) and diminishing interlock zone (DIZ) as defined by Indraratna et al. (2012). Based on the large-scale direct shear testing of ballast-geogrid interfaces, Indraratna et al. (2012) classified the ratio A/D_{50} into three distinct zones; feeble interlock zone (FIZ; with $A/D_{50} < 0.95$), optimum interlock zone (OIZ; with A/D_{50} in the range of 0.95 to 1.20) and diminishing interlock zone (DIZ; with $A/D_{50} > 1.20$). Therefore, geogrid G2 with A/D_{50} lying in the FIZ fails to confine the ballast from displacing laterally. On the other hand, the geogrid G2 when placed at the subballast-ballast interface performs better than the unreinforced conditions (Figure 6.2a). This is because the subballast-ballast interface is the weakest track interface owing to the complete absence of interlock between the bigger ballast particles and subballast containing smaller particles. Hence, the geogrid G2 that can at least cause interlocking of small sized particles, when placed at the base of ballast layer makes the interface stronger than unreinforced conditions, thereby reducing the extent of lateral displacement of ballast.

6.3 LATERAL SPREAD REDUCTION INDEX (LSRI)

The improvement in the performance of geogrid-reinforced ballast can be represented by a normalized parameter called Lateral Spread Reduction Index (LSRI), defined as the ratio of the difference in lateral displacement (δ) of unreinforced and reinforced ballast to the lateral displacement of unreinforced ballast (Equation 6.1). LSRI of zero indicates unreinforced condition whereas a value of

unity represents complete arrest of particle spreading. On the other hand, a negative value of LSRI indicates an increase in lateral displacement due to the inclusion of reinforcement.

$$LSRI = \frac{(\delta_{unreinforced} - \delta_{reinforced})}{\delta_{unreinforced}} \quad 6.1$$

The variation of LSRI with distance from the subballast-ballast interface for different geogrid types and their placement positions within the test apparatus is shown in Figure 6.3. Figure 6.3 (a) for z = 0 and Figure 6.3 (b) for z = 65 mm depict that the LSRI is a function of the geogrid type and its placement location within the test apparatus. The negative LSRI observed for geogrid G2 placed within the ballast is due to the increased lateral strains in comparison to unreinforced ballast which is an indication of ballast destabilization (Figure 6.3b). It is seen that the LSRI decreases significantly with distance from the subballast-ballast interface and subsequently becomes zero suggesting that the reinforcement has no effect in restraining the lateral movement of ballast beyond this point. The distance from the subballast-ballast interface to the point at which the LSRI becomes zero could be treated as the geogrid influence zone (GIZ). In a practical sense, it represents the zone of ballast that is subjected to enhanced confining pressure owing to the geogrid inclusion thus undergoing a smaller lateral displacement. On the other hand, LSRI represents the extent of increase in confining pressure within the GIZ, hence defines the effectiveness of reinforcement in the event of equal GIZ.

It is observed from Figure 6.3 that the GIZ is less than the full thickness of ballast for both the geogrid placement locations. A closer observation reveals that even within the GIZ, the LSRI decreases rapidly with vertical distance away from the geogrid. These observations imply that the increase in confining pressure on ballast due to the reinforcement exists only over a certain portion of the sample, with the uniform increase in confinement occurring only in about 40-50% of the total GIZ. These findings are in sharp contrast to the existing theories that inherently assume uniform increase in confinement throughout the sample height (Gray et al. 1982; Athanasopoulos 1994; Ruiken and Ziegler 2010). It may be clarified that the current study could capture the lateral strain profiles along the ballast depth and, the GIZ including the possible variation of enhanced confining pressure owing to the use of PST apparatus, with side-wall consisting of five independently movable plates.

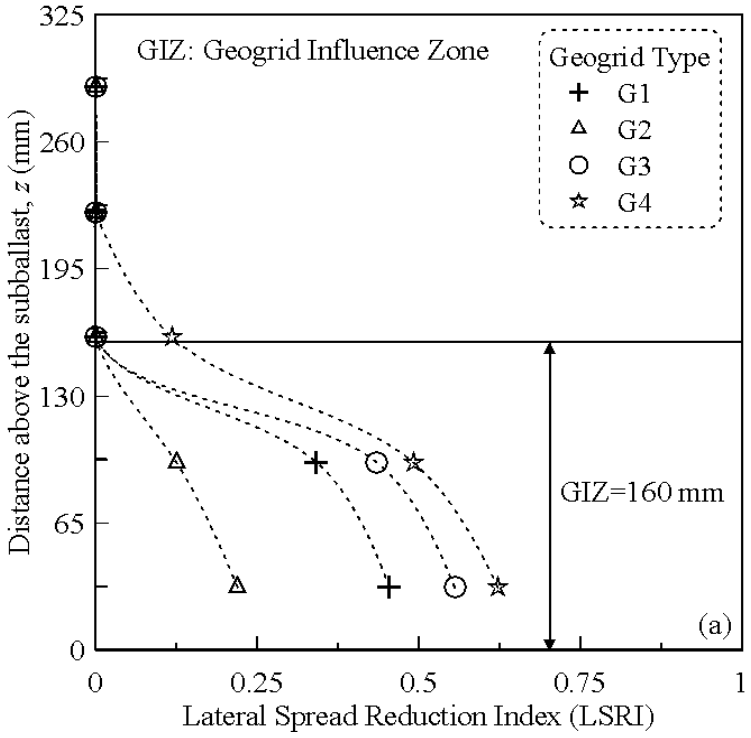

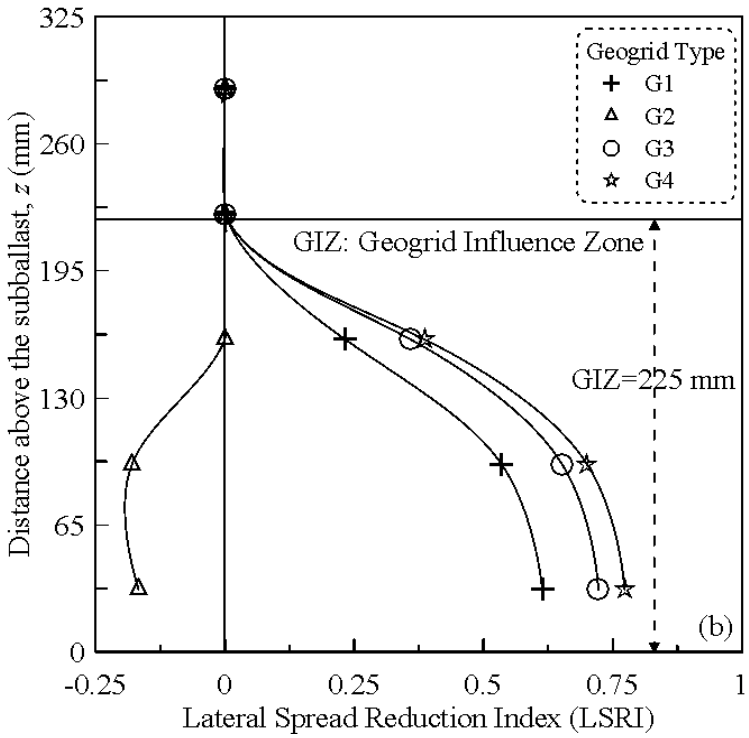

Figure 6.3 Variation of lateral strain reduction index (LSRI) with distance for geogrid placed at (a) z = 0 mm and (b) z = 65 mm

6.4 GEOGRID INFLUENCE ZONE (GIZ) FOR BALLAST REINFORCED WITH VARIOUS GEOGRIDS

Table 6.1 summarizes the GIZ and the average LSRI along the depth of ballast reinforced with various geogrids. It is observed from Table 6.1 that for a given geogrid placement position, the GIZ attained is a constant value of about 160 mm ($4.60D_{50}$) and 225 mm ($6.45D_{50}$) for various geogrids. However, the extent by which they reduce the lateral strains is different, whereby the ones effectively reducing the lateral strains are expected to improve the track performance significantly. It is further seen from Table 6.1 that the geogrids G1 and G3 offer higher GIZ of 225 mm ($6.45D_{50}$) when placed at z = 65 mm in comparison to a GIZ of 160 mm ($4.60D_{50}$)

for the grid placed at z = 0 mm. This is because the presence of denser subballast below the geogrid inhibits the particles from striking through the geogrid apertures, thereby leading to a weaker particle-geogrid interlock. On the other hand, when the geogrid is placed within the ballast a strong particle-geogrid interlock is established as the particles can now protrude through the geogrid apertures due to the presence of same material both above and below the geogrid, thereby significantly increasing the GIZ.

Table 6.1 Lateral spread reduction index (LSRI) and geogrid influence zone (GIZ) for unreinforced and geogrid-reinforced ballast

Geogrid type	*LSRI*	*GIZ (mm)*
Ballast	NA	NA
G1*	0.16	160
G1+	0.27	225
G2*	0.06	160
G2+	-0.07	0
G3*	0.20	160
G3+	0.35	225
G4*	0.25	225
G4+	0.37	225

Geogrid placement position: *Subballast-ballast interface (i.e. z = 0 mm); +65 mm above the subballast (i.e. z = 65 mm).

6.5 SETTLEMENT OF BALLAST

The vertical settlement of ballast upon cyclic loading is determined by deducting the vertical displacement at the sleeper-ballast and the ballast-subballast interface. The occurrence of vertical settlement with the number of load cycles (N) for unreinforced ballast and that reinforced with various geogrids is shown in Figure 6.4. It is observed that the vertical settlement increases rapidly during the initial 50000 load cycles for both unreinforced and geogrid-reinforced ballast. The reduced rate of vertical settlement upon further application of load cycles coincides with the reduced rate of lateral displacement in this loading regime (see Figure 6.1) highlighting that vertical settlement is caused predominantly due to the lateral displacement of ballast. Figure 6.4 further depicts that geogrid reduces the extent of settlement when compared to unreinforced ballast, which is in accordance with the results reported by the previous researchers (Matharu 1998; Brown et al. 2007; Indraratna et al. 2010; Qian et al. 2011). For instance, the geogrid G3 reduces the vertical settlement by 38% and 54% when placed at z = 0 and 65 mm, respectively. The reduction in the extent of vertical settlement due to reinforcement is attributed to the reduced lateral displacement of ballast, the effectiveness of which is proportional to the LSRI. For example, the geogrid G3 exhibiting a higher LSRI gives a relatively lower settlement of 14.7 mm in comparison to 16.5 mm for geogrid G1. In a practical sense, the reduced vertical settlement of ballast highlights the beneficial effect of geogrid in maintaining the track alignment.

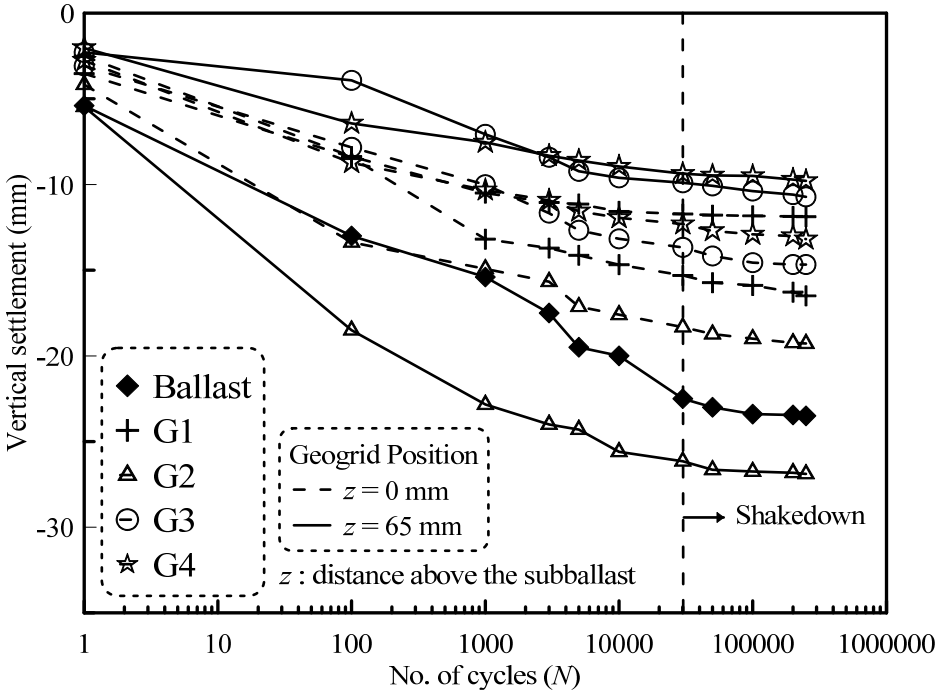

Figure 6.4 Variation of vertical settlement of unreinforced and geogrid-reinforced ballast with the number of load cycles

6.5.1 Axial strain ratio for unreinforced and reinforced ballast

It is well known that the occurrence of axial strain (ε_a) with the number of load cycles (N) is a function of the axial strain at the first cycle (e.g. Alva-Hurtado and Selig 1981). In this view, the axial strain ratio ε_{ar}, defined as the ratio of axial strain (ε_a) to the axial strain at first cycle (ε_{a1}), of both unreinforced and geogrid-reinforced ballast is plotted with respect to the number of load cycles (N) (Figure 6.5). It is evident from Figure 6.5 that ε_{ar} fall in a narrow band for both unreinforced and geogrid-reinforced ballast (irrespective of the geogrid type and its placement position). While unreinforced ballast is known to exhibit such behaviour, the current study has established that even in the case of reinforced ballast the axial strain (ε_a)

response with the number of load cycles (N) is a function of the axial strain at the first cycle.

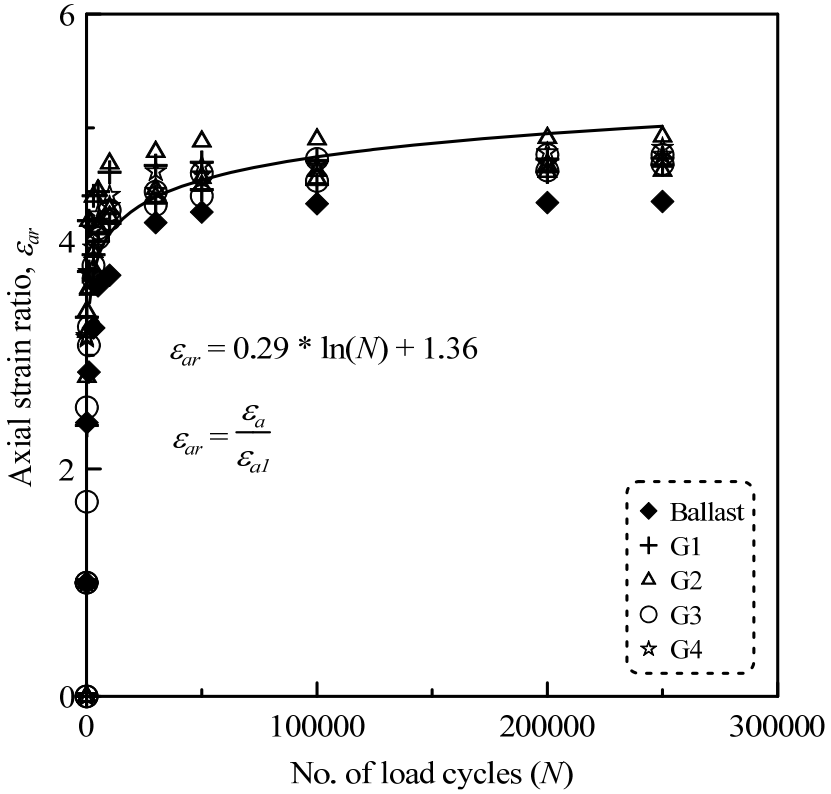

Figure 6.5 Variation of axial strain ratio with number of cycles

6.6 VOLUMETRIC AND SHEAR STRAIN IN BALLAST

The volumetric strain (ε_v) and shear strain (ε_s) in ballast can be determined by using Equation 6.2 (Timoshenko and Goodier. 1970);

$$\epsilon_v = \epsilon_1 + \epsilon_2 + \epsilon_3 \qquad 6.2a$$

$$\epsilon_s = \frac{\sqrt{2}}{3}\left\{\sqrt{(\epsilon_1 - \epsilon_2)^2 + (\epsilon_2 - \epsilon_3)^2 + (\epsilon_3 - \epsilon_1)^2}\right\} \qquad 6.2b$$

In equations 6.2 (a) and 6.2 (b), ϵ_1, ϵ_2 and ϵ_3 are the average strains in the vertical, longitudinal and transverse directions.

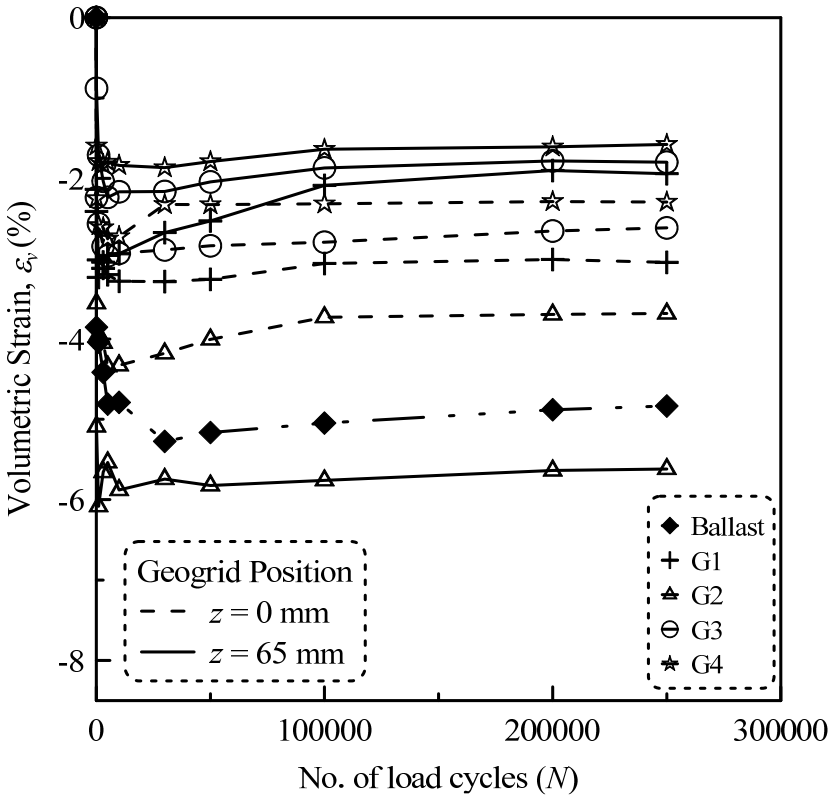

Figure 6.6 Volumetric strain of unreinforced and reinforced ballast

The variation of volumetric (ε_v) and shear strain (ε_s) with the number of load cycles (N) for unreinforced ballast and that reinforced with various geogrids is shown in Figure 6.6 and Figure 6.7. It is observed from Figure 6.6 that all the ballast samples undergo volume reduction (i.e. cyclic densification) upon cyclic loading. However, the extent of volume reduction is relatively lower for reinforced ballast implying that geogrid stabilises the track without causing any significant densification, thus maintaining sufficient voids in it that are imperative for the quick drainage of water. Similarly, the geogrid-reinforced ballast exhibits reduced shear strain in comparison

to unreinforced ballast (Figure 6.7), which is an indication of increased shear strength due to the reinforcement. These experimental observations correlate well with the field study of geosynthetic-reinforced ballasted tracks reported earlier by Indraratna et al. (2010b).

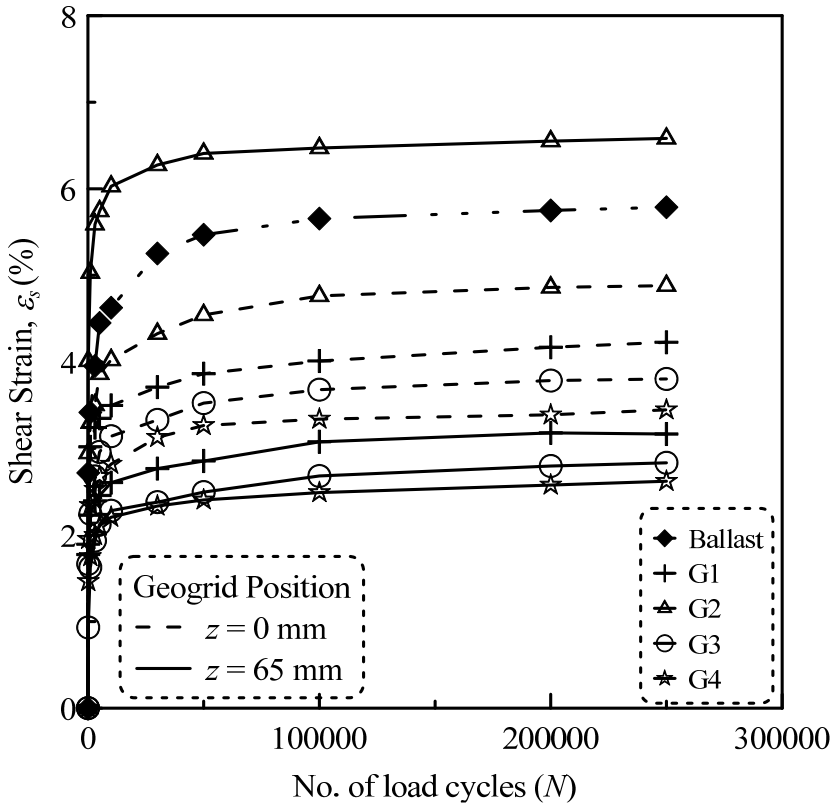

Figure 6.7 Shear strain of unreinforced and reinforced ballast

6.7 BREAKAGE OF PARTICLES

The degradation of granular materials upon loading occurs mainly due to the breakage of sharp corners, splitting of particles into two or more approximately equal parts and the attrition of asperities (Lees and Kennedy. 1975). A similar observation with respect to the degradation of ballast during cyclic loading was reported by Indraratna et al. (2005). The assessment of particle breakage is important in the sense

that it affects the vertical deformation and the ultimate strength of ballast (Raymond et al. 1976; Selig and Waters 1994), which in turn influences the track performance. In addition, the particle breakage contributes to the generation of fines which in the long-term accumulates and decreases the permeability of ballast that can eventually cause undrained failure of track during and after heavy rainfall.

In the current study, the breakage of ballast is evaluated at the end of test by determining the change in PSD of ballast upon loading. The initial and the final PSD in case of unreinforced ballast and that reinforced with geogrid G4 placed at z = 65 mm is shown in Figure 6.8. The particle breakage of unreinforced and geogrid-reinforced ballast, quantified in terms of ballast breakage index (BBI) proposed originally by Indraratna et al. (2005), is summarized in Table 6.2 BBI for unreinforced and geogrid-reinforced ballast. It is seen that unreinforced ballast undergoes a total particle breakage of 9.89%. However, the geogrid reinforcement reduces the extent of particle breakage. For example, the BBI of ballast reinforced with geogrid G3 placed at z = 0 and 65 mm is about 34% and 51% lower than that of unreinforced ballast. The reduction in particle breakage may be attributed to the interlocking of particles within the geogrid apertures that subsequently increases the confining pressure on ballast. However, owing to the different values of the LSRI and the GIZ, ballast reinforced with different geogrids undergoes different extent of breakage. For instance, as the GIZ of G1 and G3 increases from 160 mm (4.60D_{50}) to 225 mm (6.45D_{50}), the BBI reduces from 7.8% to 6% and from 6.5% to 4.8%, respectively. Here, the increased GIZ restrains a higher zone of ballast from lateral displacements that subsequently help reducing the extent of particle degradation.

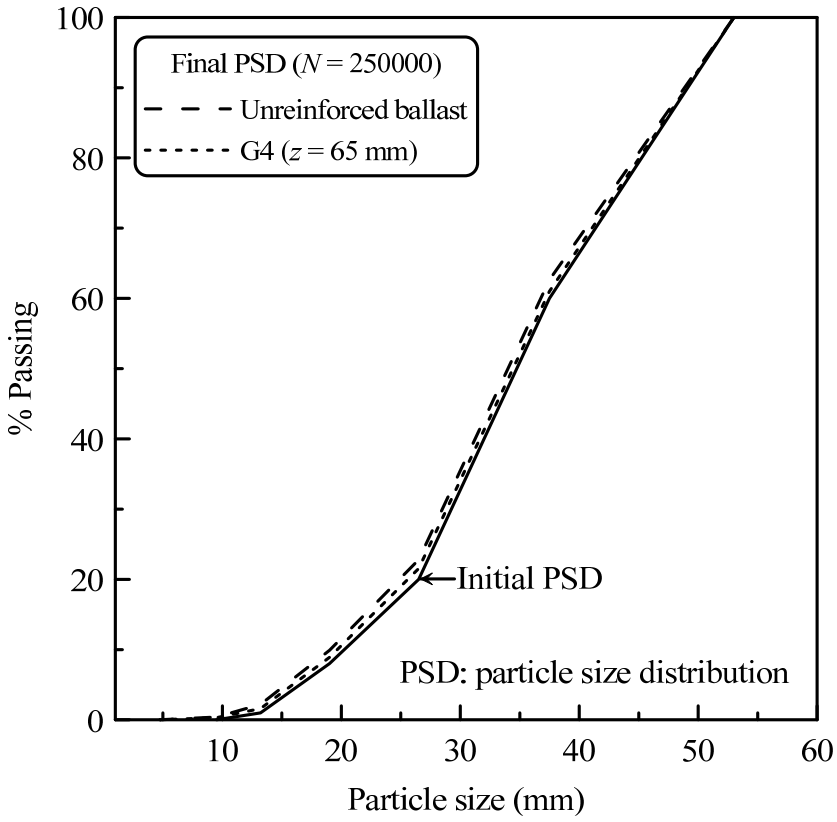

Figure 6.8 Change in PSD of ballast due to cyclic loading

Table 6.2 BBI for unreinforced and geogrid-reinforced ballast

Geogrid type	Ballast	G1*	G1+	G2*	G2+	G3*	G3+	G4*	G4+
BBI (%)	9.89	7.80	6.00	8.90	11.00	6.50	4.80	6.30	4.60

Geogrid placement position: *Subballast-ballast interface (i.e. z = 0 mm); +65 mm above the subballast (i.e. z = 65 mm).

6.7.1 Degradation of different sized particles

The particle degradation evaluated in terms of ballast breakage index (*BBI*), represents breakage of the entire ballast specimen. However, to enumerate the extent

of degradation of different sized particles within the ballast sample, the data is plotted in terms of variation of ΔW_k (the difference in percentage retained before and after testing) with the sieve size for unreinforced and geogrid-reinforced ballast. The sum of positive ΔW_k represents Marsal's breakage index, B_g.

Figure 6.9 and Figure 6.10 show the variation of ΔW_k with sieve size for unreinforced and geogrid-reinforced ballast. It is relevant to mention here that a positive ΔW_k for a given sieve size represents a decrease in percentage retained in that sieve due to particle breakage. In contrast, a negative ΔW_k in a smaller sieve indicates an increase in percentage retained in that sieve resulting from the passing of broken particles through the larger sieves. Figure 6.9 and Figure 6.10 reveal that particles in the size range of 53 to 37.5 mm are more vulnerable to breakage than smaller grains. This is due to the presence of more number of natural flaws in them (Lade et al. 1996). As expected, smaller sized particles (< 19 mm) show increase in percentage retained due to the breakage of bigger particles. Moreover, the effect of geogrid in reducing the breakage of particles, specifically the bigger ones, is also clearly evident from Figure 6.10. The value of B_g for unreinforced ballast and that reinforced with different geogrids is summarised in Table 6.3.

Table 6.3 B_g for unreinforced and geogrid-reinforced ballast

Geogrid type	Ballast	G1*	G1$^+$	G2*	G2$^+$	G3*	G3$^+$	G4*	G4$^+$
B_g	2.80	2.30	1.80	2.60	3.21	1.90	1.71	1.75	1.55

Geogrid placement position: *Subballast-ballast interface (i.e. z = 0 mm); $^+$65 mm above the subballast (i.e. z = 65 mm).

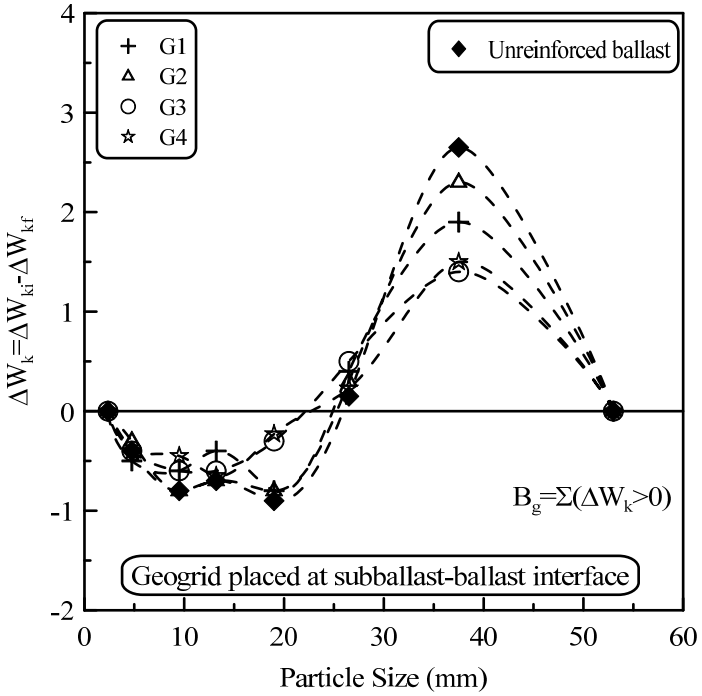

Figure 6.9 Variation of particle distribution with grain size for unreinforced and geogrid-reinforced ballast

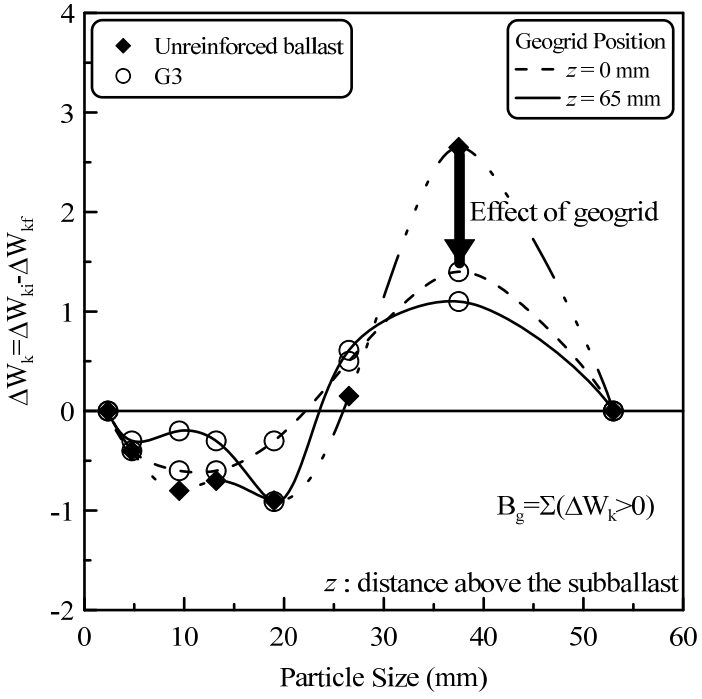

Figure 6.10 Variation of particle distribution with grain size for ballast reinforced with geogrid G3 placed at z = 0 and z = 65 mm

6.7.2 Relationship between *BBI* and Marsal's breakage index, B_g

The breakage of ballast is generally evaluated in terms of ballast breakage index (*BBI*), an index explicitly developed to assess the degradation of ballast. However, prior to BBI the degradation of ballast was evaluated in terms of Marsal's breakage index, B_g (Indraratna et al. 1998, 2004). In this context, it is difficult to compare the extent of particle breakage (*BBI*) with that available in the literature in terms of B_g. Therefore, the breakage data from the current study is plotted in the form of variation of B_g with respect to BBI (Figure 6.11). Figure 6.11 depicts that the value of B_g varies in the range of 1.55 to 3.21 for ballast samples exhibiting BBI in the range of 4.6% to 11%. It is seen that a linear relationship exists between *BBI* and B_g which could be given by Equation 6.3, as follows:

$$B_g = 0.25 \times BBI + 0.32 \qquad 6.3$$

This empirical relationship helps in the conversion of breakage from one form to another, without requiring the details pertaining to the initial and final particle size distribution of ballast, so that a quick and realistic comparison of particle degradation can be made.

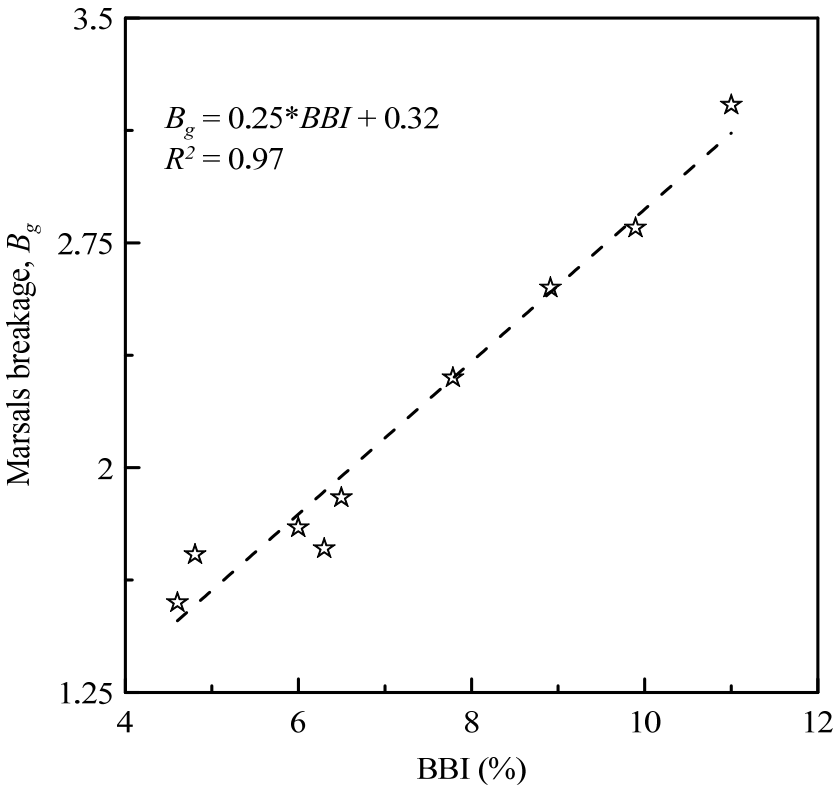

Figure 6.11 Variation of Marsal's breakage, B_g with ballast breakage index (BBI)

6.7.3 Effect of particle breakage on the volumetric and shear strain in ballast

It is well known that particle degradation leads to the cyclic densification of ballast and the reduction in shear strength due to the breakage of sharp angular projections (Indraratna et al. 1998; Thakur 2011). In this view, the variation of volumetric and shear strains in ballast with respect to the ballast breakage index (BBI) is presented in Figure 6.12 and Figure 6.13. It is evident that both volumetric strain (i.e. cyclic densification) and shear strain increases with the increase in BBI. It is to be noted here that the migration of broken fragments into the ballast voids is responsible for the increased densification with the increase in particle breakage. Similarly, the reduction in shear strength with the increase in particle breakage is responsible for the increased shear strain of ballast.

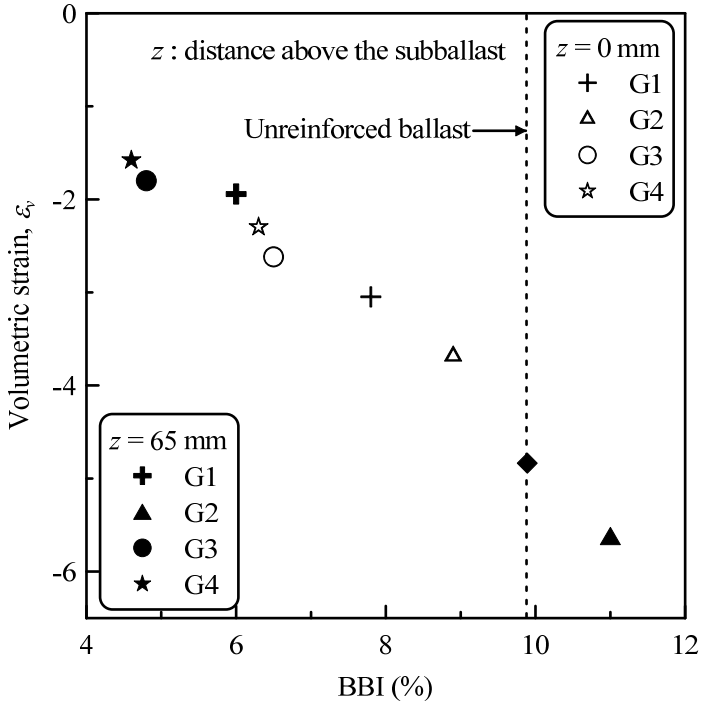

Figure 6.12 Variation of volumetric strain with the particle breakage (BBI)

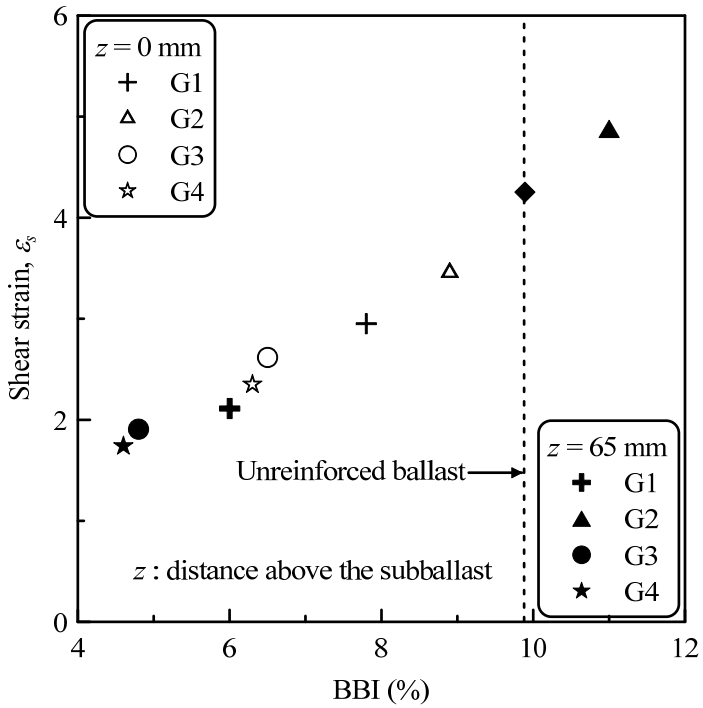

Figure 6.13 Variation of shear strain with the particle breakage BBI

6.8 ROLE OF A/D_{50} ON LATERAL SPREAD REDUCTION INDEX (LSRI)

Figure 6.14 presents the variation of average LSRI along the ballast depth with the ratio A/D_{50}, for both the geogrid placement positions (i.e. at z = 0 and 65 mm). It is noted that for geogrid placed at subballast-ballast interface, the average LSRI increases significantly from 0.06 to 0.25 as A/D_{50} increases from 0.6 to 1.20. This may be attributed to the better ballast-geogrid interlock attained as the geogrid aperture size increases for a given ballast size. The geogrid G4 with an A/D_{50} of 1.21 gives a maximum LSRI of 0.25. However, with the further increase in A/D_{50} from 1.21 to 1.85 the average LSRI decreases from 0.25 to 0.20. For the geogrid placed at 65 mm above the subballast, the average LSRI follows an almost similar trend with A/D_{50} except that the geogrid G2 exhibits a negative LSRI.

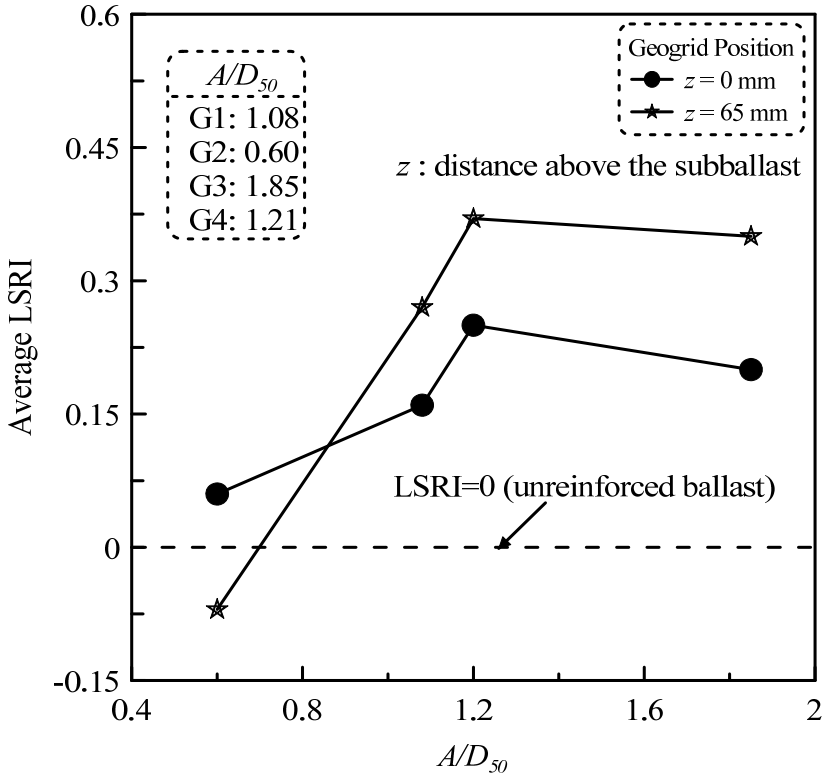

Figure 6.14 Variation of average LSRI with A/D_{50}

Figure 6.14 depicts that while the geogrid reinforcement in general arrests the lateral spread of ballast, reinforcement with an improper geogrid placed at an incorrect location can destabilize the ballast (negative LSRI). These observations emphasize the importance of properly selecting the geogrid type and placing it at a correct location if the benefits of reinforcement in track stabilization are to be accomplished.

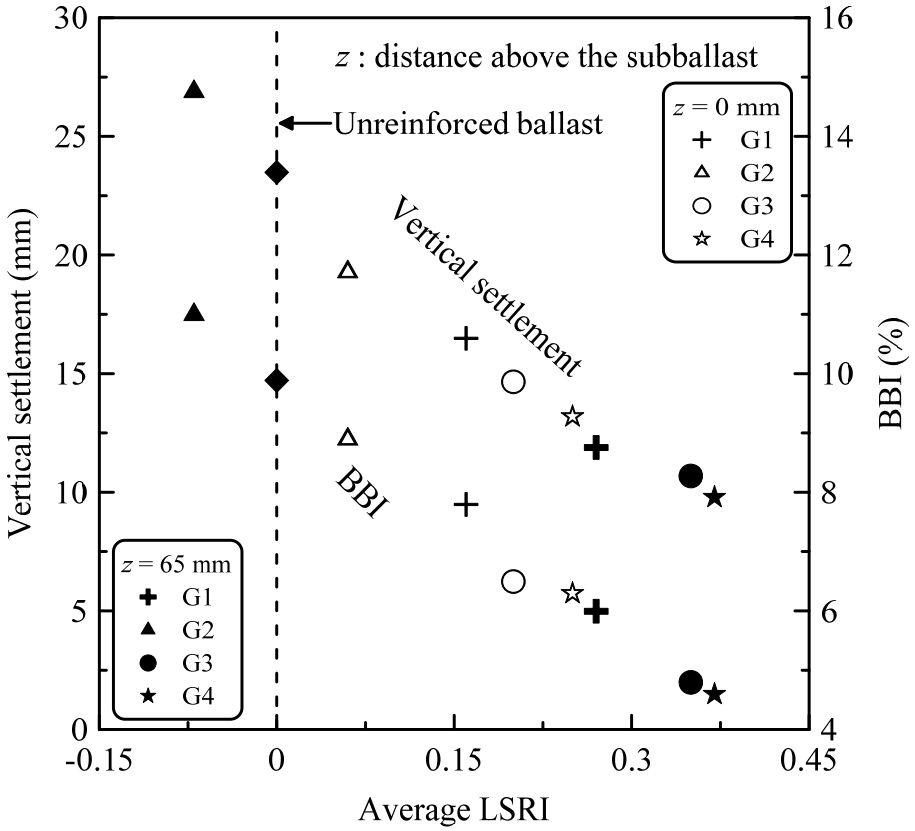

Figure 6.15 Variation of vertical settlement and BBI with LSRI

6.9 ROLE OF LSRI ON VERTICAL SETTLEMENT AND BBI

In order to establish the influence of lateral displacement of ballast on the settlement and particle breakage, the vertical settlement and BBI is plotted with respect to the average LSRI (Figure 6.15). It is observed that as the average LSRI increases both

the vertical settlement and the particle breakage reduces significantly. The vertical settlement and BBI decreases from about 23.5 to 9.8 mm and 9.89% to 4.6%, respectively, as the average LSRI increases from zero to 0.37. In other words, Figure 6.15 highlights the importance of arresting the lateral spread of ballast if the vertical settlement and particle degradation are to be reduced.

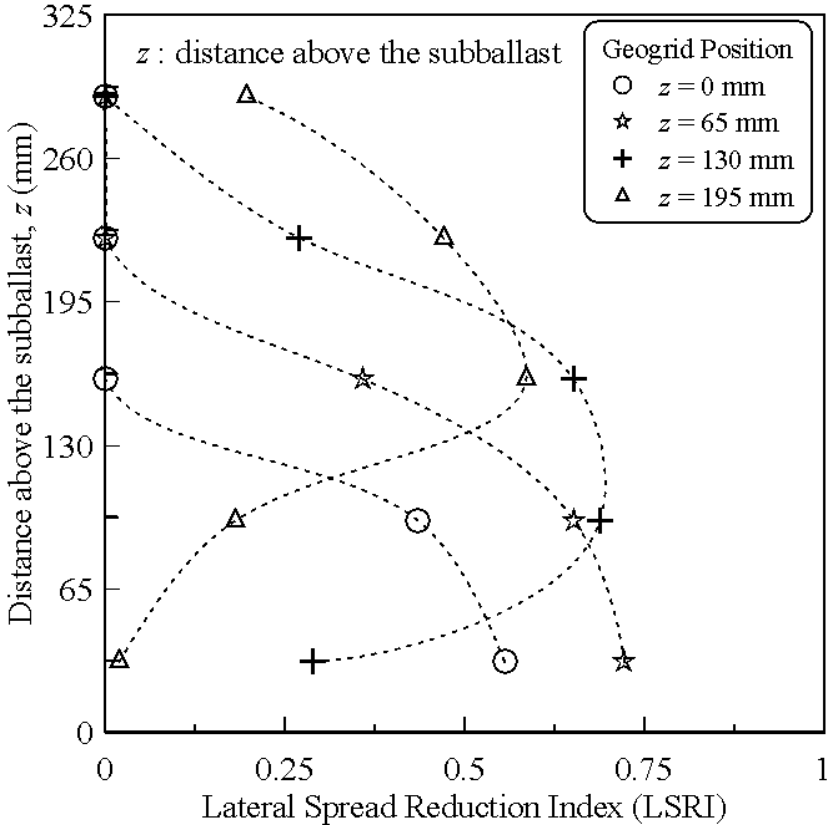

Figure 6.16 Variation of lateral spread reduction index (LSRI) with distance for different placement positions of geogrid G3

6.10 OPTIMUM GEOGRID PLACEMENT POSITION

In order to determine the optimum geogrid placement position, additional tests were carried out with geogrid G3 placed at z = 130 and 195 mm. Figure 6.16 shows the

variation of LSRI along the ballast depth for various placement positions of G3. Irrespective of the placement location, it is observed that the effect of geogrid is maximum in its immediate vicinity and decreases rapidly with the vertical distance. However, for G3 placed at z = 130 and 195 mm, the effect of reinforcement exists both above and below the geogrid unlike the geogrids placed at z = 0 and 65 mm.

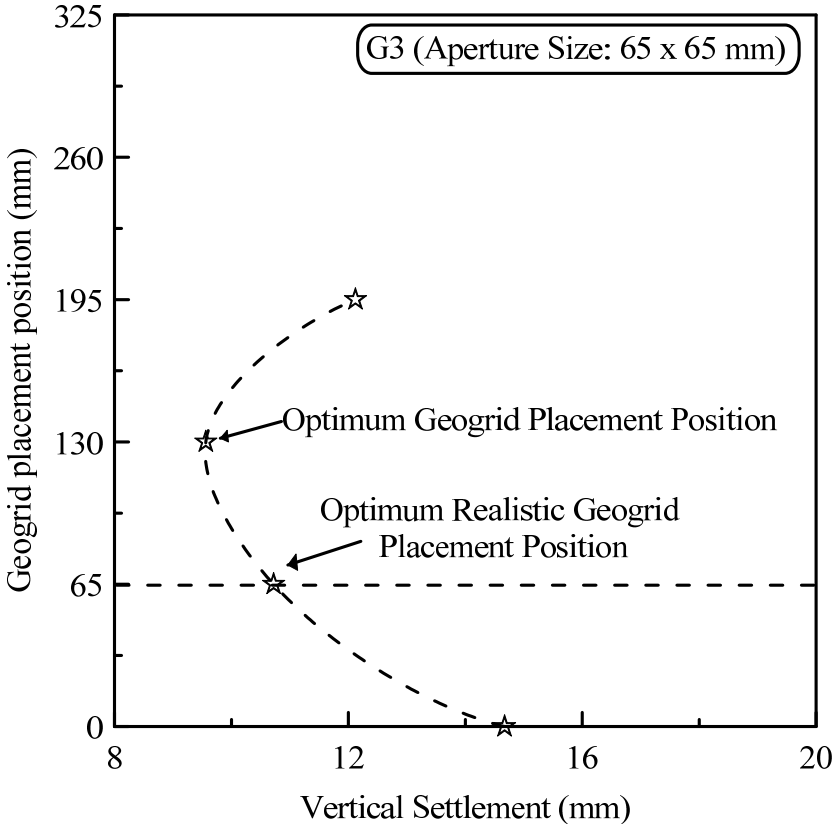

Figure 6.17 Settlement response of ballast for various placement positions of G3

The variation of settlement of ballast for different placement positions of G3 is plotted in Figure 6.17. It is clear that the settlement of ballast decreases from 14.67 mm to 10.72 mm when the placement position of geogrid is raised from zero to 65 mm above the subballast-ballast interface. A marginal decrease in the settlement of ballast from 10.72 to 9.56 mm is evident when the value of z is increased to 130 mm.

For z = 195 mm, the settlement of ballast increases again to 12.12 mm. This demonstrates that there is a threshold distance above which the ability of geogrid to effectively arrest the lateral movement of particles decreases, thus indicating that the optimum geogrid placement position is 130 mm above the subballast-ballast interface in this case. However, this placement position of geogrid may not be practically feasible as the geogrid may interfere with the ballast tamping and cleaning operations. In this context, to allow for ballast cleaning in the field, the realistic placement position of geogrid could still be treated as 65 mm above the subballast-ballast interface. However, the optimum placement location for geogrids with A/D_{50} lying in the FIZ (i.e. $A/D_{50} < 0.95$) is the subballast-ballast interface as placing them within ballast destabilizes the track.

6.11 VARIATION OF VERTICAL STRESS (σ_V) WITH BALLAST DEPTH

Two pressure cells were placed in the test chamber to capture the vertical stress variation along the ballast depth and establish the role of geogrid reinforcement in reducing the subgrade stresses (i.e. vertical stress at the subballast-ballast interface). The pressure cells used in the current study had a thickness of 12 mm and a diameter of 230 mm. They were rapid-response hydraulic earth pressure cells based on semiconductor type transducers complying the aspect ratio and size of the cell requirements as formulated by previous researchers (e.g. Selig 1980; Weiler and Kulhawy 1982; Dunnicliff 1988; Clayton and Bica 1993). One of the pressure cells was placed at the sleeper-ballast interface and the other at the subballast-ballast interface.

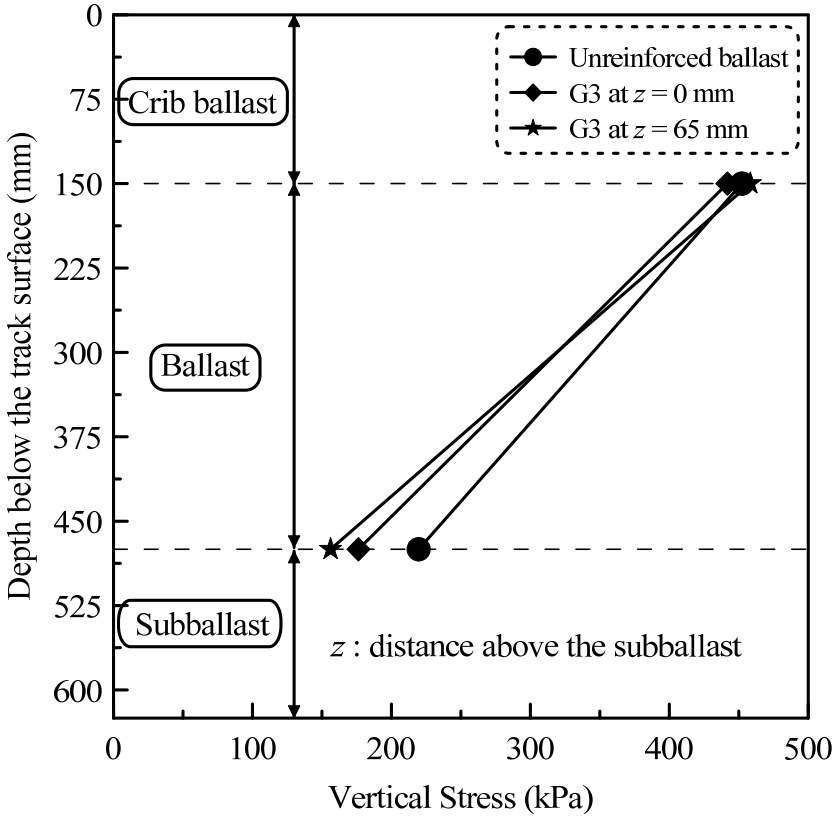

Figure 6.18 Variation of vertical stress along the ballast depth for unreinforced and geogrid-reinforced ballast

It is evident from Figure 6.18 that for unreinforced ballast, the vertical stress (σ_v) decreases significantly with depth from an applied vertical stress of 450 kPa to 220 kPa at the subballast-ballast interface. As expected, due to the better particle-geogrid interlock, the vertical stresses in subballast decreases from 176 kPa to 155 kPa, when the geogrid is placed at 65 mm above the subballast in comparison to that placed at the subballast-ballast interface. The reduction in vertical stresses due to the geogrid reinforcement is consistent with that reported in the past by Palmeira and Antunes (2010) for unpaved roads. The reduced vertical stresses in the subballast in case of geogrid-reinforced ballast also imply a subsequent reduction in the subgrade stresses. This signifies the role of reinforcement in dissipating the applied vertical stresses, to

an acceptable level at the subgrade soil, an observation that is particularly important in the case of railway tracks to be constructed on soft soils. In essence, the geogrid reinforcement of ballast would transform a portion of the applied vertical stress that otherwise would be transferred to the subgrade soil, towards increasing the confining pressure on ballast thereby enhancing the track stability.

6.12 SUMMARY

This Chapter described the permanent deformation and degradation behaviour of unreinforced and geogrid-reinforced ballast under cyclic loading. Laboratory tests were carried out using a modification to the large-scale prismoidal (triaxial) process simulation test apparatus, where one of its side walls was replaced by five independent movable plates to monitor the variation of lateral displacement with depth parallel to the ties (sleepers). During cyclic loading, both lateral displacement and vertical settlements occurred rapidly in the initial 50000 cycles implying that in reality, the newly constructed tracks would require speed restrictions to be imposed. The lateral strain variation along the ballast depth was captured for unreinforced ballast and that reinforced with various geogrids. It is shown that the geogrid reinforcement effectively arrests the lateral strains in ballast thus reducing the extent of ballast settlement and minimizing the particle breakage by about 58% and 53%, respectively. However, the effect of geogrid decreases with vertical distance from its placement position.

The degradation analysis of different sized particles reveals that the particles in the size range of 53 to 37.5 mm are more vulnerable to breakage than smaller grains.

Owing to the formation of new particles as a result of breakage of bigger particles, smaller sized particles (< 19 mm) increase by the end of test. The effect of geogrid in reducing the breakage of particles, specifically the bigger ones, is also clearly evident from the current study, thereby exemplifying the role of geogrid in stabilising the ballast. It is further shown that both volumetric and shear strain decrease due to the geogrid reinforcement of ballast. The particle degradation is shown to influence the extent of ballast densification and the shear strain in ballast layer.

Lateral spread reduction index (LSRI) and geogrid influence zone (GIZ) were proposed in the current study to assess the performance of geogrid-reinforced ballast. It is shown that LSRI is influenced by the geogrid type and its placement location. For geogrids placed at the subballast-ballast interface, the LSRI varies from 0.06 to 0.25. However, LSRI increases significantly and attains a maximum value of 0.37 for geogrid G4 placed at 65 mm above the subballast. The GIZ is found to vary from 160 mm ($4.60D_{50}$) to 225 mm ($6.45D_{50}$) based on the geogrid placement position. It is further demonstrated that the LSRI has a profound influence on the settlement and breakage of ballast with both ballast settlement and particle breakage exhibiting a significant reduction with the increase in average LSRI.

This chapter clarified that the ideal geogrid placement location is a function of A/D_{50} ratio. The optimum realistic geogrid placement location is 65 mm above the subballast for geogrids with A/D_{50} lying in the OIZ and DIZ (i.e. $A/D_{50} > 0.95$) and at the subballast-ballast interface for geogrids with A/D_{50} lying in the FIZ (i.e. $A/D_{50} < 0.95$). The geogrid also reduces the extent of vertical stress in the subballast, thus

highlighting its role in dissipating the applied train load to an acceptable level where tracks are to be constructed on soft soils.

7 THE APPLICATION OF OPTICAL-FIBER BRAGG GRATING SENSORS IN MONITORING THE RAIL TRACK DEFORMATIONS

7.1 INTRODUCTION

The lateral flow of particles during the passage of trains can reduce the horizontal residual stresses that confine the ballast, hence reducing the stability of the track (Selig and Waters. 1994). Therefore, it is important to restrain the ballast movement and continuously monitor its lateral displacement in order to prevent any track misalignment. The lateral displacement behaviour of geogrid-reinforced ballast (latite basalt) based on the large-scale model track tests under high-frequency cyclic loading were described in Chapter 6. The Chapter exemplified the role of geogrid in arresting the lateral spread of ballast. As mentioned in Chapter 5, the tests were conducted on geogrid-reinforced ballast specimens instrumented with optical-fiber Bragg grating (FBG) sensors. The FBG sensors were used as an alternative means of measuring the lateral displacement of ballast during the cyclic loading. The details pertaining to the test materials, the equipment used, and the experimental procedure followed can be found in Section 5.4 of Chapter 5. This Chapter presents and describes the details related to the FBG sensing system and discusses the lateral displacement of ballast as obtained from the optical sensors.

7.2 NEED FOR OPTICAL SENSORS IN TRACK MONITORING

The performance of a railway track is directly influenced by the complex interaction of its components in response to train loading. More specifically, the track performance depends on the effective functioning of the ballast layer and the corresponding track deformation and degradation characteristics (Alias 1984). However, the large vertical train loads combined with relatively small horizontal confining stress leads to lateral flow of ballast under the cyclic loading conditions (Baessler and Rucker 2003). The lateral flow of particles can reduce the horizontal residual stresses that confine the ballast, hence reducing the stability of the track (Selig and Waters 1994). In this context, the extent of lateral displacement of ballast during the train passage can be considered to be the most important indicator of the track stability.

The measurement of internal lateral displacement of ballast in a real track under operating conditions is generally a difficult task. While the conventional linear variable differential transformers (LVDT's) can be conveniently used to measure the lateral displacement at the ballast boundary, they run the risk of getting damaged when placed within the ballast. Moreover, any attempt to protect the LVDT's by means of steel jacketing reinforces the ballast thereby altering its volumetric behavior. Therefore, it is imperative to use a thin and flexible sensing system that can record the internal displacements in ballast while maintaining the ballast properties unchanged. The optical-fiber Bragg grating (FBG) sensors due to their high accuracy, reliability and flexibility can be treated as a suitable choice for achieving this objective. In addition, the polyamide coating to the optical fiber provides

resistance against the grinding motion of particles, thus minimizing the risk of damage to the fiber or the FBG sensor(s) when used in rail ballast. These FBG sensors were used in the current experimental study to assess their capability in measuring the lateral displacement of ballast during the cyclic loading.

7.3 BASIC STRUCTURE OF AN OPTICAL FIBER AND OPERATING PRINCIPLE OF FIBER BRAGG GRATING SENSOR

An optical fiber is a flexible fiber made of glass or plastic, designed to guide light along its length by total internal reflection. The optical fiber consists of three parts: the core, the cladding, and the coating (Figure 7.1). The core is a cylindrical rod of dielectric material and is generally made of Ge-doped glass. It is surrounded by a layer of material called the cladding. The cladding reduces loss of light from the core into the surrounding air and reduces scattering loss at the surface of the core. To protect the fiber from any physical damage, the cladding is enclosed in an additional layer of coating usually made of polyamide or acrylate.

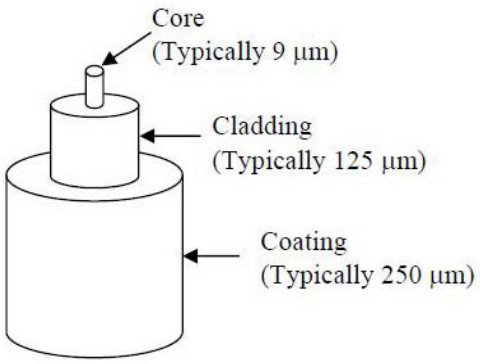

Figure 7.1 Illustration of the basic structure (i.e. core, cladding and coating) of an optical fiber

A FBG is formed by exposing the core of an optical fiber to an intense Ultraviolet interference to cause periodic changes of the refractive index. This grating structure results in the reflection of the light at a specific narrowband wavelength, known as the Bragg wavelength. The Bragg wavelength is a function of the refractive index of the fiber core and the grating period, and this condition is represented by Equation 7.1. The operation principle of fiber Bragg grating (FBG) sensors involves monitoring of the wavelength shift in the reflected wavelength spectrum. When the grating is subjected to an external loading, it undergoes a change in Bragg wavelength, the extent of which determines the magnitude of strain induced in the FBG. This is a fundamental principle that allows the fiber Bragg grating to be used as a sensor.

$$\lambda_B = 2n_e\Lambda \tag{7.1}$$

Where, λ_B is the Bragg wavelength of the FBG, n_e is the effective refractive index of the fiber core and Λ is the grating period.

7.4 APPLICATIONS OF FIBER BRAGG GRATING SENSORS IN CIVIL ENGINEERING

In comparison to the conventional electric strain gauges, the use of optical-FBG sensors have a number of obvious advantages such as (a) their ability to accurately capture the strains owing to their high sensitivity and resolution, fast response and (b) their immunity to electromagnetic and electrical signals. In this view, the use of FBG sensors as a damage detection tool in engineering applications has been on the

rise. For instance, in civil engineering applications, the FBG sensors are mainly used in the structural health monitoring (e.g. Measures 2001; Moyo et al. 2005; Connolly 2006; Majumder et al. 2008; Guo et al. 2011). The use of FBG sensors in geotechnical engineering is limited to the assessment of slope stability (e.g. Ho et al. 2006; Xu et al. 2011). In the recent past, the FBG sensors were also utilized to measure the load transferring capacity of pile foundations (e.g. Schmidt-Hattenberger et al. 2003; Lee et al. 2004). In railway engineering, the optical-FBG sensors are generally used in monitoring the strains induced in rails, counting of axles, and estimation of train weight and train speed (e.g. Lee et al. 2004; Tam et al. 2004; Yoon et al. 2011). However, the ability of FBG sensors to measure the movement of rail ballast under cyclic loading conditions is not explored in the past. It is relevant to mention here that the polyamide coating to the optical fiber offers an additional benefit by providing resistance against the grinding motion of particles, thus minimizing the risk of damage to the fiber or the FBG sensor when used in rail ballast. Therefore, the optical FBG sensors were used in the current study to investigate their suitability in measuring the lateral displacement of ballast during the cyclic loading.

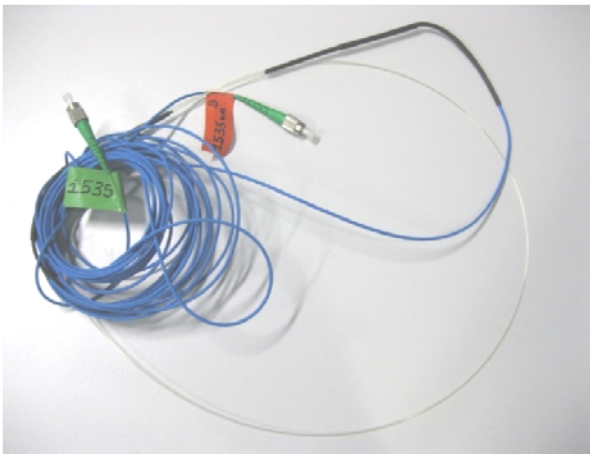

Figure 7.2 The optical fiber embedded with FBG sensor used in the current study

7.5 SMART SENSING SHEET (SSS) TO CAPTURE THE LATERAL STRAINS IN BALLAST

In order to measure the lateral strain variation along the ballast depth, a smart sensing sheet (SSS) is first made by attaching the optical fibers containing FBG sensors (Figure 7.2) to a thin and flexible polymeric sheet (prefabricated vertical drain, PVD) (Figure 7.3a). The sensing sheet had dimensions of 475 (length) x 100 (width) x 2 mm (thick). A total of four FBG sensors with a centre to centre spacing of 81 mm were attached to the SSS to record the lateral strains in ballast at different depths below the sleeper soffit. The optical fibers were glued within the grooves of PVD by means of Cyanoacrylate adhesive to ensure effective strain transfer between the polymeric sheet and the sensor. The 100 mm width of the sensing sheet employed in the current study corresponds to about 2.85D_{50} (D_{50}: mean particle size of ballast, 35 mm), thus ensuring that the strains recorded from the FBG sensors represent the average lateral displacement of ballast. It is relevant to mention that the strains in FBG sensors denote the tendency of ballast to spread laterally. The higher the strain in FBG sensors, greater is the lateral spread of particles.

The FBG sensors used in the current study had a wavelength in the range of 1535 to 1560 nm. The placement location of FBG sensors below the sleeper soffit along with their wavelengths are summarized in Table 7.1. A new set of FBG sensors were used for tests on unreinforced ballast and that reinforced with the geogrids $G1^{+}$, $G3^{+}$, and $G4^{+}$, respectively ($^{+}$geogrid placed at 65 mm above the subballast). The examination of the SSS after the testing revealed that there was no visible damage to it and all the sensors were in good condition. This can also be attributed to the further protection

provided by the PVD casing to the SSS that prevented any direct contact between the ballast and the FBG sensors. Therefore, the reusing of sensors in some of the tests is not of major concern. Nevertheless, any single SSS was used for a maximum of three tests only.

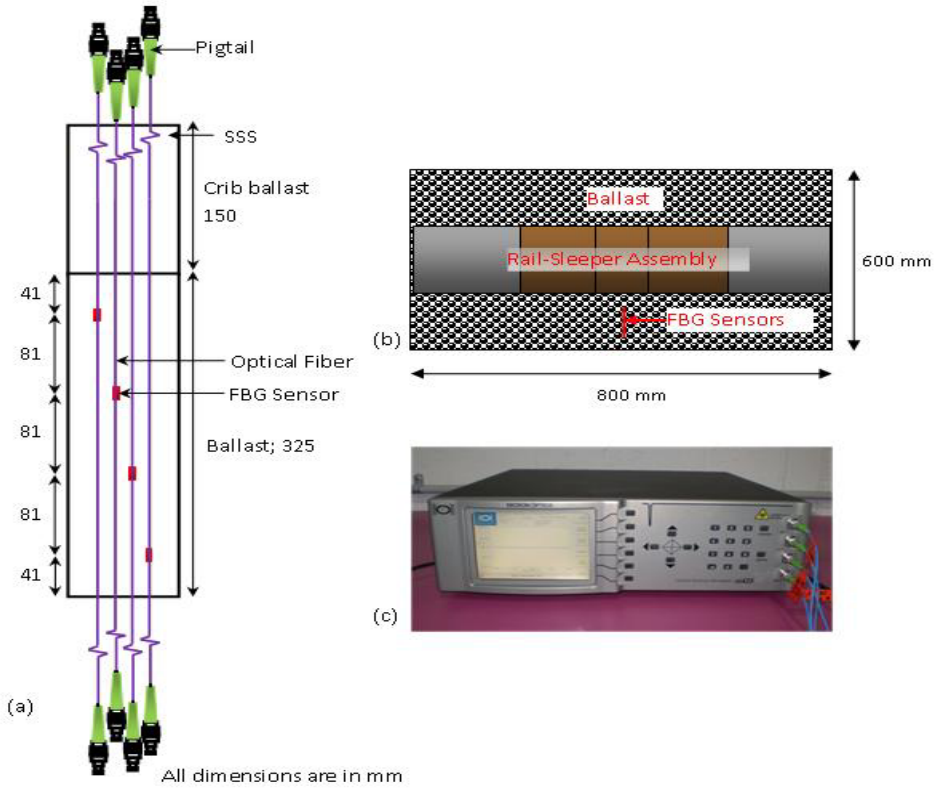

Figure 7.3 (a) Positioning of FBG sensors on the smart sensing sheet (SSS), (b) placement location of the 'SSS embedded with FBG sensors' within the test tank, and (c) interrogator used to demodulate the FBG data

Table 7.1 The placement location of FBG sensors below the sleeper soffit along with their wavelengths

Sensor No.	*Position below sleeper soffit (mm)*	*Wavelength (nm)*			
		UR, G3*, G1*	G1^{+}, G2^{+}	G4^{+}, G2*	G3^{+}, G4*
1	41	1535	1535	1535	1535
2	122	1535	1555	1540	1535
3	203	1545	1560	1550	1550
4	284	1555	1560	1560	1555

Geogrid placement position: *Subballast-ballast interface (i.e. z = 0 mm); $^{+}$65 mm above the subballast (i.e. z = 65 mm).

The sensing sheet was installed in the MPST apparatus with its width parallel to the movable side wall so that the flow of ballast parallel to the sleeper could be measured (Figure 7.3b). The SSS was supported by a set of steel rods to keep it vertically aligned during the specimen preparation (i.e. ballast placement) (Figure 7.4). Following the placement and compaction of ballast, the supporting steel rods were removed prior to loading (Figure 7.5). A dynamic 4 channel optical sensing interrogator (Si425) was employed for the demodulation of FBG sensors (Figure 7.3c). The data from FBG sensors were recorded at a frequency of 1.25 Hz. An Ethernet connection was used for the automatic data communication between the interrogator and the computer (Micron Optics Inc. 2007). The optical fibers used in the current study had pigtails on their either ends. While the pigtails from the top end of the cables were connected to the interrogator, the pigtails at the other end provided redundancy to the FBG sensing system.

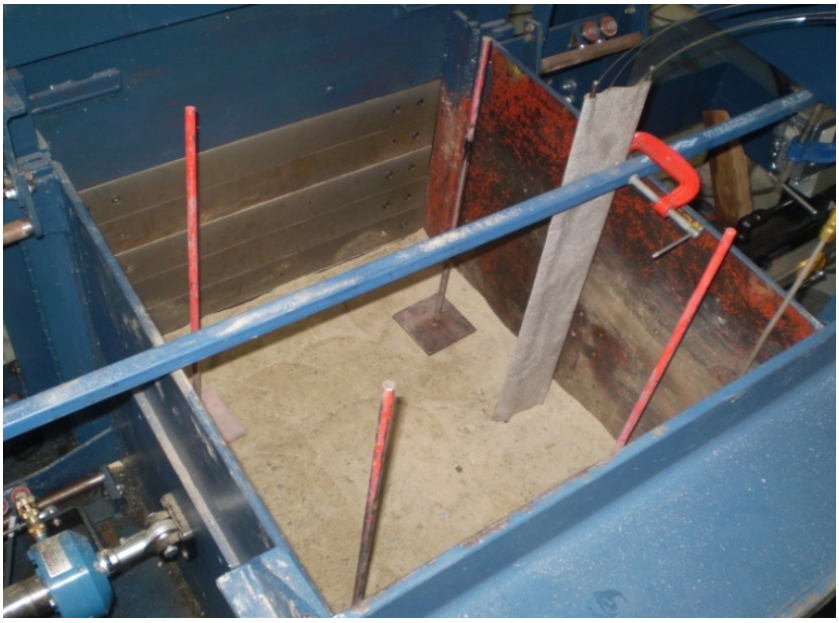

Figure 7.4 The location of SSS supported with the steel rods before the ballast placement

Figure 7.5 Photograph showing the ballasted track section instrumented with FBG sensors ready for testing

7.6 STRAIN ANALYSIS BASED ON THE FBG SENSING SYSTEM

7.6.1 The development of strains in FBG sensors with number of load cycles

Figure 7.6 presents the variation of strains in the bottom most FBG sensor of the SSS (i.e. sensor no. 4, located at a depth of 284 mm below the sleeper soffit) with the number of load cycles (N) for unreinforced ballast and that reinforced with geogrid G3. It is seen that the majority of the strains develop during the initial 50000 load cycles indicating that intense lateral spread of particles occurs during this loading regime, as also described in Chapter 6. In addition to the macroscopic behavior of ballast, the FBG sensors also captured the vibrations induced in ballast due to the high-frequency cyclic loading, as evident from the fluctuations in strains (Figure 7.6). While the lateral strains in general occur during the initial load applications, the fluctuations resulting from the vibrations due to cyclic loading continue to take place until the end of testing. These fluctuations indicate that at micro-scale, ballast undergoes both inward and outward lateral movement (relative to the sleeper position) under track operating conditions. Nevertheless, the overall particle flow is necessarily in the outward direction that eventually deteriorates the track alignment.

Figure 7.6 further reveals that the geogrid reinforcement of ballast not only minimizes the extent of lateral displacement, but also reduces the magnitude of induced vibrations in comparison to that of unreinforced ballast. The reduction in vibrations could be attributed to the increase in stiffness of ballast due to the reinforcement.

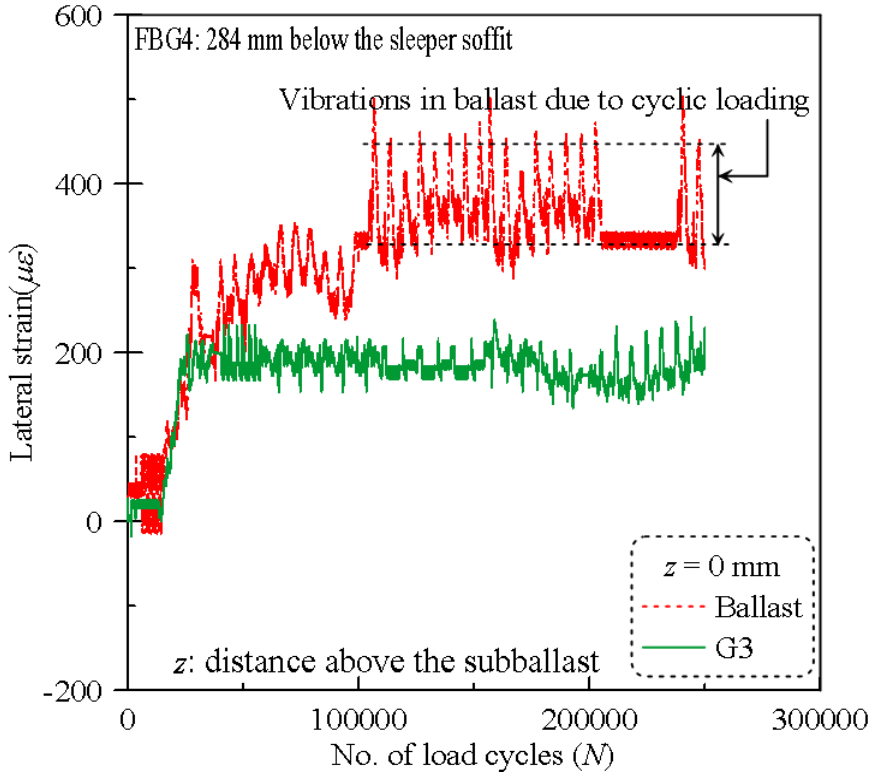

Figure 7.6 The variation of lateral strains in FBG sensor no. 4 in unreinforced and geogrid-reinforced ballast with *N*

7.6.2 The variation of lateral strains along the ballast depth from FBG sensors

The variation of lateral strains in FBG sensors (i.e. numbered 1 to 4) positioned at different depths below the sleeper soffit with the number of load cycles (*N*) is shown in Figure 7.7. It is seen that at all depths below the sleeper soffit, the variation of strains in FBG sensors follow an almost similar trend with the load applications, *N*. However, the magnitude of strains is different at different locations along the ballast depth depending upon the stress distribution pattern and in accordance with the varying intensity of inter-particle and particle-geogrid interaction.

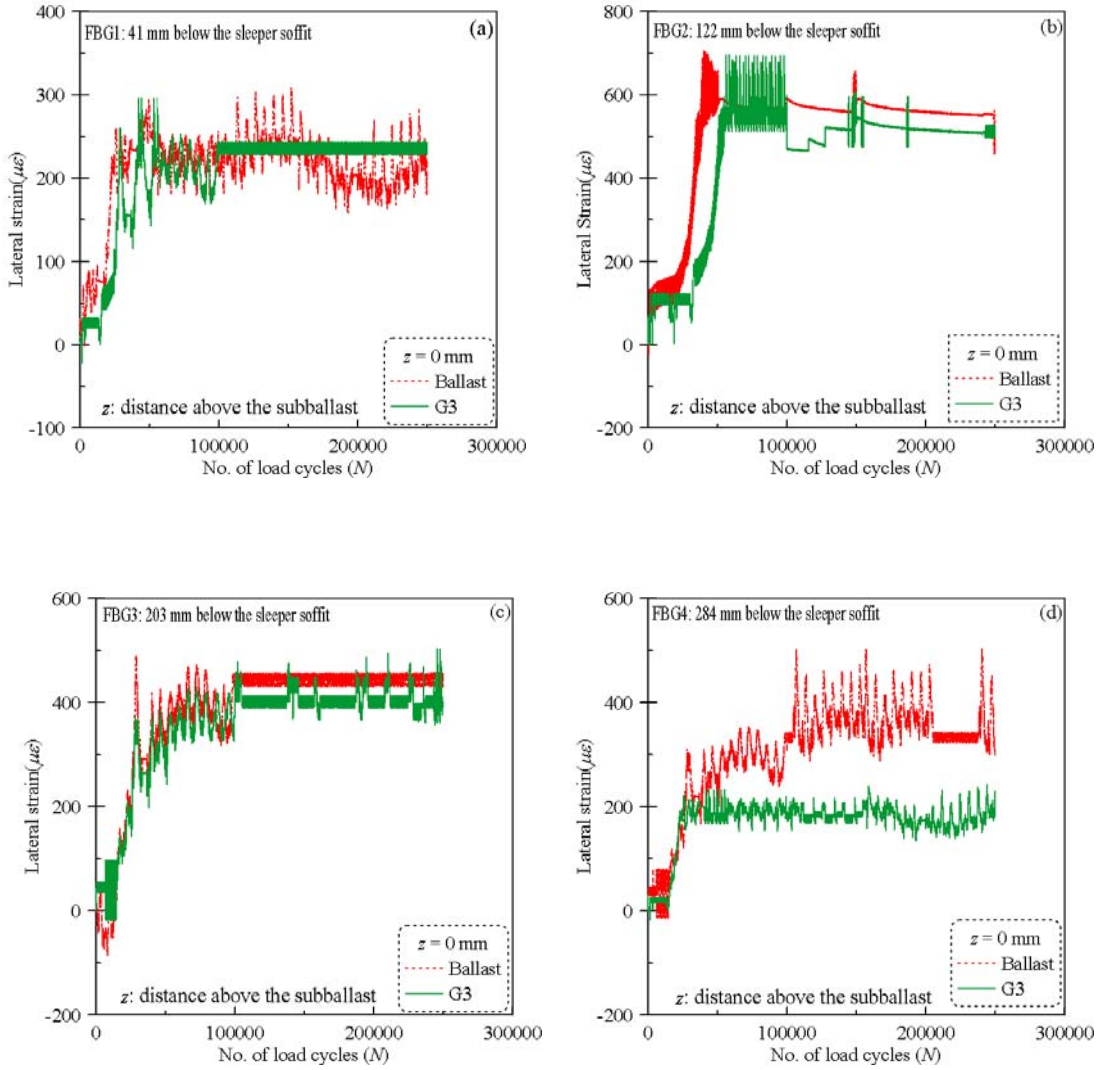

Figure 7.7 The variation of lateral strains in unreinforced and geogrid-reinforced ballast (G3 at z = 0 mm) with N, in FBG sensors located at (a) 41 mm (b) 122 mm (c) 203 mm and (d) 284 mm below the sleeper soffit

Figure 7.8 shows the development of strains in FBG sensors positioned at different depths below the sleeper soffit with N, in the case of unreinforced ballast and that reinforced with geogrid G4. The effect of geogrid reinforcement in reducing the lateral strains in ballast is clearly evident from Figure 7.8 (c) and (d). Figure 7.8 (a) and (b) indicate almost similar strains in both unreinforced and reinforced ballast.

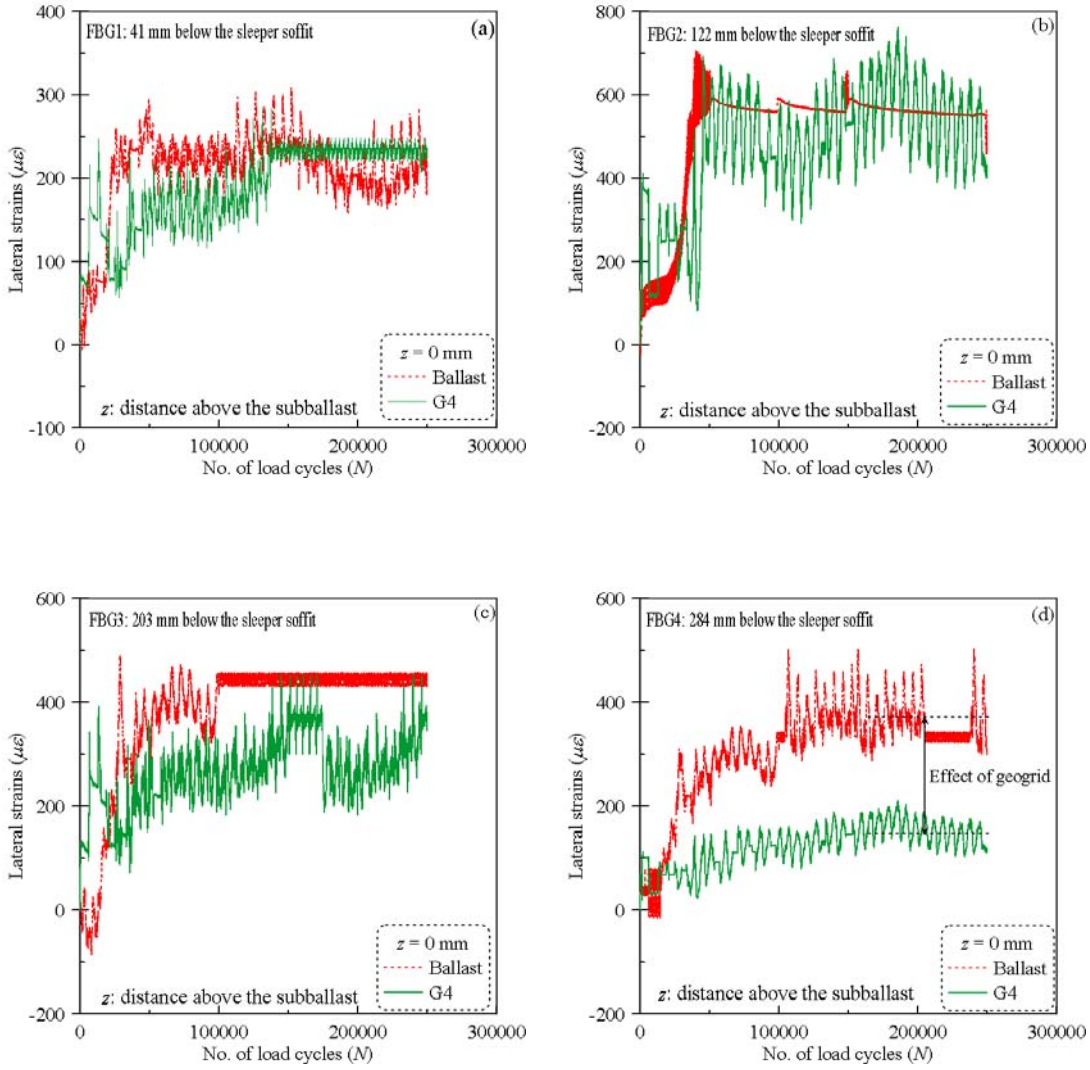

Figure 7.8 The variation of lateral strains in unreinforced and geogrid-reinforced ballast (G4 at z = 0 mm) with N, in FBG sensors located at (a) 41 mm (b) 122 mm (c) 203 mm and (d) 284 mm below the sleeper soffit

7.6.2.1 *Lateral strain profiles along the ballast depth*

Figure 7.9 presents the lateral strain profile of unreinforced ballast and that reinforced with various geogrids, as obtained from the strains in FBG sensors at the end of test (N = 250000). In order to eliminate the effect of vibrations from the FBG data, the average of lateral strain from the individual sensors (as depicted in Figure

7.10) was considered to establish the lateral strain profiles. In line with the observations made earlier in Chapter 6, Figure 7.9 depicts that the lateral strains in the immediate vicinity of geogrid are smaller in comparison to unreinforced ballast, and that the effect of reinforcement decreases with vertical distance away from the geogrid. This similarity in observations, although based on the data recorded by different measuring techniques, highlights the ability of FBG sensors in capturing the lateral movement of ballast reasonably well.

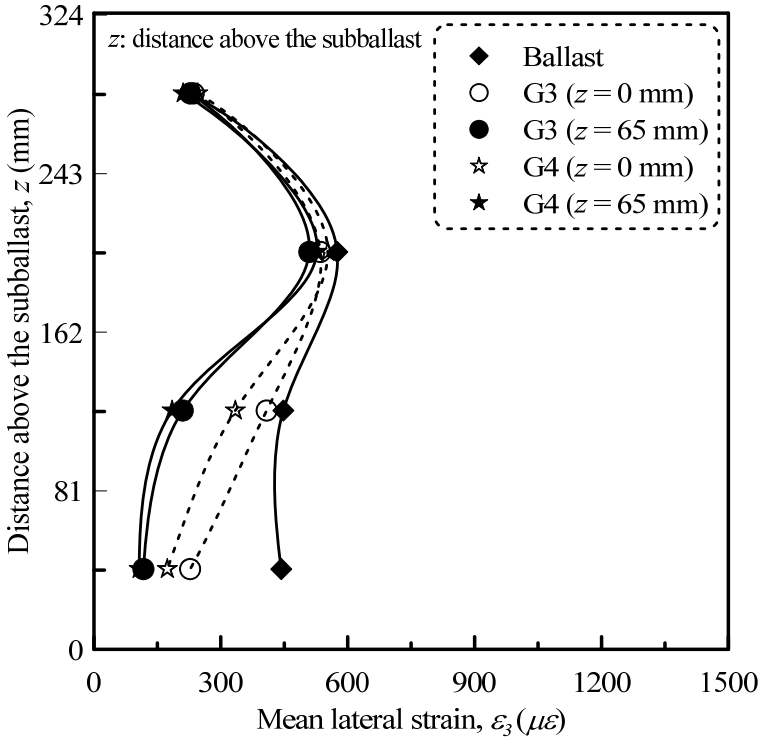

Figure 7.9 Lateral strain profile along the ballast depth as obtained from the strain in FBG sensors

It is further observed from Figure 7.9 that while the geogrid reinforcement of ballast effectively reduces the lateral spread of particles, the lateral strains are still not reduced to zero even in the vicinity of geogrid. The occurrence of slight lateral

movement in reinforced ballast could be attributed to the initial rearrangement of particles needed to establish an effective ballast-geogrid interlock.

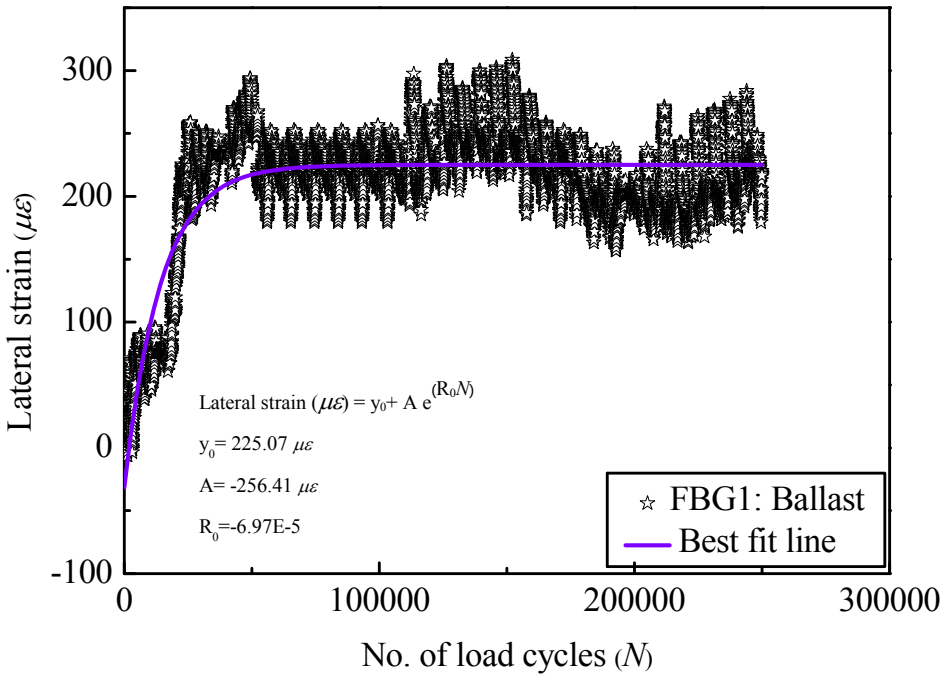

Figure 7.10 The strains developed in FBG sensor along with the best fit line representing the average lateral strain

7.6.3 Comparison of lateral strain profiles under the rail and beneath the sleeper edge

The lateral strain profiles of ballast under the rail as obtained from the FBG data are compared with that of ballast beneath the sleeper edge presented earlier in Chapter 6 (Figure 7.11). Although a direct comparison between the lateral strain profiles established at these two track sections is not possible due to the different techniques adopted for measuring the particle movement, the strain profiles at these two locations compare well with each other. However, unlike the lateral strain profiles of

ballast beneath the sleeper edge, the lateral strain profiles under the rail for both unreinforced and reinforced ballast show some fluctuations possibly due to the localized nature of data from the FBG sensors (Figure 7.11). This is because the strains recorded from the FBG sensors represent the particle spread at a small section within the test chamber, as the width of the SSS is only 100 mm in comparison to the total ballast width of 600 mm. On the contrary, the lateral displacement of particles measured beneath the sleeper edge from the movement of the modified side wall corresponds to the entire ballast width. Moreover, the lateral strain profiles under the rail are based on the data from four FBG sensors in comparison to the data from five movable plates in case of strain profiles beneath the sleeper edge.

In view of the aforementioned factors, it is envisaged that the use of two or more sensing sheets (instrumented with more than four FBG sensors, if possible) would provide better and more accurate record of the lateral movement of particles.

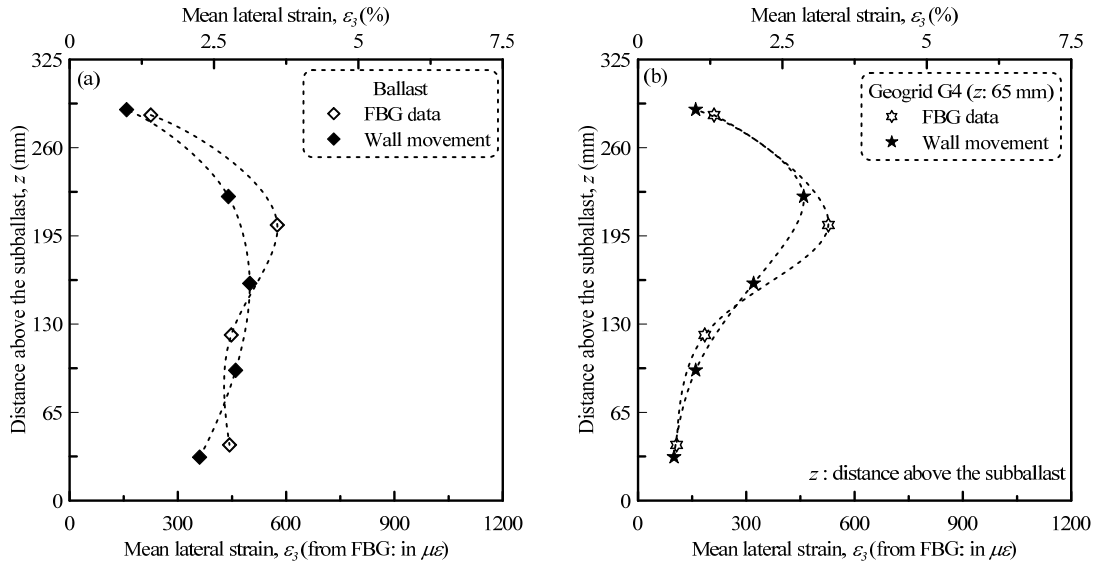

Figure 7.11 Comparison of lateral strain profiles from the FBG data (under the rail) and the wall movement (beneath the sleeper edge) in case of (a) unreinforced ballast and (b) ballast reinforced with geogrid G4

7.6.4 Conversion of strains in FBG sensors to equivalent lateral displacement

The development of strains in FBG sensors during the cyclic loading indicate the tendency of ballast to spread laterally. Therefore, it is essential to convert the strains in FBG sensors to the equivalent lateral displacement of ballast so that a realistic estimate of the current state of the track could be made. It is well known that in a typical rail track, the sleeper-ballast contact pressure is mostly concentrated in the region corresponding to about one-third length of the sleeper from its either ends (Jeffs and Tew 1996; Atalar et al. 2004). In other words, the magnitude of sleeper-ballast contact pressure immediately under the rail and beneath the sleeper edge is necessarily the same. This is also evident from the similar density of displacement vectors at these two track sections based on the numerical study of ballasted track (Figure 7.12; Vinod et al. 2013). In this context, the extent of lateral displacement of

ballast both under the rail and sleeper edge can be assumed to be identical. Therefore, the strains from the FBG sensors (ε_3) are plotted with respect to the lateral displacement of ballast beneath the sleeper edge (Figure 7.13).

It may be mentioned here that the FBG data under the rail corresponds to only four points along the ballast depth in comparison to the data from five movable plates beneath the sleeper edge. In view of this, the data from FBG-1 (i.e. topmost sensor) and FBG-4 (i.e. bottom sensor) are compared with the movement of top and bottom plates, respectively. On the other hand, the data from FBG-2 and FBG-3 are compared with the average of movement of plates 3-4 and 2-3, respectively. It is seen from Figure 7.13 that the average strains in FBG sensors follow a linear relationship with the lateral displacement of ballast. The relationship between the average strain in FBG sensors and the equivalent lateral displacement of ballast could be given by Equation 7.2.

$$Lateral\ displacement\ (mm) = 0.042 \times \epsilon_3(\mu\epsilon) \qquad 7.2$$

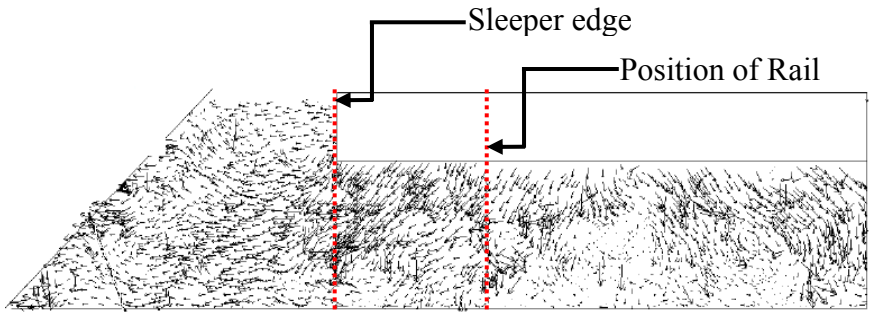

Figure 7.12 The intensity of displacement vectors beneath the rail and under the sleeper edge (Vinod et al. 2013)

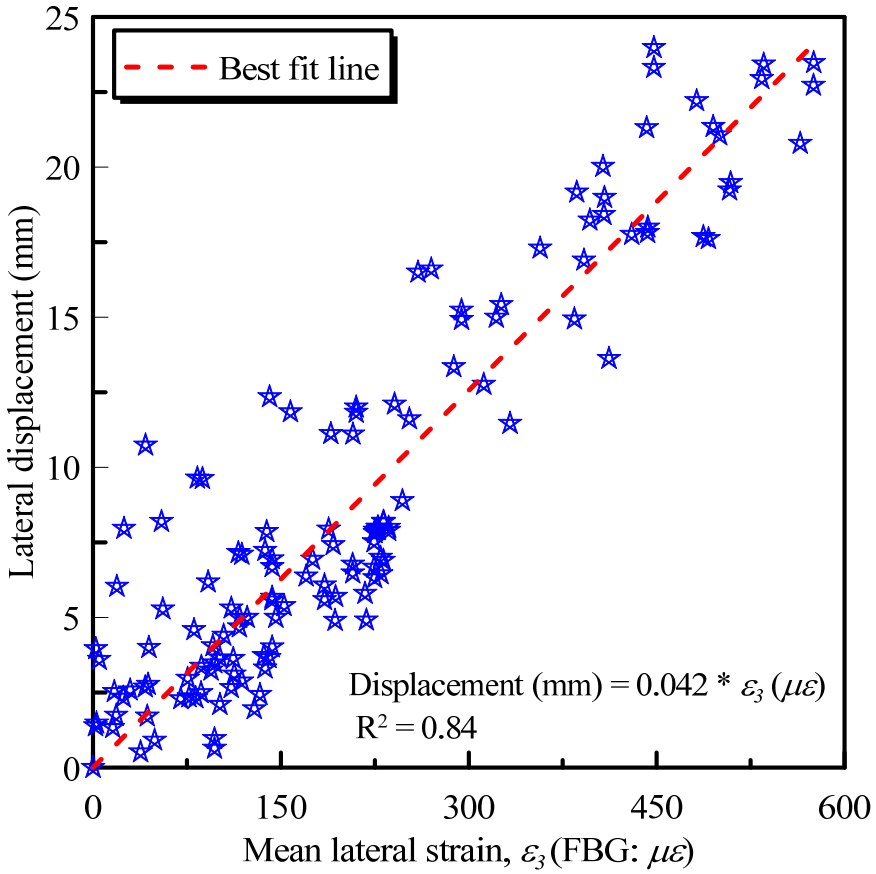

Figure 7.13 Conversion of strains in FBG sensors to equivalent lateral displacement

7.6.4.1 *Validation of the correlation between strains in FBG sensors and the lateral displacement of ballast*

To validate the correlation between the average strain in FBG sensors and the lateral movement of ballast, the equivalent lateral displacement of particles predicted based on Equation 7.2 is compared with the experimental measurements for ballast reinforced with geogrid G4 (Figure 7.14). It is evident that the empirical predictions of the lateral displacement agree reasonably well with the experimental measurements from the side-wall movement. Figure 7.15 presents the measured lateral displacements plotted with respect to the empirical predictions. It is seen that the empirical predictions fall closely along the 45-degree line, thereby further

validating the empirical model. While the FBG data from the tests on unreinforced ballast and that reinforced with geogrids $G1^{+}$, $G3^{*}$ and $G3^{+}$ is used to develop the empirical model, the data from tests on ballast reinforced with $G2^{*}$, $G4^{*}$ and $G4^{+}$ is used for its validation (here * and $^{+}$ indicate geogrid at z = 0 and 65 mm, respectively).

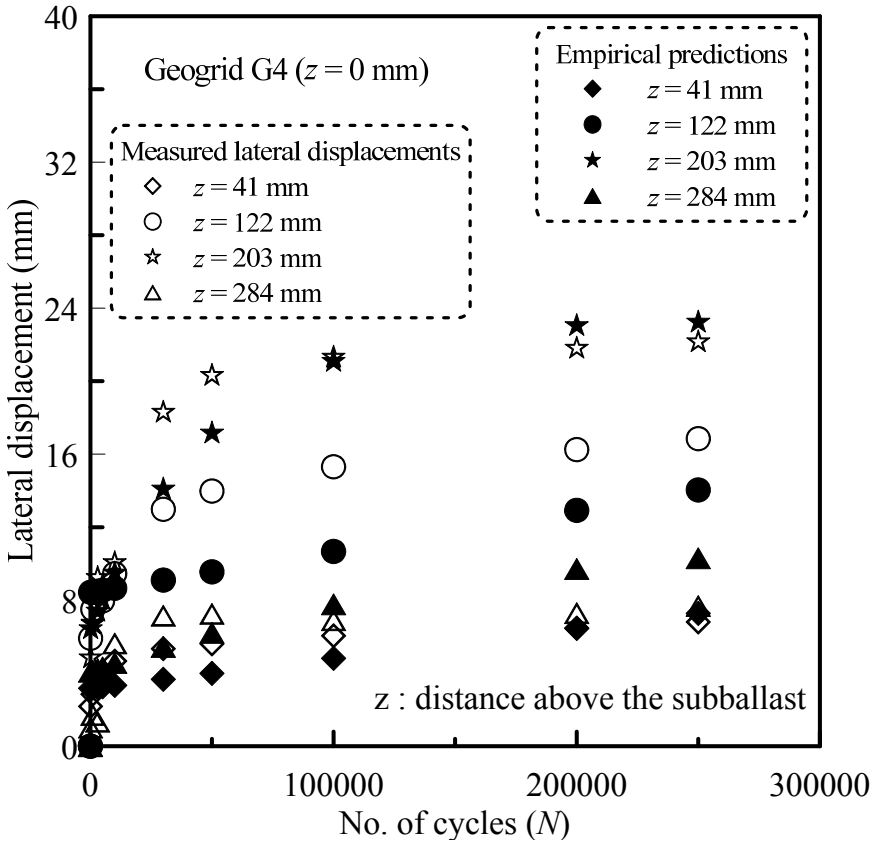

Figure 7.14 Comparison between the predicted and measured lateral displacements with number of load cycles in case of ballast reinforced with geogrid G4

In a practical sense, this empirical model assists in converting the strains from FBG sensors to the equivalent lateral displacement of ballast, thereby helping in assessing the track condition and hence the track stability. When employed as a track monitoring technique, the strains developed in the FBG sensors would serve as an

indicator of whether or not there is a necessity to carry out the ballast maintenance operations. However, further laboratory testing is necessary before this technique can be applied in the field for track monitoring purposes.

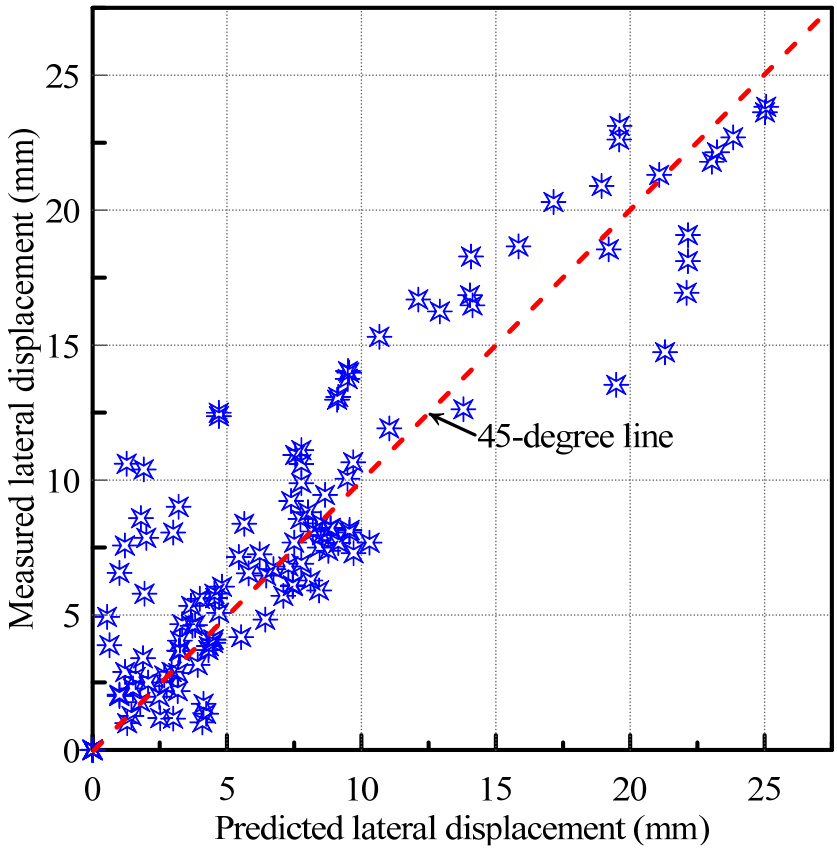

Figure 7.15 The measured lateral displacements versus the empirical predictions to validate the empirical model

7.7 SUMMARY

This Chapter investigated the possible use of optical-fiber Bragg grating (FBG) sensors in measuring the lateral displacements in ballast during cyclic loading. The results from the large-scale tests conducted on geogrid-reinforced ballast indicated that the FBG sensors successfully measured the lateral displacement of ballast. In

addition to the macroscopic behavior, the FBG sensors also captured the vibrations induced in ballast due to the cyclic loading. The lateral strain profiles of ballast were determined based on the strains in different FBG sensors installed at various depths below the sleeper soffit. It was shown that the shape of lateral strain profiles determined from the FBG sensors agreed reasonably well with that established from the movement of side wall of the MPST apparatus. Furthermore, the lateral strain profiles reconfirmed the fact that the effect of reinforcement was predominant in its immediate vicinity and decreased rapidly with vertical distance away from the geogrid, thereby highlighting the ability of FBG sensors in measuring the displacement of ballast reasonably well. Moreover, an empirical relationship was presented that could convert the strains from FBG sensors to the equivalent lateral displacement of ballast, thereby helping the practitioners to assess the track condition based on the FBG data.

The success of current experimental study encourages the use of FBG sensing system in the railway applications as a new technique to evaluate the current state of the track and hence to monitor the rail track stability. However, further laboratory testing and field trials are needed to develop the requisite design standards in order to apply the FBG sensing system in the long-term monitoring of ballast performance.

The next Chapter describes the salient conclusions of the current study and also outlines recommendations for future research.

8 CONCLUSIONS

8.1 GENERAL

This chapter presents the major conclusions of the current study and its practical implications followed by the scope for further research. This study considered the effect of geogrid reinforcement in stabilizing the ballasted rail tracks. For this purpose, laboratory experiments were carried out to study the shear strength characteristics of the ballast-geogrid interfaces, as they govern the overall performance of reinforced ballast, as detailed in Chapter 3. A process simulation test apparatus to simulate the realistic behaviour of ballast was designed and subsequently, the influence of geogrid on the permanent deformation and degradation of ballast was assessed by conducting the model track tests (Chapter 5). In addition, the study investigated the possible use of optical fiber Bragg grating (FBG) sensors in monitoring the railroad ballast deformations, as detailed in Chapter 7.

8.2 MAJOR CONCLUSIONS

8.2.1 Direct shear tests

The shear behaviour of ballast-geosynthetic interfaces was investigated using the large-scale direct shear apparatus (details in Chapter 3). Drained shearing tests were conducted on ballast-geosynthetic interfaces at various values of applied normal stresses under constant normal loading conditions. In order to optimise the geogrid type to be used to enhance the performance of a track with given ballast gradation,

geogrids with different aperture sizes were used for the testing. The important findings from the large-scale direct shear tests can be summarised as follows:

- The angle of shearing resistance of the ballast (φ) and that of the ballast-geosynthetic interfaces (δ) decreased non-linearly at relatively low confining pressures (σ_n < 100 kPa), where φ decreased from 64° to 59° when σ_n is increased from about 25 to 60 kPa.

- The non-linear shear behavior of ballast was expressed by a normalized relationship, and the values of the relevant empirical constants (i.e. *m* and *n*) for various interfaces were determined.

- Interface efficiency factor (α) was defined as $\alpha = \frac{\tan\delta}{\tan\varphi}$, where δ is the apparent friction angle of the interface and φ is the friction angle of the soil. The value of α for ballast used in the study was found to vary in the range of 0.8 to 1.16. It was lowest for the ballast-geotextile interface and highest for the ballast-geogrid (G4) interface.

- Two possible modes of ballast-geogrid interface failure were proposed. The loss of interlock and the breakage of interlocked particles were identified as the potential modes of ballast-geogrid interface failure.

- The ratio A/D_{50} has a profound influence on α. In this respect, the ratio A/D_{50} based on the variation of α is categorized into three key zones: (i) Feeble

Interlock Zone, with $A/D_{50} < 0.95$ (ii) Optimum Interlock Zone, with $0.95 < A/D_{50} < 1.20$ and (iii) Diminishing Interlock Zone, with $1.20 < A/D_{50} < 2.50$.

- The most suitable geogrid aperture size to optimize the interface shear strength is determined to be $1.20D_{50}$. The minimum and maximum aperture sizes desired to attain the beneficial effects via geogrids are established as $0.95D_{50}$ and $2.50D_{50}$, respectively.

8.2.2 Modified process simulation test (MPST) apparatus

The behaviour of ballast should ideally be studied through tests conducted on a real track under actual loading conditions. However, these tests are not only costly and time consuming but also disrupt traffic schedules. Therefore, laboratory experiments simulating field load and boundary conditions are usually carried out on ballast specimens. The realistic laboratory simulation of ballast behaviour under cyclic loading should allow the non-uniform lateral spread of particles along the ballast depth. To attain this, the process simulation test (PST) apparatus available at the University of Wollongong had to be modified (see Chapter 5). The summary modification details are as follows:

- The modification involved the replacement of the central portion of the side wall of the existing prismoidal chamber with a setup of five independent movable plates each measuring 600 mm in width and 64 mm in height assembled along the depth. A small gap of 1 mm is provided between the adjacent plates to ensure free lateral movement of each individual plate under the applied loading.

- In a real track, subballast containing smaller particles compacted to a higher density than the overlying ballast does not indicate significant lateral movement. Also, the top 150 mm of the specimen should represent crib ballast that does not carry the load but confines the ties (sleepers). This crib ballast rarely undergoes significant lateral movement. In this context, the movable plates are required only at the central portion of the side wall where the load carrying ballast is subjected to lateral movement.

- The lateral movement of plates is facilitated by means of linear bearings mounted on a steel guide rail, placed at the ends of each plate. The allowable lateral displacement is 45 mm, representing a maximum lateral strain of 5.63%.

- The MPST apparatus has plan dimensions of 800 x 600 mm and can accommodate samples measuring 650 mm in height. The shorter dimension (i.e. 600 mm) represents the centre-to-centre distance between the sleepers (ties) while the longer side (i.e. 800 mm) represents the track width. The modified apparatus is designed to simulate the track section stressed due to the applied wheel loading.

8.2.3 Model track tests

Laboratory investigations have been carried out using the large-scale MPST apparatus to study the effect of geogrid type and its placement position on the

deformation and degradation response of ballast under high-frequency cyclic loading. The outcomes of the model track tests could be summarized as follows:

- During cyclic loading, both lateral displacement and vertical settlements occurred rapidly in the initial 50000 cycles implying that in reality, the newly constructed tracks would require speed restrictions to be imposed.

- The lateral strain variation along the ballast depth was captured for unreinforced ballast and that reinforced with various geogrids. It is shown that the geogrid reinforcement effectively arrests the lateral strains in ballast thus reducing the extent of ballast settlement and minimizing the particle breakage by about 58% and 53%, respectively. However, the effect of geogrid decreases with vertical distance from its placement position.

- The degradation analysis of different sized particles reveals that the particles in the size range of 53 to 37.5 mm were found to be more vulnerable to breakage than smaller grains. Owing to the formation of new particles as a result of breakage of bigger particles, smaller sized particles (< 19 mm) increase by the end of test.

- The study established that the geogrid reduces the breakage of particles, specifically the bigger ones, thereby exemplifying the role of geogrid in stabilising the ballast.

- It is further shown that both volumetric and shear strain decrease due to the geogrid reinforcement of ballast. The particle degradation is shown to influence the extent of ballast densification and the shear strain in ballast layer.

- Lateral spread reduction index (LSRI) and geogrid influence zone (GIZ) were proposed and applied to assess the performance of geogrid-reinforced ballast.

- It is shown that LSRI was influenced by the geogrid type and its placement location. For geogrids placed at the subballast-ballast interface, the LSRI varied from 0.06 to 0.25. However, LSRI increased significantly and attained a maximum value of 0.37 for geogrid G4 placed at 65 mm above the subballast.

- The GIZ was found to vary from 160 mm ($4.60D_{50}$) to 225 mm ($6.45D_{50}$) based on the geogrid placement position.

- It was demonstrated that the LSRI had a profound influence on the settlement and breakage of ballast with both ballast settlement and particle breakage exhibiting a significant reduction with the increase in average LSRI.

- This study proved beyond doubt that the ideal geogrid placement location was a function of A/D_{50} ratio. The optimum realistic geogrid placement location is 65 mm above the subballast for geogrids with A/D_{50} lying in the

OIZ and DIZ (i.e. $A/D_{50} > 0.95$) and at the subballast-ballast interface for geogrids with A/D_{50} lying in the FIZ (i.e. $A/D_{50} < 0.95$).

- While the geogrid reinforcement in general arrests the lateral spread of ballast, reduces the ballast settlement and minimizes the particle breakage. The reinforcement with an improper geogrid placed at an incorrect location can destabilize the ballast.

- The geogrid also reduces the extent of vertical stress in the subballast, thus highlighting its role in dissipating the applied train load to an acceptable level where tracks are to be constructed on soft soils.

8.3 USE OF OPTICAL FIBER BRAGG GRATING SENSORS

The laboratory model track tests carried out using the large-scale MPST apparatus employed FBG sensors as an alternate means of measuring the deformations in ballast. The test results led to the following important conclusions;

- The FBG sensors could capture the overall lateral deformation of ballast with number of load cycles reasonably well, wherein a major portion of deformations occurred during the initial load applications.

- The strains in FBG sensors indicated that the reinforced ballast encountered lesser deformation in comparison to unreinforced specimen.

The test results encourage the use of FBG sensors in railway applications in the long-term monitoring of deformations in ballast.

8.4 PRACTICAL IMPLICATIONS

The current study has identified several important aspects of geogrid-reinforced ballast that has strong practical significance. Some of these are highlighted below;

- The geogrid reinforcement can effectively stabilize the ballast by reducing the extent of lateral and vertical deformations, and minimising the breakage of particles. However, the ability of geogrid to offer the aforementioned benefits is a function of the relative sizes of geogrid aperture size and ballast.

- The optimum geogrid aperture size to maximize the ballast-geogrid interface shear strength and inhibit the lateral spread of ballast, minimise the vertical settlement, and reduce the particle degradation under cyclic loading was determined to be in the order of $1.20D_{50}$ (D_{50} : the mean particle size of ballast).

- The optimum geogrid position is a function of the normalized aperture size, A/D_{50}. The optimum realistic geogrid position is within the ballast, 65 mm above the subballast, for geogrids with $A/D_{50} > 0.95$ (i.e. for A/D_{50} lying in OIZ and DIZ). On the other hand, optimum geogrid position is at the subballast-ballast interface for geogrids with $A/D_{50} < 0.95$ (i.e. A/D_{50} lying in the FIZ).

8.5 SCOPE FOR FURTHER STUDY

The work carried out as a part of current study has highlighted several aspects of the mechanical behaviour of geogrid-reinforced ballast including that at the ballast-geogrid interface. Although the current research has provided valuable information on the permanent deformation and degradation behaviour of geogrid-reinforced ballast, the investigation of reinforced ballast is far from being concluded. In this view, it is felt that the aspects discussed in the following section will require further examination.

- The shear strength at the ballast-geogrid interface was studied under constant normal loading (CNL) conditions in the current study. The behaviour of ballast-geogrid interfaces under constant normal stiffness (CNS) conditions can be considered as a part of future study.

- The study was carried at a loading frequency of 20 Hz. The effect of increased loading frequency on the ability of geogrid reinforcement to inhibit the lateral spread of ballast is to be studied, and its subsequent influence on the variation of LSRI along the ballast depth and GIZ is to be established.

- The study established the variation of lateral strain in ballast with vertical distance from the geogrid placement position. The variation of particle breakage (BBI) with vertical distance from the reinforcement could be considered as a part of future study.

- The current study was carried out with fresh ballast without any fouling materials present in it. In this view, further investigations are required to establish the effect of clay and coal fouling on the deformation and degradation aspects of reinforced ballast.

- Similarly, the possible effect of diminished ballast permeability owing to fouling and the implications on the deformation and degradation response of ballast should be investigated by conducting the model track tests under saturated conditions on fouled ballast.

- The study considered the effect of one single layer of geogrid of varying aperture sizes and placement position on the behaviour of ballast. The effect of geocomposite and multiple layers of reinforcement (i.e. one layer at the subballast-ballast interface and other within the ballast), including the geogrid stiffness, on the performance of ballast need to be studied. Likewise, the use of three-dimensional reinforcement (i.e. geocell) to stabilize the ballast could be considered as a part of future study.

- Only one type of ballast (i.e. latite basalt) having a same particle size distribution (PSD) and compacted to attain a similar initial density was used for the experiments. Further investigations are required to examine the effect of different types of ballast, different PSD's, and initial densities on the ballast behaviour.

REFERENCES

Abdi, M. R., and Arjomand, M. A. (2011). "Pullout tests conducted on clay reinforced with geogrid encapsulated in thin layers of sand." *Geotextiles and Geomembranes*, 29 (6), pp. 588-595 (doi: 10.1016/j.geotexmem.2011.04.004).

Abu-Farsakh, M. Y., and Coronel, J. (2006). "Characterization of Cohesive Soil–Geosynthetic Interaction from Large Direct Shear Test." *85th Transportation Research Board Annual Meeting*, January 22-26, 2006, Washington, D.C.

Alias, J. (1984). "La voie ferrée-Tome 1: Techniques de Construction et d'Entretien." *Ecole Nationale des Ponts et Chaussées*, Eyrolles, Paris, France, p. 269 (in French).

Allen, J. J. (1973). "The effects of non-constant lateral pressures on the resilient properties of granular materials." *PhD thesis*, University of Illinois, USA.

Alva-Hurtado, J. E. (1980). "A methodology to predict the elastic and inelastic behaviour of railroad ballast." *PhD thesis*, University of Massachusetts, Amherst, Massachusetts, USA.

Alva-Hurtado, J. E., and Selig, E. T. (1981). "Permanent strain behaviour of railway ballast." *Proc., 10th Int. Conf. on Soil Mechanics and Foundation Engineering*, Pergamon Press, New York, pp. 543-546.

Amsler, P. (1986). "Railway track maintenance using geotextile." *Procedings of 3rd International Conference on Geotextiles*, Vienna, pp. 1037-1041.

Anderson,W. F., and Fair, P. (2008). "Behavior of Railroad Ballast under Monotonic and Cyclic Loading." *Journal of Geotechnical and Geoenvironmental Engineering*, 134 (3), pp. 316-327.

AS 2758.7: Aggregates and rock for engineering purposes, part 7: Railway ballast. *Standards Australia*, NSW Australia, 1996.

Asadzadeh, M., and Soroush, A. (2009). "Direct shear testing on a rockfill material." *The Arabian Journal for Science and Engineering,* 34 (2B), pp. 381-396.

Ashpiz, E. S., Diederich, R., and Koslowski, C. (2002). "The use of spunbonded geotextile in railway track renewal on the St. Petersburg- Moscow line." *Proc., 7th Int. Conf. on Geosynthetics*, Nice, France, 14-19.

Atalar, C., Das, B. M., Shin, E. C. and Kim, D. H. (2001). "*Settlement* of geogrid-reinforced railroad bed due to cyclic load." *Proceedings of 15th International Conference on Soil Mechanics and Geotechnical Engineering*, Istanbul, 3, pp. 2045-2048.

Athanasopoulos, G. A. (1994). "On the enhanced confining pressure approach to the mechanics of reinforced soil." *Geotechnical and Geological Engineering*, 12, pp. 122-132.

Aursudkij, B., McDowell, G. R., and Collop, A. C. (2009). "Cyclic loading of railway ballast under triaxial conditions and in a railway test facility." *Granular Matter,* 11 (6), pp. 391-401.

Baessler, M., and Rucker, W. (2003). "Track settlement due to cyclic loading with low minimum pressure and vibrations." *System dynamics and long-term behaviour of railway vehicles, Track and subgrade,* Popp, K. and Schiehlen, W., (Editors), Springer, Berlin, pp. 337-356.

Bakeer, M. R., Sayed, M. S., Cates, P., and Subramanian, R. (1998). "Pullout and shear tests on geogrid reinforced lightweight aggregate." *Geotextiles and Geomembranes*, 16 (2), pp. 119-133.

Barksdale, R. D. (1972). "Repeated load test evaluation of base course materials." *Ph.D. Thesis*, Georgia Institute of Technology, at Atlanta, Ga.

Bathurst, R. J. and Raymond, G. P. (1987). "Geogrid Reinforcement of Ballasted Track." *Transportation Research Record* 1153, National Research Council, Transportation Research Board, Washington, D.C., pp. 8-14.

Bauer, E., and Tantono, S. F. (2009). "Numerical investigation of the interface behavior between granular soil and geogrid reinforcement." *International journal computer applications in technology*, 34 (1), pp. 23-32.

Birman, F. (1975). "Recent investigations of the dynamic modulus of elasticity of the Track in ballast with regard to high speeds." *Proc. Symp. Railroad Track Mechanics and Technology*, Princeton University, New Jersey, 21-23 April, Pergamon Press, pp. 197-221.

Birmann, F. (1966). "Recent investigations of the dynamic modulus of the track in ballast with regard to high speeds." *Proc. Symp. Railroad Track Mechanics*

and Technology, Princeton University, New Jersey, 21-23 April, Pergamon press, pp. 197-221.

Bolton, M. D. (1986). "The strength and dilatancy of sands." *Geotechnique*, 36 (1), pp. 65-78.

Broadley, J. R., Johnston, G. D. and Pond, B. (1981). "The dynamic impact factor." *Railway Engineering Conference*, Sydney, 7-10 Sep.1981, IEAust, Australia, pp. 87-91.

Brough, M. J., Ghataora, G. S., Stirling, A. B., Madelin, K. B., Rogers, C. D. F., and Chapman, D. N. (2006). "Investigation of railway track subgrade-Part 2: Case study." *Proceedings of the Institute of Civil Engineers*, *Transport*, 159 (2), pp. 83-92.

Brown, S. F. (1974). "Repeated load testing of a granular material." *Journal of soil mechanics and foundation division*, ASCE, Vol. 100, No. GT7, July, pp. 825-841.

Brown, S. F., and Hyde, A. F. L. (1975). "Significance of cyclic confining stress in repeated-load triaxial testing of granular material." *Transp. Res. Rec.* 537, Transportation Research Board, Washington, D.C., pp. 49-58.

Brown, S. F. and Selig, E. T. (1991). "The design of pavement and rail track foundations-Cyclic loading of soils." eds. O'Reilly and Brown, Van Nostrand Reinhold, Glasgow, U. K., pp. 249-305.

Brown, S. F., Kwan, J., and Thom, N. H., (2007). "Identifying the key parameters that influence geogrid reinforcement of railway ballast." *Geotextiles and Geomembranes,* 25 (6), pp. 326-335.

Cazzuffi, D., Picarelli, L., Ricciuti, A., and Rimoldi, P. (1993). "Laboratory investigations on the shear strength of geogrid reinforced soils." *ASTM Special Technical Publication* 1190, pp. 119-137.

Cancelli, A., Rimoldi, P., and Togni, S. (1992). "Frictional characteristics of geogrids by means of direct shear and pull-out tests." *In: Proceedings of the International Symposium on Earth Reinforcement Practice*, Kyushu, 1, pp. 29-34.

Charles, J A., and Watts, K. S. (1980). "The influence of confining pressure on the shear strength of compacted rockfill." *Geotechnique*, London, U K, 30 (4), pp. 353-367.

Chrismer, S. M. (1985). "Considerations of factors affecting ballast performance." *Bulletin 704 AREA – AAR Research and test department*, Report No WP-110.

Clarke, C. W. (1957). "Track loading fundamentals." *The Railway Gazette*, Part 1, pp. 45-71.

Clayton, C. R. I., and Bica, A. V. S. (1993). "The design of diaphragm type boundary total stress cells." *Geotechnique*, 43 (4), pp. 523-535.

Collins, I. F., and Boulbibane, M. (2000). "Geomechanical analysis of unbound pavements based on shakedown theory." *Journal of geotechnical and geoenvironmental engineering, ASCE,* 126 (1), pp. 50-59.

Connolly, C. (2006). "Fibre-optic-based sensors bring new capabilities to structural monitoring." *Sensor Review*, *26*, pp. 236-243.

Cui, L., and O'Sullivan, C. (2006). "Exploring the macro- and micro-scale response of an idealised granular material in the direct shear apparatus." *Geotechnique,* 56 (7), pp. 455-468.

Dalton, C. J. (1973). "Field Durability Tests on Ballast Samples as a Guide to the Significance of the Specification Requirements." *Canadian National Railways*, Technical Research Center, St. Laurent, Quebec, January, p. 78.

Dash, S. K., and Shivadas, A. S. (2012). "Performance Improvement of Railway Ballast Using Geocells." *Indian Geotechnical Journal*, 42 (3), pp. 186–193 DOI 10.1007/s40098-012-0017-3.

Desai, C. S., Zaman M. M., Lightner, J. G., and Siriwardane, H. J. (1984). "Thin-layer element for interfaces and joints." *International Journal of Numerical and Analytical Methods in Geomechanics*, 8 (1), pp. 19-43.

Diyaljee, V. A. (1987). "Effects of stress history on ballast deformation." *Journal of geotechnical engineering, ASCE,* 113 (8), pp. 909-914.

Drucker, D. C., Gibson, R. E., and Henkel, D. J. (1957). "Soil mechanics and work hardening theories of plasticity." *Transactions, ASCE*, 122, pp. 338-346.

Dunnicliff, J. (1988). *Geotechnical instrumentation for monitoring field performance*, Wiley, New York.

Dunlap, W. A. (1966). Deformation characteristics of granular materials subjected to rapid, repetitive loading." *PhD thesis*, Texas A&M University, Texas, USA.

Eisenmann, J., (1970). Stress distribution in the permanent way due to heavy axle loads and high speeds, *AREA Proceedings*, 71, pp. 24-59.

Eisenmann, J. (1972). "Germans gain a better understanding of track structure." *Railway Gazette International*, 128 (8), pp. 305-312.

Eisenmann, J., Leykauf, G. and Mattner, L. (1993). "Deflection and settlement behaviour of ballast." *Proc. 5th International Heavy Haul Railway Conference*, Beijing, 1993, pp. 193-227.

Eisenmann, J., Leykauf, G. and Mattner, L. (1994). "Recent development in German railway track design." *Proceedings of Institution of Civil Engineers Transportation*, Paper 10107, Transport Board Railway Panel, 105, May, London, pp. 91-96.

Esveld, C. (2001). Modern railway track, MRT-Productions, Zaltbommel, The Netherlands.

Feng, D. M. (1984). "Railroad ballast performance evaluation." *MSc degree project report*, Report No. AAR84-311P, Dept of Civil Engineering, University of Massachusetts, Amherst, USA.

Fernandes, G., Palmeira, E. M., and Gomes, R. C. (2008). "Performance of geosynthetic-reinforced alternative sub-ballast material in a railway track." *Geosynthetics International*, 15 (5), pp. 311-321.

Frederick, C. O., and Round, D. J. (1985). "Vertical track loading." Track technology, Thomas Telford, London, pp. 135-149.

Frohling, R. D. (1998). "Prediction of spatially varying track settlement." *Conference on Railway Engineering*, Rockhampton, 7-9 September, IE Aust., Australia.

Geol, J. P.C. (2011). "The use of geogrids on mainline and intermodal facility projects." AREMA, September, 2011.

Goebel, C. H., Weisemann, U. C. and Kirschner R. A. (1994). "Effectiveness of a reinforcing geogrid in a railway subbase under dynamic loads." *Geotextiles and Geomembranes*, 13, pp. 91-99.

Gray, D. H., Athanasopoulos, G., and Ohashi, H. (1982). "Internal/external fabric reinforcement of sand." *Proceedings of the Second International Conference on Geotextiles*, Las Vegas, Industrial Fabrics Association, 3, pp. 611-616.

Guérin, N., Karam Sab., and Moucheront, P. (1999). "Identification expérimentale d'une loi de tassement du ballast." (in French) *Canadian Geotechnical Journal*, 36, pp. 523-532.

Guo, H., Xiao, G., Mrad, N., and Yao, J. (2011). "Fiber Optic Sensors for Structural Health Monitoring of Air Platforms." *Sensors*, 11, pp. 3687-3705.

Haeri, S. M., Noorzad, R., and Oskoorouchi, A. M. (2000). "Effect of geotextile reinforcement on the mechanical behavior of sand." *Geotextiles and Geomembranes,* 18 (6), pp. 385-402.

Hardin, B. O. (1985). "Crushing of soil particles." *Journal of Geotechnical Engineering*, ASCE, 111 (10), pp. 1177-1192.

Harrison, H. D., Selig, E. T., Dean, F. E. and Stewart, H. E. (1986). "Correlation of concrete tie track performance in revenue service and at the facility for accelerated service testing." Vol. 1 – a detailed summary, Battelle Columbus Laboratories and University of Massachusetts, Final Report, Report No. DOT/FRA/ORD-84/02.1, August 1984, p. 156.

Ho, Y. T., Huang, A. B., and Lee, J. T. (2006). "Development of a fibre Bragg grating sensored ground movement monitoring system." *Measurement Science and Technology*, 17, pp. 1733-1740.

Hornícek, L., Tyc, P., Lidmila, M., Krejciríková, H., Jasanský, P and Brešt'ovský, P. (2010). "An investigation of the effect of under-ballast reinforcing geogrids in laboratory and operating conditions." *Proceedings of the Institution of Mechanical Engineers, Part F: Journal of Rail and Rapid Transit,* 224, pp. 269-277.

Indraratna, B., Wijewardena, L.S.S., and Balasubramaniam, A.S. (1993). "Large-scale testing of greywake rockfill." *Geotechnique*, 43 (1), pp. 37-51.

Indraratna, B., Ionescu, D., Christie, H. D. and Chowdhury, R. N. (1997). "Compression and degradation of railway ballast under one-dimensional

loading." *Australian Geomechanics Journal*, Australian Geomechanics Society, IEAust, December, Barton, Australia, pp. 48-61.

Indraratna, B., Ionescu, D., and Christie, H. D. (1998). "Shear Behavior of Railway Ballast based on Large Scale Triaxial Testing." *Journal of Geotechnical and Geoenvironmental Engineering*, *ASCE,* 124 (5), pp. 439-449.

Indraratna, B. and Ionescu, D. (1999). "Deformation of ballast under static and dynamic loading." *Proceedings of the 2nd International Symposium on Pre-failure Deformation of Geomaterials*, 2, Torino, 28-30 September 1999, Balkema, Rotterdam, pp. 283-289.

Indraratna, B., Ionescu, D., and Christie, H. D. (2000). "State-of-the-art Large Scale Testing of Ballast." *In: Conference on Railway Engineering CORE2000: Railway Technology for the 21st Century*. Adelaide, 21-23 May 2000, pp. 208-220.

Indraratna, B., Ionescu, D., and Christie, H. D. (2000). "State-of-the-art large scale testing on ballast." *Conference on Railway Engineering Proceedings*, Adelaide, 15-18 May 2000, IE Aust, Barton, Australia, pp. 92-102.

Indraratna, B., Ionescu, D., Salim, W., and Christie, H. D. (2001). "Stress-strain and degradation behaviour of railway ballast under static and dynamic loading, based on large-scale triaxial testing." *Proceedings of the 15th International Conference in Soil Mechanics and Foundation Engineering*, Vol. 3, Istanbul, 25-28 August 2001, Turkey, pp. 2093-2099.

Indraratna, B., Salim, W., and Christie, D. (2002). "Improvement of recycled ballast using geosynthetics." *Proc. 7th International Conference on Geosynthetics*, Nice, France, pp. 1177-1182.

Indraratna, B., and Salim, W. (2003). "Deformation and degradation mechanics of recycled ballast stabilised with geosynthetics." *Soils and Foundations*, 43 (4), pp. 35-46.

Indraratna, B., Khabbaz, H., Salim, W., Lackenby, J., and Christie, D. (2004). "Ballast characteristics and the effects of geosynthetics on rail track deformation." *International Conference on Geosynthetics and Geoenvironmental Engineering, ICGGE*, Bombay, India, pp. 3-12.

Indraratna, B., Lackenby, J., and Christie, D. (2005). "Effect of confining pressure on the degradation of ballast under cyclic loading." *Geotechnique*, 55 (4), pp. 325-328.

Indraratna, B., and Salim, W. (2005). Mechanics of ballasted rail tracks-A geotechnical perspective, Taylor & Francis/Balkema, London.

Indraratna, B., Khabbaz, H., Salim, W., and Christie, D. (2006). "Geotechnical properties of ballast and the role of geosynthetics in rail track stabilisation." *Ground Improvement,* 10 (3), pp. 91-101.

Indraratna, B., Shahin, M. A., and Salim, W. (2007). "Stabilisation of granular media and formation soil using geosynthetics with special reference to railway engineering." *Ground Improvement,* 11 (1), pp. 27-43.

Indraratna, B., Nimbalkar, S., and Christie, D. (2009). "The performance of rail track incorporating the effects of ballast breakage, confining pressure and geosynthetic reinforcement." *8th International Conference on the Bearing Capacity of Roads, Railways, and Airfields*, London, UK: Taylor and Francis Group., pp. 5-24.

Indraratna, B., Thakur, P. K., and Vinod, J. S. (2010a). "Experimental and Numerical Study of Railway Ballast Behavior under Cyclic Loading." *International Journal of Geomechanics*, 10 (4), pp. 136-144.

Indraratna, B., Nimbalkar S., Christie, D., Rujikiatkamjorn, C., and Jayan Vinod. (2010b). "Field Assessment of the Performance of a Ballasted Rail Track with and without Geosynthetics." *Journal of Geotechnical and Geoenvironmental Engineering*, 136 (7), pp. 907-917.

Indraratna, B., Salim, W., and Rujikiatkamjorn, C. (2011). *Advanced rail geotechnology- ballasted track*, CRC Press, London.

Indraratna, B., Sd. K. Karimullah Hussaini., and Vinod, J.S. (2012). "On the shear behavior of ballast-geosynthetic interfaces." *Geotechnical testing journal*, ASTM, 35 (2), pp. 305-312 (DOI: 10.1520/GTJ103317).

Ionescu, D., Indraratna, B., and Christie, H. D. (1996). "Laboratory evaluation of the behaviour of railway ballast under static and repeated loads." *Proc. of the 7thAustralia New Zealand Conference on Geomechanics*, 1-6 July 1996, Adelaide, Australia, pp. 86-91.

Ionescu, D., Indraratna, B., and Christie, H. D. (1998a). "Behaviour of railway ballast under dynamic loads." *Proc. 13th South East Asian Geotechnical Conference*, Taipei, 9-12 November, 1, Balkema, Rotterdam, pp. 69-74.

Ionescu, D., Indraratna, B., and Christie, H. D. (1998b). "Deformation of railway ballast under dynamic loads." *Conference on Railway Engineering*, Rockhampton, 7-9 September, IE Aust, Australia, pp. 111-118.

Ionescu, D. (2004). "Evaluation of the engineering behaviour of railway ballast." *PhD Thesis*, University of Wollongong, Wollongong, NSW, Australia.

Janardhanam, R., and Desai, C. S. (1983). "Three-dimensional testing and modelling of ballast." *Journal of geotechnical engineering*, ASCE, 109 (6), pp. 783-796.

Jeffs, T., and Marich, S. (1987). "Ballast characteristics in the laboratory." *Conference on Railway Engineering*, Perth, 1987, pp. 141-147.

Jeffs, T. (1989). "Towards ballast life cycle costing." *The 4th International Heavy Haul Railway Conference*, 11-15 September, pp. 439-445.

Jeffs, T., and Tew, G. P. (1991). A Review of Track Design Procedures: Sleepers and Ballast, 2, railways of Australia.

Kempfert, H. G., and Hu, Y. (1999). "Measured dynamic loading of railway underground." *Proc. 11th Pan-Am. Conf. on Soil Mech. & Geotech. Eng.,* Brazil, pp. 843-847.

Kennedy, J. (2011). "A full-scale laboratory investigation into railway track substructure performance and ballast reinforcement." *PhD thesis*, Heriot-Watt University, UK.

Kerr, A. D. (1976). "On the stress analysis of rails and ties." *AREA Proceedings*, 78, p. 19.

Knutson, R. M. (1976). "Factors influencing the repeated load behaviour of railway ballast." *Ph.D. Thesis*, University of Illinois, at Urbana, Ill.

Knutson, R. M., and Thomson, M. R. (1977). "Resilient response of railway ballast." Transportation research record, 651, pp. 31-39.

Koerner, R. M. (1998). *Designing with geosynthetics*, 4th ed., New Jersey: Prentice Hall.

Lackenby, J. (2006). "Triaxial behaviour of ballast and the role of confining pressure under cyclic loading." *PhD Thesis*, University of Wollongong, Australia.

Lackenby, J., Indraratna, B., McDowell, G., and Christie, D. (2007). "Effect of confining pressure on ballast degradation and deformation under cyclic triaxial loading." *Geotechnique*, 57 (6), pp. 527-536.

Lade, P. V., Yamamuro, J. A., and Bopp, P. A. (1996). "Significance of particle crushing in granular materials." *Journal of Geotechnical Engineering*, *ASCE*, 122 (4), pp. 309-316.

Lee, K. Y., Lee, K. K., and Ho, S. L. (2004). "Exploration of Using FBG Sensor for Axle Counter in Railway Engineering." WSEAS Transactions on Systems, 6 (3), pp. 2440-2447.

Lee, W., Lee, W-J., Lee, S-B., and Salgado, R. (2004). "Measurement of pile load transfer using the fiber Bragg grating sensor system." *Canadian Geotechnical Journal*, 41 (6), pp. 1222-1232.

Lee, K., and Farhoomand, I. (1967). "Compressibility and Crushing of Granular Soils in Anisotropic Compression." *Canadian Geotechnical Journal*, 4 (1), pp. 68-86.

Lees, G., and Kennedy, C. K. (1975). "Quality, shape and degradation of aggregates." *Journal of Engineering Geology*, 8, pp. 193-209.

Lentz, R. W., and Baladi, G. Y. (1981). "Constitutive equation for permanent strain of sand subjected to cyclic loading." *Transportation research record*, 810, pp. 50-54.

Leps, T. M. (1970). "Review of shearing strength of rockfill." *Journal of the Soil Mechanics and Foundation Division*, *ASCE*, 96, pp. 1159-1170.

Le-Pen, L. M., and Powrie, W. (2011). "Contribution of base, crib and shoulder ballast to the lateral sliding resistance of railway track: a geotechnical perspective." *Proceedings of the Institution of Mechanical Engineers Part F: Journal of Rail and Rapid Transit*, 225 (2), pp. 113-128 (DOI: 10.1177/0954409710397094).

Liu, S. H., Sun, D., and Matsuoka, H. (2005). "On the Interface Friction in Direct Shear Test." *Computers and Geotechnics*, 32 (5), pp. 317-325.

Liu, C-N., Ho, Y-H., and Huang, J-W. (2009). "Large scale direct shear tests of soil/PET-yarn geogrid interfaces." *Geotextiles and Geomembranes,* 27, pp. 19-30.

Luo, Y., Yin, H., and Hua, C. (1996). "Dynamic response of railway ballast to the action of trains moving at different speeds." *Proceedings of the institution of mechanical engineers, Part F: Journal of rail and rapid transit*, 210 (2), pp. 95.

Majumder, M., Gangopadhyay, T. K., Chakraborty, A. K., Dasgupta, K., Bhattacharya, D. K. (2008). "Fibre Bragg gratings in structural health monitoring-Present status and applications." *Sensors and Actuators- A*, *147*, pp. 150-164.

Marachi, N. D., Chan, C. K., and Seed, H. B. (1972). "Evaluation of properties of rockfill materials." *Journal of the Soil Mechanics and Foundations Division*, *ASCE*, 98, pp. 95-114.

Marsal, R. J. (1967). "Large scale testing of rockfill material." *Journal of the Soil Mechanics and Foundations Division*, *ASCE*, 97 (2), pp. 27-43.

Marsal, R. J. (1973). "Mechanical properties of rockfill." In: *Embankment Dam Engineering*, Wiley, NY, pp. 109-200.

Matharu, M. S. (1994). “Geogrid cut ballast settlement rate on soft substructures.” *Railway Gazette Intenational*, 150 (3), pp. 165-166.

McDowell, G. R., Bolton, M. D. and Robertson, D. (1996). “The fractal crushing of granular materials.” *J. Mech. Phys. Solids*, 44 (12), pp. 2079-2102.

McDowell, G. R., Harireche, O., Konietzky, H., Brown, S. F., and Thom, N. H. (2006). “Discrete element modelling of geogrid-reinforced aggregates.” *Proceedings of the Institution of Civil Engineers Geotechnical Engineering,* 159, January 2006, GE1, pp. 35-48.

McDowell, G., and Stickley, P. (2006). “Performance of geogrid-reinforced ballast.” *Ground Engineering,* 39 (1), pp. 26-30.

Measures, R. M. (2001). *Structural monitoring with fiber optic technology*, Academic Press, 2001.

Micron Optics, Inc. (2004). Si425 Optical Sensing Interrogator Instruction Manual, Atlanta, USA.

Morgan, J. R. (1966). “The response of granular materials to repeated loading.” Proc., 3rd Conf., ARRB, pp. 1178-1192.

Moyo, P., Brownjohn, J. M. W., Suresh, R., Tjin, S. C. (2005). “Development of fiber Bragg grating sensors for monitoring civil infrastructure.” *Engineering Structures,* 27, pp. 1828-1834.

Nancey, A., Imbert, B., and Robinet, A. (2002). "Thick and abrasion resistant geotextile for use under the ballast in railway structures." *7th International Conference on Geosynthetics*, Nice, France, 3, pp. 1191-1194.

Ni, Q., Powrie, W., Zhang, X., and Harkness, R. (2000). "Effect of particle properties on soil behaviour: 3-D numerical modeling of shear box tests." *Numerical Methods in Geotechnical Engineering*, *ASCE*, Geotechnical Special Publication No. 96, pp. 58-70.

Nakata, Y., Kato, Y., Hyodo, M., Hyde, A. F. L., and Murata, H. (1999). "One-dimensional compression behaviour of uniformly graded sand related to single particle crushing strength." *Soils and Foundations*, 41 (2), pp. 39-51.

Neil, D. M. (1976). "Railtrack design ballast and subgrade." *Rail and Reclamation Workshop on Materials and Methods for Low Cost Road*, Leura, Australia, 6-10 September, pp. 637-661.

Norman, G. M. and Selig, E. T. (1983). "Ballast performance evaluation with box test." *AREA, Bul. 692, Proceedings 84*, May, pp. 207-239.

Olowokere, D. O. (1975). "Strength and deformation of railway ballast subject to triaxial loading." *M.S. Thesis*, Dept. of Civil Engineering, Queen's University, Kingston, Ontario, Canada.

Orange, N. T. (1988). "Permanent way research and development studies by Australian National." *Proc. 7th International Rail Track Conference*. Rail Track Assoc. Australia, October, Auckland, pp. 427-431.

ORE. (1970). “Stresses in the rails, the ballast and the formation resulting from traffic loads.” *Office for research and experiments, International union of railways*, Utrecht, Holland Question D71, Report No. 10, Vol. 1 and 2.

ORE. (1978). “The dynamic effects due to increasing axle loads from 20 to 22.5 tonnes and the estimated increase in maintenance costs.” D. 161.1, Report No. 4, September, Utrecht, Holland, p. 67.

Palmeira, E. M., and Antunes, L. G. (2010). “Large scale tests on geosynthetic reinforced unpaved roads subjected to surface maintenance.” *Geotextiles and Geomembranes,* 28, pp. 547-558.

Profillidis, V. A. (1995). “The mechanical behaviour of the railroad tie.” *Journal of Structural Engineering*, ASCE, 58, pp. 245-256.

Qian, Y., Tutumluer, E., and Huang, H. (2011). “A Validated Discrete Element Modeling Approach for Studying Geogrid-Aggregate Reinforcement Mechanisms.” *In: Geo-Frontiers 2011: advances in geotechnical engineering, Ed: Jie Han and Daniel A. Alzamora;* pp. 4653-4662.

Railtrack. (2000). *Railtrack Line Specification*, RT/CE/S/006 Issue 3: Track Ballast.

Raymond, G. P., Gaskin, P. N. and Svec, O. (1975). “Selection and performance o frailroad ballast.” *Proc. Symp. Railroad Track Mechanics and Technology*, Princeton University, New Jersey, 21-23 April, Pergamon Press, pp. 369-387.

Raymond, G. P., Lake, R. W. and Boon, C. J. (1976). "Stresses and deformations in railway track." *Canadian Institute of Guided Ground Transport*, Queen's University at Kingston, Ontario, November, CIGGT Report No 76-11, pp. 171.

Raymond, G. P., Lamson, S. T. and Law, J. E. (1983). "A review of current track structure design and future track research requirements." *Canadian Institute of Guided Ground Transport*, Queen's University at Kingston, Ontario, August, CIGGT Report No. 83-6 TP 4861E, pp. 52.

Raymond, G. P. (1978). "Design for railroad ballast and subgrade support." *Journal of soil mechanics and foundation division*, ASCE, 104, January, pp. 45-60.

Raymond, G. P. and Williams, D. R. (1978). "Repeated load triaxial tests on a dolomite ballast." *Journal of the Geotechnical Engineering Division*, ASCE, 104 (GT7), July, pp. 1013-1029.

Raymond, G. P., and Diyaljee, V. A. (1979). Railroad ballast sizing and grading." *Journal of the Geotechnical Engineering Division*, ASCE, 105 (GT5), pp. 676-681.

Raymond, G. P., and Bathurst, R. J. (1987). "Performance of large-scale model single tie-ballast systems." *Transportation Research Record*, 1131, pp. 7-14.

Raymond G. P. and Bathurst, R. J. (1990). "Test results on exhumed railway track geotextiles." *4th International Conference on Geotextiles, Geomembranes and related products*, The Hague, The Netherlands, 1, pp. 197-202.

Raymond, G. P., and Bathurst, R. J. (1994). "Repeated-load response of aggregates in relation to track quality index." *Canadian Geotechnical Journal*, 31 (4), pp. 547-554, 10.1139/t94-063.

Raymond G. P. (1999). "Railway rehabilitation geotextiles." *Geotextiles and Geomembranes,* 17(4), pp. 213-230.

Raymond, G. P. (2002). "Reinforced ballast behaviour subjected to repeated load." *Geotextiles and Geomembranes*, 20, pp. 39-61.

Raymond, G. P., and Ismail, I. (2003). "The effects of geogrid reinforcement on unbound aggregates." Geotextiles and Geomembranes, 21 (6), pp. 355-380.

Robnett, Q. L., Thompson, M. R., and Hay, W. W. (1975). "Ballast and foundationmaterials research program." Technical data based report Report No. FRA/OR & D-76-138, prepared by University of Illinois for the U. S. DOT, Federal Railroad Administration, July, p.62.

Ruiken, A., and Ziegler, M. (2010). "Recent findings about the confining effect of geogrids from large scale laboratory testing." *9th International Conference on Geosynthetics, Brazil,* pp. 691-694.

Sadeghi, J., and Askarinejad, H. (2007). "Influences of track structure, geometry and traffic parameters on railway deterioration." *International Journal of Engineering, Transactions B: Applications*, 20 (3), pp. 292-300.

Salim, W. (2004). "Deformation and degradation aspects of ballast and constitutive modelling under cyclic loading." *PhD Thesis*, University of Wollongong, Australia.

Salim, W., and Indraratna, B. (2004). "A new elastoplastic constitutive model for coarse granular aggregates incorporating particle breakage." *Canadian Geotechnical Journal*, 41 (4), pp. 657-671.

Sarsby, R. W. (1985). "The influence of Aperture size/Particle size on the efficiency of grid reinforcement," *Second Canadian Symposium on Geotextiles and Geomembranes*. Edmonton Alberta, September 1985, pp. 7-12.

Sato, Y. (1995). "Japanese studies on deterioration of ballasted track." *Special supplement to Vehicle system dynamics*, 24, Swets and Zeitlinger B. V. Publishers, Lisse, pp. 197-208.

Schmidt-Hattenberger, C., Straub, T., Naumann, M., Borm, G., Lauerer, R., Beck, C., and Schwarz, W. (2003). "Strain measurements by fiber Bragg grating sensors for in-situ pile loading tests." Proceedings of SPIE, 5050, pp. 289-294.

Schultze, E., and Coesfeld, G. (1961). "Elastic properties of ballast." *Proc. 5th International Conference on Soil Mechanics and Foundation Engineering*, Dunond Publishers, Paris, France, pp. 323-327.

Schuettpelz, C., Fratta, D., and Edil, T. B. (2009). "Evaluation of the zone of influence and stiffness improvement from geogrid reinforcement in granular materials", *Transportation Research Record*, pp. 76-84.

Selig, E. T. (1980). "Soil stress gage calibration." *Geotechnical Testing Journal*, 3 (4), pp. 153-158.

Selig, E. T. and Alva-Hurtado, J. E. (1982). "Predicting effects of repeated wheel loading on track settlement." *Proc. 2nd International Heavy Haul Railway Conference*, Colorado Springs, pp. 476-487.

Selig, E. T., and Waters, J. M. (1984). Track Geotechnology and Substructure Management, Thomas Telford.

Selig, E. T., and Waters, J. M. (1994). Track geotechnology and substructure management, Thomas Telford Services Ltd., London, UK, p. 428.

Selig E. T. (1998), "Ballast deformation: Its causes and cures." Railway Track and Structures, May, AAMR, New-York, USA, pp. 25-31.

Shahu, J. T., Rao, K. N. S. V., and Yudhbir. (1999). "Parametric study of resilient response of tracks with a sub-ballast layer." *Canadian Geotechnical Journal*, 36 (6), pp. 1137-1150, (DOI: 10.1139/t99-054).

Sharpe P., Brough M., and Dixon, J. (2006). "Geogrid trials at Coppull Moor on the West Coast Main Line." *Railway Foundations*, 6, pp. 367-375.

Shin, E. C., Kim, D. H., and Das, B. M. (2002). "Geogrid-reinforced railroad bed settlement due to cyclic load." *Geotechnical and Geological Engineering*, 20, pp. 261-271.

Shenton, M. J. (1974). "Deformation of railway ballast under repeated loading conditions." *British Railways Research and Development Division*.

Shenton, M. J. (1975). "Deformation of railway ballast under repeated loading conditions." *In: Kerr(ed): Railroad track Mechanics and Technology*, Proc. Of a symposium held at Princeton univ., pp. 387-404.

Shenton, M. J. (1985). "Ballast deformation and track deterioration." *Proc. Conf. Track Technology*, University of Nottingham, 11-13 July 1985, Thomas Telford Ltd, London, pp. 253-265.

SNCF. (1950). "Société Nationale des Chemins de fer français-French National Railway Corporation."

Stewart, H. E. (1982). "The prediction of track performance under dynamic traffic loading." *PhD thesis*, University of Massachusetts, Amherst, Massachusetts, USA.

Stewart, H. E. (1986). "Permanent strains from cyclic variable-amplitude loading." *Journal of geotechnical engineering*, ASCE, 112 (6), pp. 646-660.

Suiker, A. S. J. (2002). "The Mechanical Behaviour of Ballasted Railway Tracks." Delft University Press, the Netherlands, 2002.

Suiker, A. S. J., Selig, E. T. and Frenkel, R. (2005). "Static and cyclic triaxial testing of ballast & subballast." *J. of Geotech. & Geoenv. Eng*., 131 (6), pp. 771-782.

Sweere, G. T. H. (1990). "Unbound granular basis for roads." *PhD thesis*, University of Delft Delft, The Netherlands.

Tam, H. Y., Liu, S. Y., Guan, B. O., Chung, W. H., Chan, T. H. T., and Cheng, L. K. (2004). "Fiber Bragg Grating Sensors for Structural and Railway

Applications." *In Proceedings Photonics Asia 2004: Advanced Sensor Systems and Applications II 5634 (Beijing, PR China)*, pp. 85-97.

Tang X., Chehab, G.R., and Palomino, A. (2008). "Evaluation of geogrids in stabilizing weak pavement subgrade." *International Journal of Pavement Engineering,* 9 (6), pp. 413-429.

Thakur, P. K. (2011). "Cyclic densification of ballast and associated deformation and degradation." *PhD Thesis*, University of Wollongong, Wollongong, NSW, Australia.

Thom, N. H., and Brown, S. F. (1988). "The effect of grading and density on the mechanical properties of a crushed dolomitic limestone." *Proceedings of the 14th Australian road research board conference*, part 7, pp. 94-100.

Timmerman, D. H. and Wu, T. H. (1969). "Behavior of Dry Sands Under Cyclic Loading." *Journal of the Soil Mechanics and Foundations Division*, ASCE, July, pp. 1097-1112.

Timoshenko, S.P., and Goodier, J.N. (1970): *Theory of Elasticity*, McGraw Hill, New York, 1970.

Trevizo, C. (1991). *FAST/HAL Ballast experiment*, Paper 16, AAR, Transp. Test Center-Pueblo, Colorado, p. 9.

T.S. 3402: *Specification for supply of aggregate for ballast*, Rail Infrastructure corporation of NSW, Sydney, Australia, 2001.

Tutumluer, E., Huang, H., and Bian, X. (2012). "Geogrid-Aggregate Interlock Mechanism Investigated through Aggregate Imaging-Based Discrete Element Modeling Approach." *International Journal of Geomechanics*, 12 (4), pp. 391-398 (DOI: 10.1061/ (ASCE) GM.1943-5622.0000113).

Uzan, J. (1999). "Granular characterisation for mechanistic pavement design." *Journal of transportation engineering,* 125 (2), pp. 108-113.

Vinod, J. S., Indraratna, B., and Sitharam, T. G. (2013). "DEM simulations of granular materials during cyclic loading." *International conference on case histories in geotechnical engineering*, April 29-May 4, Chicago, USA (in press).

Walls, J. C., and Galbreath, L. L. (1987). "Railroad ballast reinforcement using geogrids." In: *Proceedings of Geosynthetics,* 87 (1), New Orleans, pp. 38-45.

Weiler, W. A., and Kulhawy, F. H. (1982). "Factors affecting stress cell measurements in soil." *Journal of Geotechnical Engineering Division*, 108 (GT12), pp. 1529-1548.

Werkmeister, S. (2003). "Permanent Deformation Behaviour of Unbound Granular Materials in Pavement Constructions." *PhD thesis*, Technische Universitat Dresden, Germany.

Wheat, P., and Smith, A. (2008). "Assessing the marginal infrastructure maintenance wear and tear costs of Britain's railway network." *Journal of Transport Economics and Policy*, 42, pp. 189-224.

Wrigley, N. E. (1989). "The Durability and Aging of Geogrids." *Proc. GRI-2, Durability and Aging of Geosynthetics*, Publ. by Elsevier Appl. Sci., London and New York, pp. 110-134.

Xu, D. S., Yin, J. H., Cui, P., Pei, H. F., Zhu, H. H., and Hong, C. Y. (2011). "Monitoring and analysis of internal displacements of a slope and relationship with rainfall infiltration." *Proceedings of 3rd International Postgraduate Conference on Infrastructure and Environment*, Hong Kong, 11-12 July 2011, 1, pp. 117-123.

Yan, Y., and Ji, S. (2010). "Discrete element modeling of direct shear tests for a granular material." *International Journal for Numerical and Analytical Methods in Geomechanics,* 34 (9), pp. 978-990.

Yoon, H-J., Song, K-Y., Kim, J-S., and Kim, D-S. (2011). "Longitudinal strain monitoring of rail using a distributed fiber sensor based on Brillouin optical correlation domain analysis." *NDT&E International*, 44, pp. 637-644.

Zicha, Z. H. (1989). "High-speed rail track design." *Journal of transportation engineering*, ASCE, 115 (1), pp. 68-83.

APPENDIX A: PHOTOGRAPHS OF THE GEOSYNTHETICS USED IN THE STUDY

G1		**G2**	
G3		**G4**	
G5	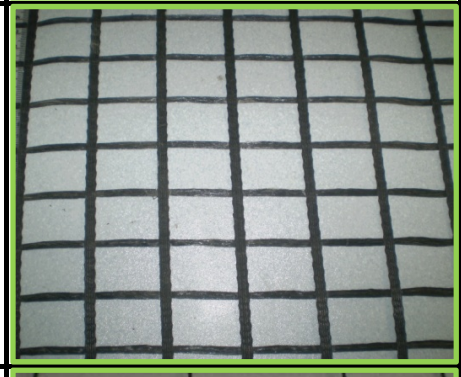	**G6**	
G7	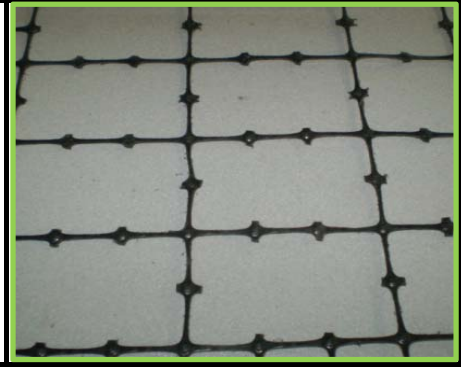	**Geotextile**	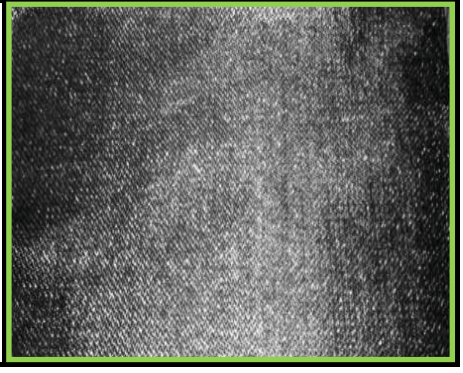

APPENDIX B: LATERAL DISPLACEMENTS IN BALLAST BENEATH THE SLEEPER EDGE

B.1 LATERAL MOVEMENT OF PLATES NUMBERED 2 TO 5 OF THE MPST APPARATUS

The variation of lateral displacements in unreinforced and geogrid-reinforced ballast with the number of load cycles (N) determined from the movement of plates numbered 2 to 5 of the MPST apparatus are depicted in Figure B.1 to Figure B.4. Similar to the lateral displacement behaviour observed from the movement of plate 1 (Figure 6.1 of Chapter 6), it is clear from Figure B.1 to Figure B.4 that the lateral displacements occur mainly during the initial 50000 load cycles after which the displacements remain relatively constant. In line with the results reported in Chapter 6, the role of geogrid in restraining the lateral displacement in ballast is clearly observed. However, due to the varying level of ballast-geogrid interaction depending upon the geogrid type and its placement location, different plates exhibit different amount of lateral displacement.

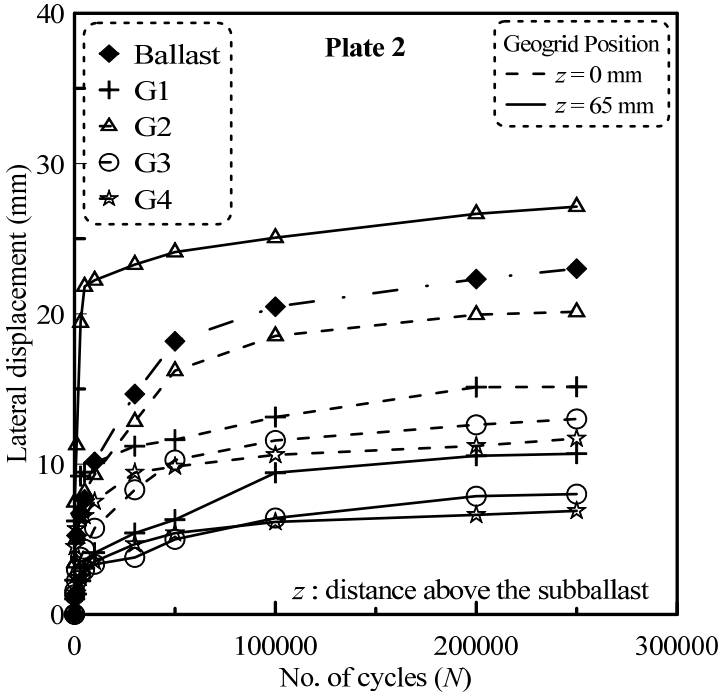

Figure B.1 Lateral displacement in unreinforced and geogrid-reinforced ballast as determined from the movement of plate 2

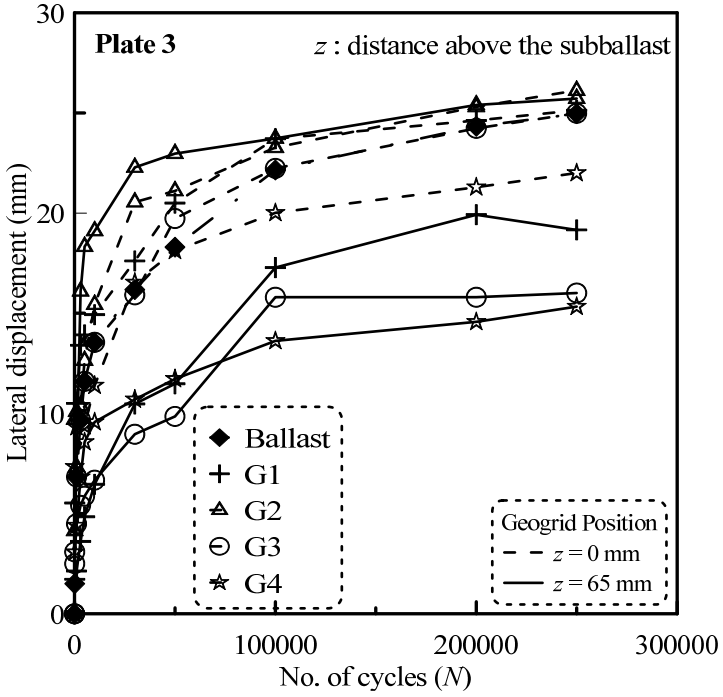

Figure B.2 Lateral displacement in unreinforced and geogrid-reinforced ballast as determined from the movement of plate 3

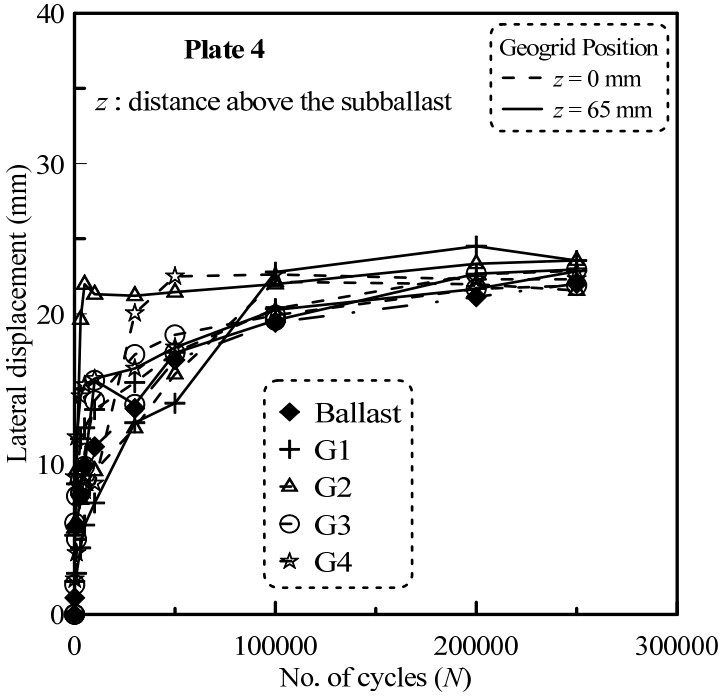

Figure B.3 Lateral displacement in unreinforced and geogrid-reinforced ballast as determined from the movement of plate 4

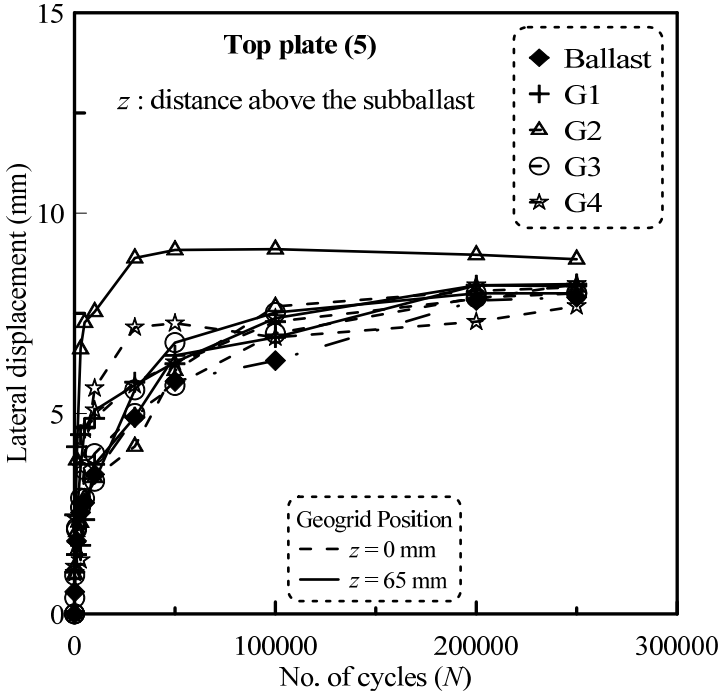

Figure B.4 Lateral displacement in unreinforced and geogrid-reinforced ballast as determined from the movement of plate 5